Applications and Analysis of Stiffened Side Shell Panel Failure for Naval Patrol Craft

by

LT Matthew K. A. Mothander, USCG

B.S. Naval Architecture and Marine Engineering (with honors)
United States Coast Guard Academy, 2005

Submitted to the Department of Mechanical Engineering in Partial Fulfillment of Requirements for the Degrees of

Master of Science in Naval Architecture and Marine Engineering

and

Master of Science in Mechanical Engineering

at the
Massachusetts Institute of Technology
June 2009

Signature of Author:.....
Department of Mechanical Engineering
May 8th, 2009

Certified By:.....
Dr. Tomasz Wierzbicki, Professor of Applied Mechanics
Thesis Supervisor

Certified By:.....
CDR Trent Gooding, USN, Associate Professor of the Practice of Naval Construction and Engineering
Thesis Reader

Accepted By:.....
Dr. David Hardt, Ralph E. and Eloise [redacted] Professor of Mechanical Engineering
Chairman, Department Committee for Graduate Studies

This Page Intentionally Left Blank

Applications and Analysis of Stiffened Side Shell Panel Failure for Naval Patrol Craft

by

LT Matthew K. A. Mothander, USCG

Submitted to the Department of Mechanical Engineering on May 8th, 2009 in Partial Fulfillment
of the Requirements for the Degrees of
Master of Science in Naval Architecture and Marine Engineering
and
Master of Science in Mechanical Engineering

Abstract

Over their lifetime, naval patrol craft are subjected to many different types of loading scenarios, most of which are perfectly safe. In rare instances, through a variety of different reasons, these craft are loaded beyond their means, resulting in structural failure.

This thesis focuses on how side shell stiffened panel failure occurs from a global and local perspective, bridging the gap between a real life problem and mechanics theory in an effort to reduce uncertainty in the ship structural design and construction process. It incorporates aspects of basic ship structural design theory, detailing static and dynamic shipboard loads, progressive collapse behavior, and global causes of hull strength reduction. Locally, it examines stiffened panel failure modes due to axial loading through a comparison analysis with consideration for sources of panel strength loss. Finally, this thesis discusses methods for avoidance and mitigation of failure in the future at the design, construction, and operational levels.

On the global level, this thesis draws from two incidents in the last decade where U.S. Navy and U.S. Coast Guard patrol craft have had class-wide incidents of structural failure. These failures have ranged from buckling, to yield, to fracture. Each ship's background is discussed, and primary stress calculations are presented with design margins based on classification societies, along with an engineering analysis of the failures that occurred on each vessel. Internal and external factors for overall hull strength reduction are examined and applied to each case, including considerations for slamming and saltwater corrosion.

Using one of the failure incidents that took place on the U.S. Coast Guard 123', local failure modes are examined across several analysis methods for axially loaded panels. Buckling and ultimate load values are calculated through a parametric design space, while boundary conditions and geometric properties are varied. Finite element analysis and proven analytical methods are used, including those developed by Von Karman. A comparison analysis is completed using experimental data, where local causes for strength reduction in panels are considered, including construction imperfections, shearing, residual stresses, cracking, and initial deflection.

Thesis Supervisor: Dr. Tomasz Wierzbicki
Title: Professor of Applied Mechanics

Thesis Reader: CDR Trent Gooding, USN
Title: Associate Professor of the Practice of Naval Construction and Engineering

This Page Intentionally Left Blank

Biographical Note

LT Matthew K. A. Mothander is a 2005 graduate of the United States Coast Guard Academy where he received a Bachelor of Science in Naval Architecture and Marine Engineering (with honors). Commissioned as an Ensign in the United States Coast Guard in May of 2005, he served aboard U.S. Coast Guard Cutter Spencer (WMEC-905) from June 2005 until May 2007, as the Damage Control Assistant and assistant Chief Engineer. During this time, he participated in Hurricane Katrina relief operations, alien migrant interdiction operations in the Straits of Florida and Windward Pass, and confiscated over 3000 kg of illegal narcotics. Upon departure from MIT, Matthew plans to work in the U.S. Coast Guard office of Naval Engineering, located at Coast Guard Headquarters in Washington, DC.

Acknowledgements

First and foremost I would like to express my sincere appreciation to Professor Wierzbicki for guiding me through this research and exposing me to material and wisdom, both in his classes and in our meetings, which helped me fulfill my goals for this thesis. I would also like to thank LCDR Frank Pierce of CG-9 for the information on which much of my thesis is based, LT Joseph Rizzo of U.S. Coast Guard Cutter Tybee, Rich d'Entremont and Peter Witherell of PSNS detachment Boston for information and insight on both the WPB and the PC. Additionally, I would like to acknowledge Dr. Yaning Li and LCDR Josh LaPenna for all of their help with ABAQUS/CAE and finite element methods. Lastly, I would like to thank my wife, Colleen, for always knowing when it was time to go to the lab to work and when it was time to take time off and come home.

Table of Contents

Table of Figures

This Page Intentionally Left Blank

Table of Tables

This Page Intentionally Left Blank

Introduction

i. Why Discuss Ship Strength?

Before recorded time, man has been using ships of all shapes and sizes to move themselves and materials across the globe. Today, more than 88% of the world's trade travels by sea – a source we count on everyday to deliver goods we depend on. Regardless of their shape and size, the millions of ships that have been constructed both for recreation and for profit all have one thing in common: they all rely on structural strength and the ability to maintain watertight integrity to float. But just how strong does a ship have to be to float? This is such a broad statement that it is almost silly to analyze it at a level like this. Clearly there are a vast number of different factors that affect ship structural strength but the overarching variables encompass what the ship is made of and what the payload is going to be. People often forget that a large percentage of the structural strength of the ship is devoted to ensuring the ship does not buckle, crack, or yield under its own weight. Naval architects work closely with marine structural engineers during the design process to ensure that appropriate structural loading scenarios are considered. This analysis can be accomplished in a variety of different ways. Before it all can be completed however, design teams must first understand the design philosophy and the reasoning behind construction in the first place.

The design philosophy is arguably the most difficult decision making process in the realm of shipbuilding. After payload determinations are made, significant decisions relating to range, speed, survivability, crew comfort and mission effectiveness have to be made. It is from these building blocks that a design is born, construction occurs, and the finished product is finally launched and put into service. But what happens if, that ship is discovered to have some type of structural problem? What happens if the ship develops global and local buckling, cracking, or bending? How could it have been avoided and what were the tell-tale signs that could have served as a warning? These are questions today's naval architects and marine engineers hope to never ask.

ii. Motivation

Structural problems were much more prevalent in the past than they are today. During the eight years during and following World War II, the 2,710 Liberty ship fleet built exclusively to help with the war experienced significant structural problems. In all, nearly 1500 instances of significant brittle fracture or other sources of structural damage were reported. In 12 cases, a Liberty ship literally broke in two without warning, including one particularly tragic instance

where 10 lives were lost (1). Figures 1 and 2 detail both a surviving Liberty ship as well as examples of the structural failures seen in this class.

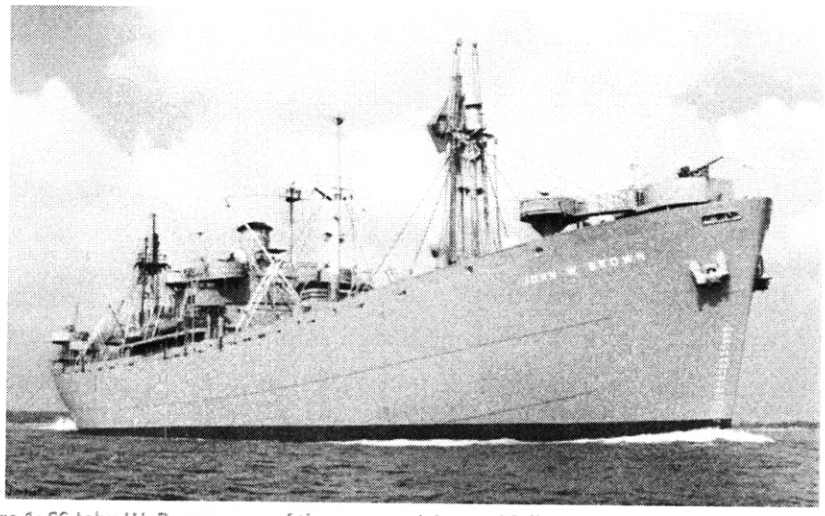

Figure 1: SS John W. Brown, one of the two surviving and fully operational Liberty ships today.

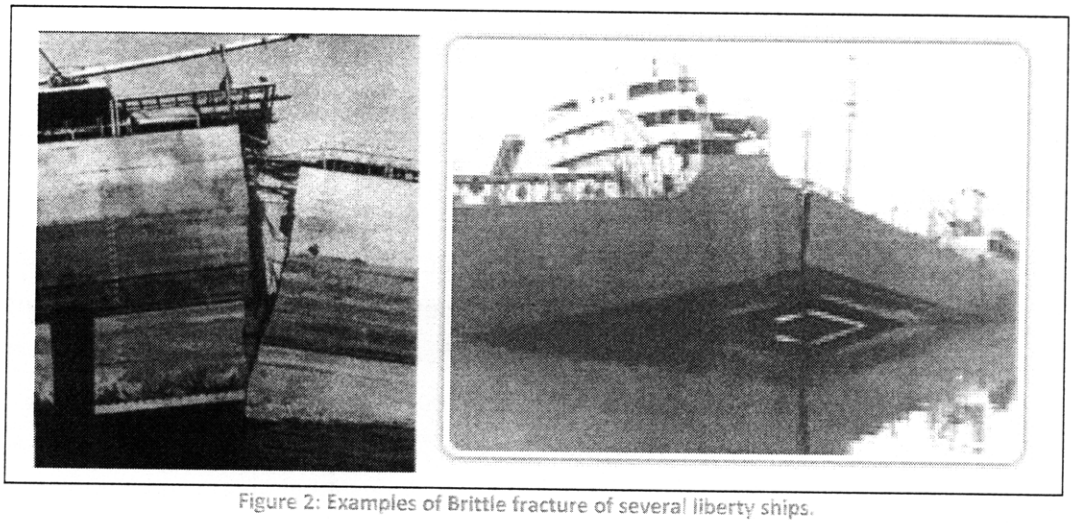

Figure 2: Examples of Brittle fracture of several liberty ships.

Due to these catastrophic missteps, it is therefore applicable to examine the worst case scenario: the structural integrity of the vessel has come into question, buckling has occurred and the load is such that ultimate failure follows. While it may not be precisely brittle fracture as was determined (and fixed) in the Liberty ship case, the causes of buckling and ultimate failure of hull, side shell, and deck stiffened panel members due to excessive longitudinal loading and hull strength reduction are still a very real threat to the shipbuilding industry. In order to properly examine this problem, one must start at the beginning with a discussion of the fundamentals of ship structural design.

With an understanding of longitudinal strength and applied loads, it is possible to examine what kind of relatively significant and insignificant factors cause a reduction in hull strength which can ultimately lead to hull failure under certain conditions. In almost all cases,

the "spectacular ship failure" event where a ship just suddenly breaks in two will not occur, chiefly due to the ductility of today's structural steel. Rather, it is often that two or three or more significant sources of loading, coupled with various factors that reduced design strength, ultimately cause worn steel to surpass its yield point. In worst case scenarios, steel surpasses its ultimate failure point and subsequent fracture strain. The question is, with the proper design software tools of today, how does this occur? Proper safety margins incorporated in classification society rules based on principle hull dimensions, hull materials and primary missions should mitigate any and all occurrences of such incidents. Furthermore, advanced design and analysis software also plays an increasingly important role in predicting a vessel's structural strength. Regardless, what is seen on a computer screen in a theoretical design is slightly to significantly different from the finished product because after all, human hands create ships through the manipulation and molding of natural resources and are by no means always identical to computer modeled theory.

iii. Incidents

To explore these questions, two specific instances were examined where U.S. Naval and U.S. Coast Guard patrol craft experienced longitudinal failure of various kinds. Failure included cracking with propagation and buckling in several different instances and modes. Traditionally, the U.S. Government has had no problems designing and constructing sound vessels through traditional contract means. Although the ship design and construction process for each of these two ships were two completely separate entities, they share several commonalities: Both ships were built by the same shipyard, both are based on the same proven British hull design, and both ships were retrofit with a stern launch consisting of 9' and 13' for the U.S. Navy and U.S. Coast Guard, respectively. The timeline of failure is different for each class of ship however, as the U.S. Naval Ship failed pre-extension while the Coast Guard Cutter only failed after the extension process was completed. Additionally, it should be noted in the applicable case that by itself, the retrofit cannot be ruled a primary cause of failure. The classes of ships in question are the U.S. Navy Cyclone Class PC 179' (originally a 170') and the U.S. Coast Guard Cutter Island Class WPB 123' (originally a 110') (2) (3). These ships can be seen on the following page in Figures 3 and 4. While the 179' PC (and its pre-retrofit 170' siblings) is still in service today performing various critical missions for the Department of Homeland Security and the Department of Defense, the fleet of U.S. Coast Guard 123' WPB's sit idle in Curtis Bay, Maryland, as a result of a decision made at the highest levels of uniformed service (2).

Figure 3: U.S. Navy (and U.S. Coast Guard) 179' Patrol Craft.

Figure 4: A CAD rendition of the United States Coast Guard 123' Patrol Craft. This Cutter was first built as a 110' Patrol Boat and retrofit with a stern launch as part of the Deepwater Program.

iv. Objectives

Due to ongoing investigation by Coast Guard Technical Authority of the U.S.C.G. failure causes, this thesis will not investigate in particular detail on why each ship failed on a global scale. Rather, it will examine relevant ship theory on a macro-to-micro sliding scale bridging the gap between real life events and detailed structural mechanics to understand how failure occurs, translating it into a scenario that can be accessed from an academic standpoint. This is accomplished through discussion of the mechanics of failure through global and local regimes, encompassing shipboard stress analysis and an examination of internal and external factors that

reduce the strength of ship hulls. Additionally, a local level analysis and comparison of axially loaded stiffened side shell panel of the 123' in experimentation, finite element, and analytical areas from a baseline level show how design ideals and computer analysis leave out or inadequately model many of the uncertainties and strength degradation factors in ship building. The science of ship structural design is, in no uncertain terms, one of the most complicated and dynamic processes in the design spiral. This is a look at a single, though very important, sliver from this particular field that is still evolving every day.

This Page Intentionally Left Blank

Chapter 1: The Ship Design and Construction Process

1.1 Fundamentals of Ship Structural Design

Ships are, by no small margin, man's largest moving engineering marvel. From the giant supertankers surpassing 300,000 LT to the U.S. Navy's 90,000 LT super carriers, the complexity and ingenuity of ship structural design rivals some of the world's greatest structures. In fundamental terms, the reason a ship floats is simple and is given by Archimedes principle:

$$Mg = \rho g V \quad [1]$$

$$\text{If } Mg = W, \text{ and } \rho g = \gamma, \text{ then}$$
$$W = \gamma V \quad [2]$$

This balance of forces in the vertical direction causes a ship to float and satisfy Newton's laws of static equilibrium. This is the most basic "law" of ship design. Structural loads consisting of the ship's own weight (internal loads) and outside forces (external loads) create a need for hull design that goes beyond a simple balance of forces. This chapter will examine these basic principles not only from an engineering approach, as expected, but also (and more importantly) from a design approach.

1.1.1 Longitudinal Strength

The analysis of longitudinal strength starts with a simplifying assumption that in terms of structural response, a ship can be modeled as large girder. This girder is supported by the force of buoyancy pushing upward and weighted down by the steel, machinery, equipment and personnel that make up the ship. Along with the basic principle that these two forces are equal, knowledge of the loading distribution, and the location of the vertical and transverse center of gravities (VCG) and (TCG), play a role in determining longitudinal strength.

Basic beam theory is used in naval architecture practice to make estimations of the maximum load, shear, and bending moment distributions found along the hulls of high speed naval vessels. Beam theory, as it is applied to ships, is discussed at length in Zubaly's *Applied Naval Architecture*, (4). In order to determine the distributions that are present in the beam-theory hull girder approach, several underlying assumptions must be made as listed below:

- Plane sections remain plane
- The girder is prismatic by nature
- Any and all responses are not coupled

- The girder material is homogenous and elastic

Beam theory develops relationships between weight and buoyancy as it is distributed along the length of the beam and can be expressed by *b(x)* and *w(x)*, buoyancy and weight per unit length (4).

Buoyancy per unit length depends on the "fineness" characteristic of the ship and is described most often by the Prismatic Coefficient (C_p). In the case of this type of naval vessel, the buoyancy per unit length at either end will be much less than at the mid-ship section. The weight per unit length is dictated by the distribution of weight within the ship. Complex weight distribution analysis in the final iteration of design will usually yield the most accurate results for weight for various loading conditions. The net force in the vertical direction is the load, described below in Equation 3:

$$l(x) = w(x) - b(x) \quad [3]$$

Graphically over the length of the ship, *l(x)* has a zero net area, which is required in equilibrium.

As in beam theory, the location and magnitude of the shearing forces present is written as the integral of the distributed load, *l(x)*. Equation 4 below describes this function:

$$V(x) = \int_{AP}^{FP} l(x)dx \quad [4]$$

The relationship between the bending moment distribution and shear force distribution is identical to that of the shearing force and loading per unit length. The magnitude of the bending moment, *M(x)*, is calculated by integrating *V(x)* over the length of the ship:

$$M(x) = \int_{AP}^{FP} V(x)dx \quad [5]$$

An example of the load-shear-moment diagram as a function of ship length (along with weight and load components) for an arbitrary ship is shown in Figure 5. It must be noted that the maximum bending moment that is estimated by this static equilibrium method is only one part of the maximum allowable bending moment. This is known as the *still water bending moment*. In reality, the maximum bending moment is made up of both static and dynamic loads contributing to the overall stressing of the hull (4).

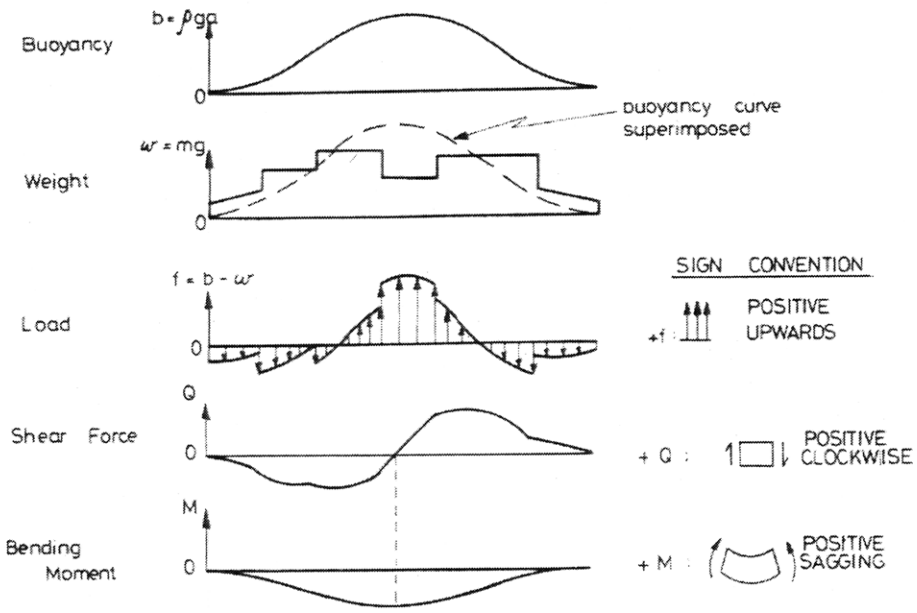

Figure 5: Buoyancy through bending moment curves in still water ship structural analysis. This figure is reproduced from (5).

When subjected to a moment, the overall hull girder will have a tendency to bend downward or arch upward as both external and internal forces change over time. This phenomenon is called hull girder *hogging* or hull girder *sagging*. This is shown in Figure 6:

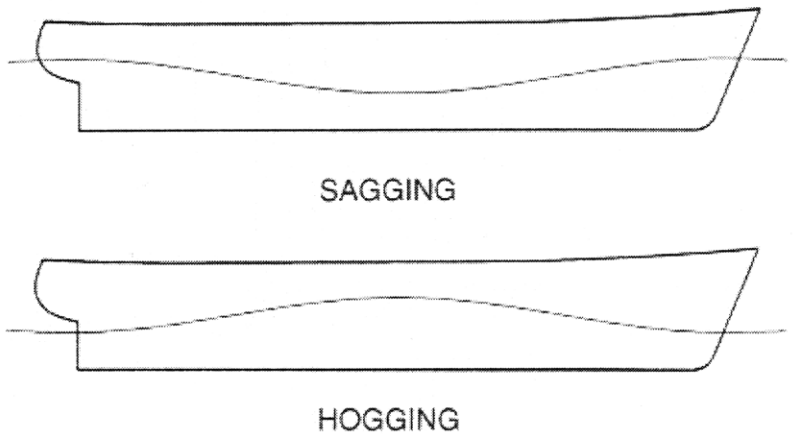

Figure 6: Simplification of a superimposed sagging and hogging wave. In basic structural analysis, a trochoidal wave is superimposed on the hull (4).

Typically in the early stages of design, a ship's hull girder strength is evaluated by determining the allowable stresses associated with a bending moment caused by a quasi-static trochoidal wave whose parameters are a function of the ship's length.

1.1.2 Primary, Secondary, and Tertiary Stresses

Bending moments discussed in the preceding section are a result of the net vertical forces subjected to a ship's hull that is modeled in its simplest form as a beam. When a beam is subjected to a moment, the reaction of the beam is to compress and extend linearly according to the magnitude of that moment. The resulting stresses can be computed according to the well known flexural formula, seen as Equation 6. This derivation can be seen in Hibbler's *Mechanics of Materials* (6) or any other strength of materials textbooks and is the result of beam theory and its associated moment curvature relationship.

$$\sigma = \frac{My}{I} \qquad [6]$$

In this case, the bending stress σ over a girder with a given moment and moment of inertia is maximized farthest from the neutral axis, where y is the distance from that axis. When this holds true, $y=c$ and the relationship between the moment of inertia and c is called the section modulus. It essentially quantifies the ship's ability to resist bending, seen below (4):

$$Z = \frac{I}{c} \qquad [7]$$

Unless the hull's neutral axis is at exactly half the depth of the hull, there will be two section modulus calculations, one for the deck and one for the keel. Generally, the neutral axis of the midship section is typically found at 0.4*Depth, that is, 40% of the way from the keel to the strength deck. This implies the largest bending stresses will usually occur at the strength deck. In a structural failure scenario, various factors can reduce the effective section modulus of a ship's hull, which in turn can increase the bending stresses on the hull past a given threshold (usually the yield stress) to failure (5).

The different types of stresses experienced by the hull can be broken down into three distinct categories: primary stresses and its associated shear stress, secondary stresses and tertiary stresses. Visual representations of each of these stresses can be seen in Appendix 1.1.

Primary Stresses and Shear Stress

Primary stresses encompass how the hull responds as a whole. The theory rests on beam theory and holds the same assumptions as we see in a basic longitudinal strength analysis discussed in 1.1.1. Primary stresses can occur in the vertical, lateral, or torsion directions. Generally, the primary stresses caused by moments in the lateral and twisting directions are orders of magnitude less than that of the vertical primary stresses and therefore are not a driving

factor in design. While certain types of bending stress are of little consequence, a type of stress that has design relevance in overall primary response analysis is shear stress. Shear stress describes the tendency to "slip" due to opposing, in plane forces. In ship design, shear is measured by shear flow, which is the gradient of shear stress within a fixed body. It is given by Equations 8 and 9:

$$q = \frac{Q}{I}m \qquad [8]$$

$$m = \int_0^s ytds \qquad [9]$$

The derivation of this formula can be seen in Hughes's *Ship Structural Design* (5) in full and will not be shown here.

Secondary Stresses

Secondary stresses encompass the behavior of the individual stiffened panels that make up the hull of the ship due to lateral loading. Secondary stresses can be amplified due to hydrodynamic pressure if the stiffened panels are below the waterline. Secondary stresses develop on the actual sub-panel sections between the stiffeners, which can be seen below as Figure 7 (7). In a traditional, longitudinally framed stiffened panel, the loaded edges of each panel consist of the orthogonal, transverse stiffeners placed at intervals along the hull. The unloaded edges then consist of other, adjacent longitudinally stiffened panels.

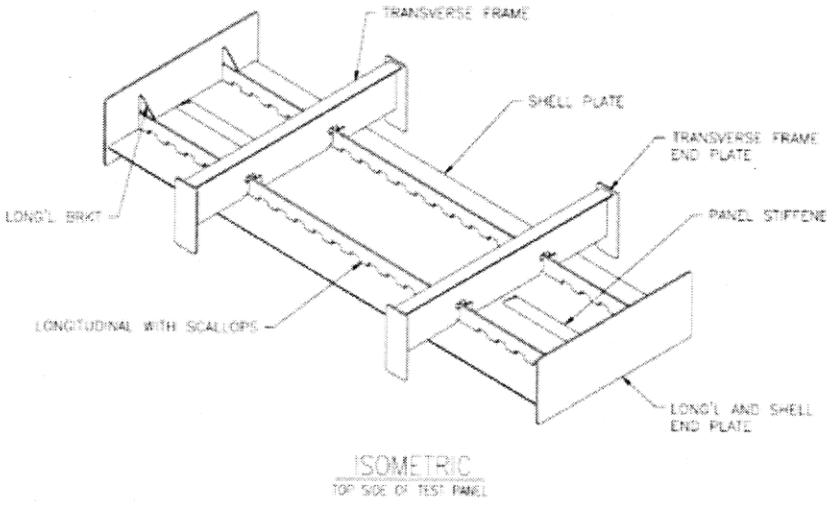

Figure 7: Isometric view of 123' side shell panel used for testing. This panel will be used later to analyze local structural strength under a variety of different variables for the 123' WPB.

Stiffeners are traditionally assumed to act as simply supported boundary conditions for each sub-panel section.

Tertiary Stresses

Tertiary stress is caused by the bending and deformation of the individual plates that make up a stiffened panel. Like stiffened panels subjected to secondary stresses, these plates are subjected to axial loading and have specified boundary conditions made up of the attached stiffeners. Tertiary stresses can potentially make up a large portion of the stresses that add to failure. Typically, consideration for tertiary stresses can be included using the Heller-Jasper method, discussed in References (8) and (4). Graphical examples of all three types of stresses can be seen in Appendix 1.1.

1.2 Structural Design Methodology

The first section of this chapter described the basics of longitudinal strength, the responses of the hull girder and familiarized terms that are prevalent in the structural design process. But what exactly drives structural design requirements? Why even build a certain type of ship in the first place? What are the relative important portions of design considerations such as safety, survivability, upfront cost and lifecycle cost? These questions are usually answered in the early stages of design and embodied in the design philosophy.

1.2.1 Philosophy

The design philosophy of a warship (U.S. Navy, or otherwise) derives from the capability and cost requirements for the ship. A capabilities document typically outlines required missions, weapon and defense capabilities, speed, range and endurance capabilities, and habitability concerns. As with any design, various trade-off studies are required in order to achieve any sort of optimal finished product. In one particular method of optimization, specific weights are assigned to each chosen design parameter and fed into an evaluation framework (or calculator of sorts) that produces what is often known as the "Overall Measure of Effectiveness" (OMOE) (9). A sample model of this method and further discussion can be seen in Appendix 1.2.

It is important to understand that design philosophy affects ship *structural* design at its very highest level. The design philosophy and the types of missions that the warship will eventually hold determine the type of hull that will be used. Traditional high speed naval vessels (patrol boats, fast destroyers and frigates) typically have a mono-hull, sleek, high length-to-width ratio look about them. After the hull selection process is completed, actual structural design of the hull falls on the structural engineer.

1.2.2 Design Approaches

In the Naval Architecture world, there are essentially two major paths to take when working on the structural design of a ship. Both methods require geometric properties be essentially known and a specific design philosophy to be completed, and each method is intended to achieve a similar end result. Regardless of the method, ship structural design focuses on two major aspects of the ship: *Hull Girder Design* (discussed in section 1.1.1) and *Midship Section Design*. The midship section is essentially the strongest portion of this beam and represents the ability or inability for the ship to flex as load-induced stresses are dissipated throughout the hull. The two approaches that are available to achieve these designs are the "Rules" based and "Rationally-Based Optimization" approaches (5). A third method which uses portions of both methods is currently employed by the U.S. government for warship structural design (9).

Classification Societies and the Rules-Based Approach

When those in the maritime community talk about a vessel being in compliance with the "rules," they are referring to various groups or organizations that are explicitly non-governmental, that regulate and check applicable standards for the design and construction of all ships. A table of some of the predominant classification societies can be seen in Appendix 1.3.

As there is no law that binds any shipbuilder to follow the standards set forth by these societies, these classification societies bear no financial or legal burden on the ship itself and merely provide guidance on construction and implementation of the ship and its systems (10). As it turns out however, almost every ship and/or boat all over the world is built to the standards of one of these classification societies. This is due to flagging and insurance requirements imposed by countries and insurance companies that will ultimately hold some, if not all, of the previously discussed legal and financial responsibility.

The American Bureau of Shipping, one of the predominant classification societies is the basis for the rules-based design approach of many U.S. vessels. Although there is no specific requirement to follow these rules, they provide effective safety margins and robust design approaches to limit complications that could cause failure. Standards in ship strength set forth by ABS can be broken down into three categories or "minimums" (11). They are as follows:

- Maximum bending stress midships ($M_{tot} = M_{sw} + M_w$)
- Nominal permissible bending stress (calculated based on ship characteristics)
- Required section modulus (calculated based on ship characteristics)

If some or all of these criteria are not met, the ship cannot be certified. The overall premise creating a design using the rules-based approach is essentially a simple iterative process. More information can be seen in References (10) and (12).

The rules-based approach is very robust and sound, however in a volatile economy and an overarching concern for cost, it often provides too much (or too little) of a safety margin. Unknown safety margins and overdesign can potentially bring significant cost increases and unwanted weight issues to the table. The alternative approach helps mitigate some of these concerns.

The Rationally-Based Optimization Approach

The rationally-based design approach is a type of structural design that emphasizes user defined inputs coupled with computer optimization to create an efficient, structurally sound finished product. Dr. Owen Hughes has been a pioneer in the field of structural design, who defines this approach in his ship structures book published by The Society of Naval Architects and Marine Engineers or *SNAME*: "Design which is directly and entirely based on structural theory and computer-based methods of structural analysis and optimization, and which achieves an optimum structure on the basis of a designer-selected measure of merit" (5). This approach requires four major analysis procedures:

- Calculation of loads
- Calculation of the ship's response to those loads
- Calculation of limiting values of each response
- Optimization of the loads and responses

By its own definition, it is clear that this method is out of necessity, computer based. While this method, enabled by computing power, has led to to major strides in ship design, the industry still requires classification societies to ensure rules compliance due to insurance needs.

Warship Design

Before the emergence of major independent ship design firms, Coast Guard and Naval warships were designed completely in-house (9). As times have changed, however, so have methods, though these methods have not evolved completely into today's commercial design industry. In the U.S. government's most recent shipbuilding projects, the ship's concept design was born from a single or multiple concept designs coupled with mission capability requirements. In-house, preliminary design is typically completed with all major systems incorperated and analysis completed for payload, weight, strength and so forth. This design is then taken to industry where various companies have the opportunity to bid on a "winner take

all" or "joint" contract. In recent contract awards both in the Navy and Coast Guard ship construction projects, joint contracts have been awarded where several large companies or shipyards have worked together to create detailed concept design and a finalized product. These projects have seen great successes but also have met great failures (13) (9). Naval structural design methodology has evolved over time and publications have been written to govern the design under a modification of the rules-based approach. These publications were published, and are still maintained by the Naval Sea Systems Command, otherwise known as NAVSEA. The NAVSEA structural design manual details the different aspects of the way the U.S. Navy has conducted ship design in the past and present (14). In recent years, the U.S. government has taken the requirements set forth by NAVSEA and its understanding of special requirements of a surface combatant and developed a set of new documents titled "The Naval Vessel Rules" (9), in incorporation with ABS. These rules are not available to the general public for security reasons and essentially have provided U.S. Navy naval architects and their contractors with the specifications and allowances for the future of the U.S. fleet.

1.3 Warship Construction

Until now, discussion has primarily focused on how ships are designed. In the preceding sections, the rules-based approach and the rationally-optimized design approach have been examined and compared over a variety of different criteria. At the conclusion of the design phase, when all feasibility and cost studies have been completed, it is then up to the construction company or companies to put the design to fabrication. In the case of naval warship detailed design and construction, the designer and the fabricator are usually one and the same (9). These companies are not left up to their own measures, however. In-house oversight, consisting of senior technical advisors employed by the government (both military and civilian personnel), follow and approve as necessary each step of the construction process. On the construction side this is usually accomplished in the form of inspections during fabrication and upon completion of various ship systems. The generic, military construction process based on shipyard operations today in the United States is briefly discussed in the following sections, as well as specific circumstances that shipyards often encounter when retrofitting and repairing ships already in service.

1.3.1 The Construction Process

It is very difficult, nearly impossible even, to create a single "checklist" of tasks that describe how to build a ship from design plans. Every shipyard as a separate entity completes tasks a little differently, has different procedures and a different way to monitor work. In a

general sense, the end product is the same, but the method to create the product once the design is complete is usually somewhat different (15).

Each shipyard involved in production will have a certain "Production Approach," which governs the flow of material into the finished product. Lamb's *Ship Design and Construction* details some of the criteria examined when deciding on the type of approach (16):

- Product demand
- Demand variability and predictability
- Product complexity
- Product mobility
- Material type and associated joining technology
- Product variety within a single production system
- Degree of customization or variation among products of any single type

Although none of the afore mentioned criteria will be described in detail, the result of an analysis for a government contract has almost always resulted in a customized modeled from a fabrication technique known as the "Group Technology Approach."

To apply the group technology approach in ship construction, shipyards look at and then optimize the similarities between intermediate-type products. They then evaluate demand and create production lines that optimize both quality and economics due to these similarities. In a typical naval shipyard, these production lines are located either right next to the main assembly areas or a short drive away. It is from these production lines that the pieces for eventual subassembly and ship erection are found (16).

1.3.2 Dry-Dock Repairs and Retrofitting of Naval Ships

For any vessel, let alone a naval combatant, regular scheduled dry docks are a normal part of the ship's lifespan. In some cases, the maintenance and repair dry-dock periods are performed where the ship was built, but more often they are completed (especially when it comes to the Government) at a nearby shipyard who happens to be the lowest bidder. When it comes to lifespan, the U.S. Navy tends towards decommissioning ships at or before their predicted service life, and building new vessels. The U.S. Coast Guard on the other hand, continuously stretches cutters past normal life expectancy through programs such as Deepwater (to be discussed later) and the Mid-life Extension Project, or MEP. The MEP project is basically a fancy name for an extensive, multi-million dollar dry-docking, retrofit, and repair period ranging from 6 months to a year in length. Cutters undergoing the MEP process are brought to the U.S. Coast Guard Yard from all over the United States, where in-house supervision can take place.

In extreme scenarios meant to extend the service life of a ship, along with new systems and updated compartments, the actual hull is extended to better serve the mission profile of the ship. This was the case with the ships that will be discussed in this study. With any dry-docking, repair, or retro-fit however, comes some risk that the ship will actually be worse off than before. This is better understood once the effects of human limitations and uncertainty in the design and construction process are considered.

1.3.3 Understanding the Effects of Human Limitations and Uncertainty

Optimists might say that the abilities of humans to design and build are limitless. In a sense, they are correct. The technological advances seen over the last 100 years surpass the advances of the last thousand years 10,000-to-1. Still, any man-made structure cannot be ideal in every way. Advances in computers, automation, and robotics have enabled the construction process to approach such a point, but humans will never truly be able to create anything with absolutely no flaws.

Ships, by nature, are constructed using advanced steel forming and welding techniques that have been fine tuned throughout the history. Still, these techniques are not an exact science. Additionally, there are vast uncertainties about the environments that the ship will encounter through its lifetime. The definition of "ideal" in this context then becomes "made within certain tolerances and margins" (17). Structural failure, then, occurs when the actual differs from the predicted by more than the tolerances and margins allowed for. A good example of a design tolerance is seen in the U.S. Navy design standards for hull girder strength, SDS 100-1. This standard incorporates a minimum of 1.0 Ton-per-square-inch stress margin for combat ships that accounts for weight growth, changes in the loading distribution, and the uncertainties associated with corrosion, residual stresses, deflection and imperfections. This is the standard for warship construction today, and this thesis touches on the uncertainties of the strength reduction factors that can ultimately cause a ship to fail.

This Page Intentionally Left Blank

Chapter 2: Ship Strength and Loading

The analysis of the structural strength of a ship requires a mutual understanding of structural loading, the associated stresses, and the response of the ship as a whole. The strength assessment starts with determining the material properties for calculations and only ends when every one of the thousands of structural members have been designed with appropriate safety margins and validated by a governing authority, government or otherwise. It is typically easiest to commence the structural analysis of a warship by first examining the associated material properties and then determining loads and finally potential risks for hull strength reduction that have to be taken into consideration during design and construction.

2.1 Ship Material Properties

The construction of U.S. warships is nearly a 100% steel market. In some cases, the superstructure of a warship is made out of lighter weight aluminum, fabricated through explosion welding techniques. Typically, the entire structure is made up of a single type of steel, but with retrofits, dry-dock repairs, and any other dockside repairs, there is a possibility for the type of steel to vary.

Why Steel?

The use of steel in ships has evolved over time but the reasoning behind the use of any material in construction is relatively the same. In *Applied Naval Architecture* by Zubaly, (4) the author lays out a set of basic criteria for the materials used to form the structural core of a ship. These criteria are listed below:

- Availability and cost
- Uniformity
- Ease of fabrication
- Ease of maintenance
- Resistance to distortion with applied load

When these requirements are set forth, it is easy to see that steel is often an appropriate choice. Amongst this list lies the chief cause for concern in ship building: strength versus weight at cost. In this market, mild to mid range steel has proven to be inexpensive to make, inexpensive to build with, and easy to fix.

Material Properties of Steel

The strength of steel (or any similar material for that measure) is determined through several ratios based on Hooke's Law and quantified in terms of stress and strain. The linear relationship between stress (σ) and strain (ε) is known as the Modulus of Elasticity and essentially represents material stiffness. This linear relationship only applies when steel is in the elastic region. The modulus of elasticity is sometimes called Young's Modulus, after Thomas Young, and is represented by the variable E (6).

In the case of a particular type of steel, engineers tend to rely on stress – strain or load – strain diagrams to quickly review material properties. This diagram portrays the steel in the elastic range where the stress – strain relationship is linear and in the plastic range, post yield, until ultimate stress and finally to fracture. The diagram below shows a typical stress-strain diagram for mild steel from the elastic range all the way to fracture.

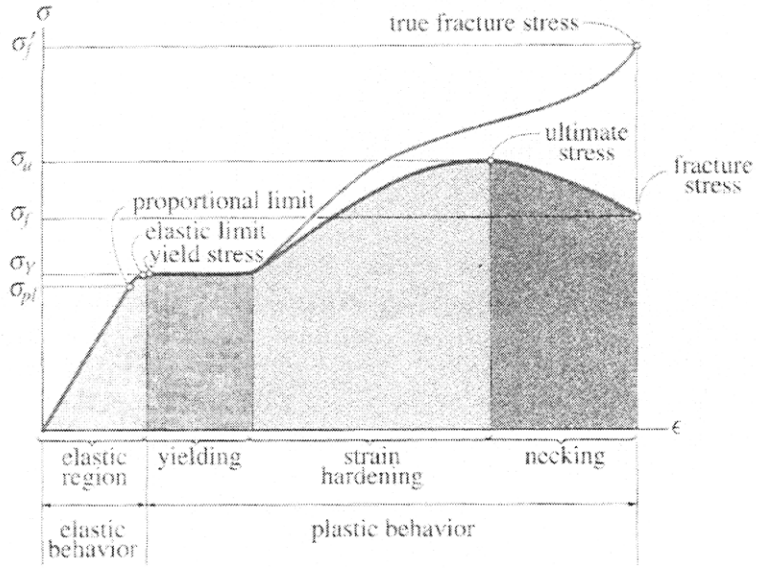

Conventional and true stress-strain diagrams for ductile material (steel) (not to scale)

Figure 8: Stress-Strain diagram for mild steel. This figure is reproduced from Reference (6)

It should be noted that there exists a difference between "true" stress and engineering stress shown in Figure 8 above. During normal design, this does not present any cause for concern because structures are normally built to remain in the elastic region, where very little difference exists (6).

Steel found in Ships

There are several types of "ordinary" steel that are approved by ABS and are commonly used to build both commercial shipping and U.S. warships. They all are rated for tensile strengths that fall in acceptable ranges and generally are differentiated by their relative toughness. In addition to these steels there are several high strength steels that are approved and generally only used in special situations due to cost. Like many ships that have been through a multitude of different dry-docks and retrofits, the 123' U.S. Coast Guard Cutter examined in this work is built of several different types of steels and has an aluminum strength deck and superstructure. The ship below is a finite element replica of the 123' showing all the different types of steel used aboard.

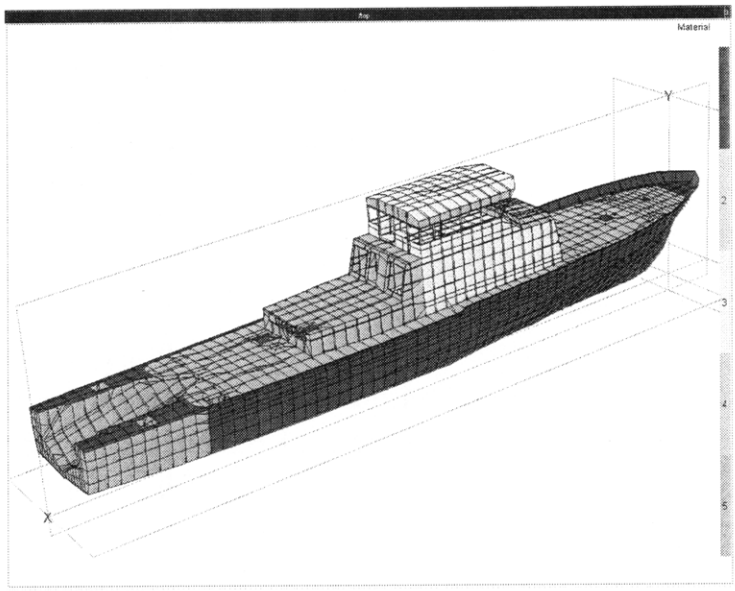

Figure 9: MAESTRO Model showing material properties by type. This form of the hull was generated with the analysis program MAESTRO (18).

By color code, the red and green portions of the hull are mild (BS 4360) and high strength steel, respectively, while the orange deck and yellow superstructure are two different types of aluminum.

By comparison, the Navy PC 179's hull is constructed entirely of BS 4360 steel which happens to be the same steel that was used to construct the 110' and used in the 110' to 123 conversion processes. Like the 123', the 179's superstructure is also made of aluminum. A complete description of the material properties are seen as part of References (18) (19).

2.2 Shipboard Loading

First and foremost, a ship must be built to withstand the load imposed by its own weight. This is called the "lightship" and remains very constant throughout the life of the ship with small

adjustments coming during structural repairs. In the case of both ships discussed in this study, this weight was changed substantially during the hull extension. The discussion of shipboard loads is generally divided into several categories, namely static loads, dynamic loads, and impact loads (20).

2.2.1 Static Loads

Static loads make up those that define opposing forces in a particular loading condition of a ship. These loads do not have an instantaneous change and generally have a pre-determined centroid location on the ship depending on their distribution. The main static shipboard loads are the overall displacement of the ship in its loading condition and the equal and opposite buoyant force. These loads only change when the overall ship displacement changes due to a variety of different circumstances. Some of these are below, but this list is certainly not all-inclusive (4).

- Change in liquid load (fuel, potable water, ballast, grey water, sewage)
- On/Offload of Cargo
- Change in Structure

In design, ships are usually afforded a growth margin that accounts for a gradual increase in overall displacement over time due to the accumulation of sea growth and material buildup. In addition to these main contributions to the static load aboard ship, thermal effects and hydrostatic hull pressures contribute to hull stresses. Ships must also be designed to withstand the infrequent static load conditions imposed by dry-docking evolutions and minor grounding events (20).

2.2.2 Dynamic Loads

Dynamic loads are loads that vary over a given time frame. These loads can be quantified by assigning an amplitude (A) and frequency of vibration (Hz) or even described mathematically as a probabilistic spectrum. The latter is usually used to describe wave induced loads since this type of loading extends well into the probabilistic realm. The response, however, to the load is often simplified into vibration amplitude-frequency data (20). Dynamic loading, especially excessively violent dynamic loading, is often the ultimate difference in structural failure. Both low frequency and high frequency dynamic loading are discussed in the proceeding sections.

Low Frequency

Low frequency dynamic shipboard loading are varying loads that have a nominal frequency up to several seconds in length. This frequency between load peaks is generally lower

than the first mode of the natural frequency of the vessel. Low frequency dynamic loads include, but are not limited to, the following (20):

- Wave induced loads.
- Inertial movements as the ship accelerates and decelerate in its six degrees of freedom.

Low frequency loads make up a great portion of the dynamic loads that exert stresses on the ship. During the design process, it is these loads and the requisite static loads that derive the baseline strength requirements in a design.

Highly accurate evaluation of wave-induced loading requires extensive knowledge of hydrodynamics and an understanding of how time varying fluid forces interact with inertial motions of the hull. To simplify these variables, a process called strip theory is used. Strip theory allows engineers to use the relatively large length to width ratio of the wetted surface of a ship to eliminate variables and boundary conditions in a very complex and dynamic problem (20). The elements considered in strip theory are listed below:

- Froude-Krylov Force
- Wave-Diffraction pressure Force
- Hydrostatic Restoring Force
- Damping Force
- Added Mass Force

All of these forces accounting for low frequency dynamic loads on the hull are sufficiently discussed in any hydrodynamics textbook. It is the compilation of these forces that the naval architecture community has simplified into the quasi-static trochoidal wave seen in many CAD programs that analyze ship structural design (20). The trochoidal wave is discussed in Section 4.2.

High Frequency

High frequency loads are described as loads that meet or exceed the first mode of natural vibration of the ship (20). These dynamic loads range from forced vibrations due to machinery or shafting to hydrodynamic in-balances in the propulsive equipment. The magnitudes of these loads usually are comparatively small, but coupled with natural frequency characteristics, large loads can develop through resonance.

2.2.3 Impact Loads

Impact loads make up another area of concern for naval architects. Impact loading is often violent and unexpected and usually, if the magnitude of the load is great enough, causes the

ship to essentially shudder, or vibrate fiercely. Types of impact loading found in warships include large grounding events, impact with other vessels, piers or structures or weapons discharge, although the most common type of impact loading is the slamming phenomenon. Slamming occurs when the resultant of wave loading and inertial forces draw the bow of the ship out of the water and then subsequently slams back down into the water as the ship tries to achieve static stability in the seaway (21).

Unlike low frequency dynamic loads or static loads which have a direct and often immediate impact on the overall strength of the ship, high frequency and impact loads are, coupled with other factors discussed in the following sections, often the cause of hull strength degradation over time (20). It is this strength degradation that leads to direct failure in static and low frequency dynamic load response scenarios.

2.3 Factors in Strength Reduction

The question of strength reduction (from design standards) over time or during the initial construction phase comes up again and again after a ship suffers a debilitating or catastrophic failure due to excessive loading. There are many possible causes for strength reduction due to the inherently complex nature of ships and the variety of different and unpredictable loads they must withstand. The major causes for structural failure are discussed in the following sections but it must be noted that these causes are not all inclusive; they merely describe the most likely causes based on evidence and an understanding of the properties of shipbuilding materials.

2.3.1 Residual Stresses

Residual stresses in steel are often overlooked because of their "residual" nature. They can exist in a solid elastic body (that includes metals used in ship construction) and are present regardless of external loading. These stresses can be caused during forming, cold working, or welding of the material, or even during simple thermal expansion due to temperature gradients. Studies by the Ship Structures Committee (SSC) show that compressive-like residual stresses can cause reduce buckling loads by a substantial amount if left unchecked (22). Most often, residual stresses are a result of fabrication techniques required in ship construction, namely rolling and welding.

During the rolling of fabrication steels, residual stresses are caused by uneven cooling. In rolling, residual stresses are typically a function of the geometry. In some cases, if left untreated, residual stresses during rolling can reach as high as 80 MPA (23).

Welding is a skill that is developed over time that often takes years and years to master. Welding large steel structures where welding beads are struck for many feet or even yards presents a daunting task to ensure the steel is not modified in a way that could be detrimental to its strength. Like rolling, residual stresses are created in welding from the uneven thermal gradients and their resultant incompatible strains although with slightly different distribution characteristics (23). Generally, these residual stresses can be mitigated with techniques such as rapid quenching or annealing. Shipyards tend to develop their own "best way" to reduce these effects.

Heat Flow and Transient Thermal Stresses

In order to determine where residual stresses come from in thermal scenarios, it is important to examine what actually happens during welding in terms of material distortion. High tensile residual stress can cause serious problems for any welder and can have an extremely adverse effect on the strength of the weld. It is known that incompatible strain generated in and around the welding site is the cause of residual stresses but how these strains are formed is the important part of the analysis. Incompatible strains are the building blocks of residual stress and are the result of heat flow and transient thermal stresses (23).

Understanding heat flow and how it translates into transient thermal stress does not have to be examined within the constraints of a geometrically complex structure such as the hull form of a ship. Instead, presenting a 2-D infinite plate will still yield a simple understanding and provide a stepping stone into transient thermal stresses. The following figure shows the progression of a weldment and its resulting thermally induced residual stress (23)

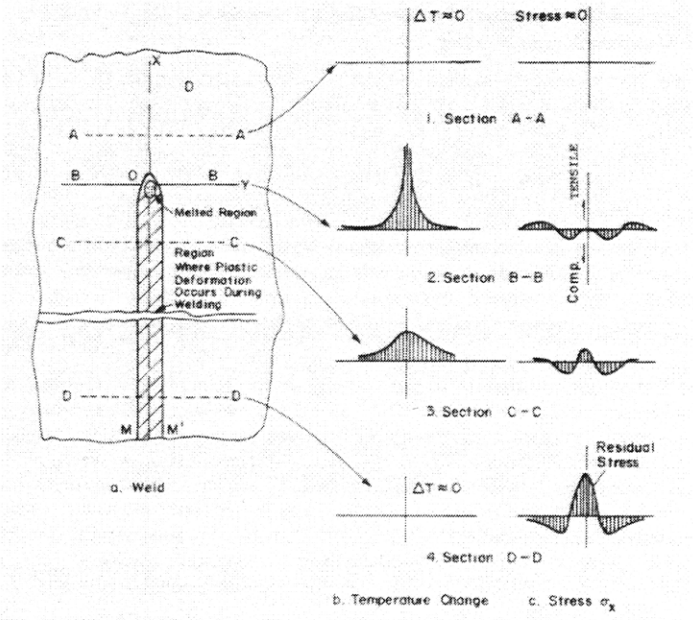

Figure 10: The Progression of Residual Stresses from a typical, unrestrained one-pass weld.

On the most basic level, it is through the solutions to this analysis in the context of the specific material, geometric, and fabrication parameters that the distribution of incompatible strains can be determined. The sum of the area of the compression and tension sections of the calculated stresses in this diagram can all be equated to zero and satisfy the definition of residual stress (23).

Residual Stresses Caused by Welding

Residual stresses that are produced by the process of welding come in two forms: Those that are produced by the welding of two pieces of metal that are unrestrained, and those that are a result of post weld reactions due to prior restraint during welding. Figure 10, seen on the previous page, shows the typical distribution of stresses in the unrestrained, fairly simple, one pass weld.

Estimations of residual stresses in simple plates is best completed by assuming a typical residual stress exists and, in the tension zone next to the weld, the magnitude of the residual stress equals the yield stress. These assumptions allow for the derivation of Equation 10:

$$\sigma_r = \sigma_y \frac{2\eta}{b/t - 2\eta} \qquad [10]$$

In this case, η is the eccentricity ratio which can be calculated from the slenderness parameter of a plate, seen in Reference (5).

While Equation 10 provides a fairly good approximation method for calculating residual stresses in simple plates, this method becomes less accurate as more complex geometries are introduced. If specific weld characteristics are known, the extent of residual stresses present in stiffened panels with normal proportioned stiffeners can be estimated using weld geometry and empirical data:

$$\sigma_r = \frac{c_1 a_w}{bt + A_s} c_2 \qquad [11]$$

In this case, a_w is the cross-sectional area of the weld and the coefficients given by c_1 and c_2 define shrinkage force and stress reduction due to shakedown in the weld, respectively.

Residual stress is easy to understand but incredibly difficult to measure and gauge accordingly. During ship construction, whenever fabrication is necessary, residual stresses tend to be produced. This is especially obvious when one looks at the hull and superstructures of several classes of ships in the U.S. Fleet. This waviness along the shell plating is called the hungry horse look. By themselves, residual stresses do not present a serious issue to the integrity

of a structure. It does become an issue, however, when plates under residual stresses are subjected to large-magnitude compression or tension loading in as in the case of a ship in heavy seas.

2.3.2 Eccentricity: Initial Deflections

In the real world, pure axial loading hardly ever exists and in a mega-structure such as a large ship, it occurs even more rarely. Similarly, initial deflections (which can be caused by eccentricity) or imperfections in plates and columns (caused by welding or forming) can, in essence, cause virtual bending stresses that can be stronger than residual stresses in rare cases.

Hughes (5) uses a variation of Euler column theory to describe the effects of eccentricity. This theory is discussed in detail in Section 3.1.1. When eccentric loading is introduced into a simply supported column, the governing equation adds a term for initial deflection and additional deflection. These terms are given by δ and w and are seen as part of the modified, simplified governing equation, below:

$$\frac{d^2y}{dx^2} = -\frac{P}{EI}(\delta + w) \qquad [12]$$

In this case, P describes the load while EI is the stiffness factor of the column. Solving (12) provides a mathematical solution for the "magnified" deflection using a baseline load if any deflection is present. If P_E describes the ideal Euler buckling load and P is the actual load on the object, the magnification factor is given by:

$$\phi = \frac{P_E}{P_E - 1} \qquad [13]$$

With regards to this magnification factor, Hughes makes two very important points which directly relate to ship integrity issues. The first is that as eccentricity increases, the initial buckling load decreases, though later it will be shown that this does not have an appreciable effect because the decrease usually is small. The second is that the initial magnitude of deflection, whether large or nearly insignificant, has no real bearing on the overall strength of the column as the load approaches the Euler buckling load (5). A graphical representation of this can be seen in Appendix 2.1.

On a ship, hull plating deflections are typically out of plane and can be classified as transverse deflections and longitudinal deflections. While transverse initial deflections are mostly associated with large stiffener welding and have little or no effect on hull strength, longitudinal initial deflections tend to pose a little more noteworthy problem. Still, studies in

which ultimate strength characteristics were examined after accounting for longitudinal wave-like initial deflections showed that for reasonable and typical initial deflections, strength is decreased only just slightly and can be considered negligible. This is shown in a finite element example of plate loading in Chapter 5.

It is clear that initial deflections associated with normal workmanship or construction do not have an appreciable effect on reducing hull strength, but what about the abnormal occurrences during the life of the ship? Some of these might include collision with the pier or another vessel, improper dry-docking or running aground, or even battle damage. In these cases, from the perspective of damage control, there are usually more immediate problems to worry about than the overall buckling strength of the ship as long as collapse strength is not within reach. Due to the relative difficulty of experimental testing on board ships which have experienced any or all of these circumstances, no real unclassified data exists (The U.S. Navy has done extensive live-but-classified testing on the susceptibility of its fleet) (9). To remedy this, several software platforms are available which provide a method to assess bending moment and associated stresses in the case that a structural member becomes compromised, due to a variety of different causes.

2.3.3 Slamming and Vibration Effects

To this point, human-controlled factors contributing to hull strength reduction have been considered. However, the effects of excessive vibration are at best, partially human-controlled. During the design phase, the hull's natural frequency can be estimated and certain forcing frequencies can be avoided within operation, but no real control exists beyond this point. Briefly introduced as a high-frequency dynamic load, the loading and resulting vibratory response caused by slamming is a significant cause for the degradation of the strength of a hull over time.

Slamming

In order for slamming to occur, two requirements are needed. The first is the emergence of the bow and second, the relative velocity (ft/s) of the hull and the wave surface must exceed a threshold given by Equation 14. Here, L is the ship's LBP and the multiplication factor is an empirically derived constant (21).

$$V^* = .53\sqrt{L} \qquad [14]$$

What exactly happens during the slamming phenomena is important in understanding how it can contribute over time to strength reduction for a hull. For simplification, the slamming event can essentially be broken up into three main phases: Phase I occurs while the bow section is out of the water and the flat bottom is approaching the surface, Phase II encompasses the

impact until full wetting occurs, and Phase III brings the ship back to equilibrium. During Phase I, the predominant forces are air flow and wave-air interaction until the moment of impact. Phase II dominant forces are a mix of friction forces as water flow across the body and a cushioning effect. In Phase III, pressures become static and an increasing buoyancy effect is introduced as the ship settles into the water (21).

Defining slamming in these terms simplifies an extremely complex problem. While it does not nearly provide sufficient means to analytically describe slamming in variable seas, it can be effective enough in relative terms of this work. The vibratory response of the slamming phenomenon is felt almost entirely in the first mode of natural vibration. The severity of the response is strongly correlated with the wave's incident wavelength. The closer the wavelength is to the length between perpendiculars (LBP), the larger the vibratory response (21).

Estimating 1st order Natural Vibration Characteristics

The coincidence of the first mode of natural frequency and forced (machinery driven) vibrations, coupled with the magnification of the amplitude of vibration due to slamming effects, warrants calculation of the first mode of natural frequency. This can be used to determine if any resonance may have occurred in either real-world case of structural failure.

Approximating the natural frequency of a ship (two-node vertical frequency) can be completed within fairly narrow limits using a process which requires a great amount of data collection and manipulation. This method is discussed in Reference (24). To circumvent this often long and drawn out process, structural engineers sought a new, empirically based method using experimentation and a ship's general characteristics. Schlick was the first to come up with such a formula, at the end of the 19th century. One-hundred and fifty years later, Liddel improved Schlick's formula which had previously not considered added mass (24). Equation 15 below shows the final result:

$$N_{cycles/min} = \phi \sqrt{\frac{I}{(2 + \frac{B}{3T})\Delta L^3}} \qquad [15]$$

Seen above, main components of Equation 15 include the empirically based constant ϕ which changes based on platform type and the displacement, the mid ship moment of inertia, and length of the ship. More information on different variations of empirical formulas to determine the first mode natural frequency can be seen in References (24) and (25).

Using the correct empirical constant provides a fairly accurate approximation of the first mode of natural frequency. From this result, the second and third modes of natural frequency can be calculated using empirically derived multipliers. These multipliers are seen in Table 1:

Frequency	1st	2nd	3rd
Multiple	1.00	2.22	3.45

Table 2: Higher order natural frequencies as a function of the fundamental frequency (25).

While these vibration characteristics are merely estimations, it is up to the engineers aboard ship to determine if issues with resonance are potentially speeding up the fatigue-induced failure process. Actual vibration characteristics can easily be determined for any ship using an accelerometer and a computer system that can analyze the results.

2.3.4 Corrosion

Corrosion is a hull strength reduction factor that, once it starts, is nearly impossible to control through human factors. In ships that are nearing the end of their service lives, it is such a big cause for concern that many ship salvage programs have a function to allow for corrosion-caused strength degradation. Decreased manning on U.S. Navy and U.S. Coast Guard ships dictates that considering corrosion as a major means of strength degradation is still very crucial. Paint coatings and zinc sacrificial anodes are several ways that ships deal with this problem but the corrosive power of the ocean will never cease to exist.

For corrosion to occur, an anode (which corrodes) and a cathode must be present. Along with these two materials, an electronic path must be present, along with an electrolyte (26). The tendency for corrosion to occur depends on the magnitude of the voltage developed between the anode and the cathode. Salt water is a very strong and tenacious electrolyte but in many cases (obviously not on the outer hull) it can be removed by a simple freshwater wash down (26).

From an engineering perspective, ships should be designed for a worst-case corrosion scenario based on the strength of the measures in place (both active and passive) to combat its progression. This includes the consideration for "stress corrosion cracking." Stress corrosion cracking is essentially cracking that occurs due to tensile stresses coupled with a specific environment prone to corrosion. A ship at sea presents such a situation. In this case, tensile stresses do not even have to exceed the ultimate stress of the particular effected material and outwardly visible corrosion does not have to be present prior to fracture (27). More information on the mechanics of stress corrosion cracking, identification of corrosion prone areas, and corrosion control systems can be seen in References (27) and (26).

Chapter 3: Fundamentals of Plates, Panels, and Hulls

After considering all of the global loadings and factors that reduce ship strength it is important to recognize an imminent shift from the global realm into the local realm. In a worst case scenario, a ship is built so poorly that it fails globally in a violent collapse (such as Euler column failure) where no additional strength is retained as the relative displacement grows larger and larger. Governing bodies in ship design specifications and good design practices in general obviously prevent this global, catastrophic failure from happening, so local failure analysis of the hull is critical. This is accomplished by first looking at buckling and ultimate strength analysis of plates and panels and applying this theory in shipboard applications.

3.1 Buckling Theory of Plates and Panels

Buckling theory of plates and panels starts with an even more basic fundamental approach: Euler column buckling. Globally, a ship can be loosely modeled as a beam or beam-column with time-dependent load and boundary condition changes. Locally, variations of this theory are applied with specific changes in rigidity formulation and boundary conditions to arrive at closed form solutions. The following subsections use the explanation of Euler Column theory to show viable methods for analytically calculating axial loads for simple plates and longitudinally stiffened panels.

3.1.1 Buckling Theory of Euler Columns

Pure-elastic buckling of the Euler column considers both ends to be simply supported, and the edges along the length of the column to be free. Unlike panels which will be discussed later, after column buckling occurs they usually cannot be considered to hold any additional strength (28). The complete derivation on which the abbreviated derivation (seen below) is based can be seen in any mechanics text. The governing equation for this type of "perfect" column buckling is given by the Euler differential equation with a line load (q) equal to 0:

$$EI\frac{d^4w}{dx^4} - P\frac{d^2w}{dx^2} = q = 0 \qquad [16]$$

In this case, P equals the buckling load and EI is the rigidity constant given by Young's Modulus and the moment of inertia. Figure 11 on the following page shows a visual image of the column with simply supported end conditions:

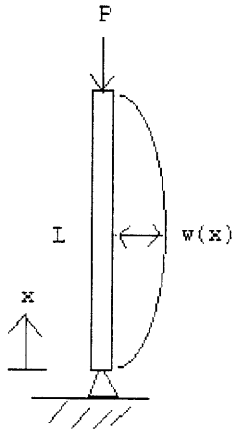

Figure 11: Column buckling through local Equilibrium. The lowest Eigen-value of the governing equation defines the critical buckling load.

A variation of this equation that includes consideration for eccentricity is seen as Equation 12 in Chapter 2. The buckling load is considered to be positive and appropriate simply supported boundary conditions are applied as follows:

$$w(0) = w(l) = 0 \quad [17]$$

$$\frac{d^2w}{dx^2}(0) = \frac{d^2w}{dx^2}(l) = 0 \quad [18]$$

Applying boundary conditions to Equation 16 and dividing through by *EI* yields the modified governing equation:

$$\frac{d^2w}{dx^2} + \frac{Pw}{EI} = 0 \quad [19]$$

The general solution to Equation 19 can then be written as follows with consideration for the simply supported boundary conditions:

$$w = C_1 sinkx,\ k = \sqrt{\frac{P}{IE}} \quad [20]$$

Using this solution, the family of solutions that will satisfy Equation 19 is found when $kl = n\pi$. The lowest form of this solution gives the Euler column buckling load:

$$P_E = \frac{\pi^2 EI}{l^2} \quad [21]$$

Higher order solutions and solutions with variable end boundary conditions are derived by simply using different integer values for *n* and different values for *l*.

The preceding abbreviated derivation of the Euler buckling load assumes that purely elastic, "collapse" buckling occurs. There is a point, however, when the geometric dimensions of the column are such that yield occurs prior to global buckling. This can be determined by equating the material-dependent yield stress to the buckling stress and determining the threshold slenderness ratio (ß) needed for elastic buckling to occur. This is seen mathematically below, but note ß of the Euler column is not the same as the slenderness ratio parameter for an ideal plate:

$$\sigma_y = \sigma_{cr} = \frac{\pi^2 E}{\beta_{cr}{}^2}, and\ \beta_{cr} = \pi\sqrt{\frac{E}{\sigma_y}} \quad [22]$$

Using appropriate material properties for mild steel (further discussed in Chapter 5) ß equals 85.5. Using the radius of gyration, it can be determined that an ideal column will yield rather than buckle for any rectangular shape whose overall length is less than $23.9 \times h$. This derivation can be seen in Reference (29). This relationship becomes important when determining the appropriate method for analytically approximating longitudinally stiffened panels under longitudinal uniform axial load.

3.1.2 Buckling Theory of Plates

The mathematical gap between the elastic buckling of columns and the buckling of plates can be bridged by considering a plate which behaves like a wide column. In this case, the boundary conditions remain the same and the plate buckles in mode I, or overall mode. The only difference is that the rigidity of the column is now removed and replaced by plate flexural rigidity (5). The formula for wide column buckling is seen below:

$$P_{cr} = \frac{\pi^2 D b}{a^2} \quad [23]$$

Where D is the flexural rigidity, a is the length of the unloaded edge and b is the length of the loaded edge. D is given by Equation 24:

$$D = \frac{Eh^3}{12(1-v^2)} \quad [24]$$

In this case, flexural rigidity of a plate considers Young's Modulus, plate thickness, Poisson's ratio and a multiplier. In the case of Equation 23 with regards to plate strength, it is quite inefficient to use a simple plate in the same manner as a wide column with Euler boundary conditions. A plate with stiffeners or supported edges however, is much more practical and is able to carry much more axial load.

Simply Supported Plate Buckling

There exists a closed form solution for the buckling of a rectangular plate *(a x b)* with simply, simply supported boundary conditions and a uniformly distributed load, P_x, along each applicable edge at x = [*0, a*]. A diagram of a simply, simply supported plate can be seen in Appendix 3.1 and is also reproduced in Chapter 5. The governing equation for plate buckling given this prescribed load can therefore be written as follows (30).

$$D\nabla^4 w + \frac{P_x}{b}\frac{d^2w}{dx^2} = 0 \quad [25]$$

Equation 25 accounts for all directions of the load tensor under the given boundary conditions. More explanation of how this general governing solution was obtained can be seen in Reference (30). The boundary conditions for the simply, simply supported plate can be written as:

$$w = 0 \; for \; \Gamma \quad [26]$$

$$M_{nn} = 0 \; for \; \Gamma \quad [27]$$

Given these simply, simply supported boundary conditions, a solution can be written for *w* as:

$$w = C_1 \sin\left(\frac{m\pi x}{a}\right) sin\left(\frac{n\pi x}{b}\right) \; for \; m, n = 1,2 \quad [28]$$

Substituting Equation 28 into the governing equation and simplifying, assuming the critical load will be determined when *n=1* for all *a* (based on Eigen-Value buckling) gives:

$$\frac{P_x}{b} = \frac{\pi^2 D}{b^2}\left(\frac{mb}{a} + \frac{a}{mb}\right)^2 \quad [29]$$

Cancelling like-variables and substituting the squared term for a single variable presents the widely accepted analytical equation for critical buckling load. Here, *m* is indicative of the buckling wavelength.

$$k_c = \left(\frac{mb}{a} + \frac{a}{mb}\right)^2 \quad [30]$$

$$P_{cr} = k_c \frac{\pi^2 D}{b} \quad [31]$$

In a simply, simply supported boundary condition, k_c may be found analytically by first determining the appropriate wavelength parameter and then applying the geometrical parameters of the plate. A diagram of a simple plate buckling event with simply, simply supported boundary conditions and a wavelength parameter of three can be seen in Appendix 3.1. Wavelength parameter transitions occur when corresponding m and $m+1$ curves have equal ordinates, and m can be determined simply from the relationship of a/b. This is shown in the k_c versus a/b diagram, seen in Appendix 3.2 (30).

It should be noted the relationship between a/b and m only really lasts through the fourth wavelength parameter, that is a/b ≤ 4. If a continues to increase without an increase in b, the plate is considered a *very long plate* and tends to buckle in half waves whose relative lengths are approximately the width of the plate (30).

Other Boundary Condition Considerations

For a given simple plate with boundary conditions other than Euler or simply, simply supported, a closed form finite analytical solution cannot be obtained. Plates that exhibit clamped boundary conditions, or variations thereof, fall into this group. Numerical solutions have been obtained for each respective set of boundary conditions by employing the Raleigh-Ritz method and a method employing infinite series (5). In order to analytically determine buckling loads with these boundary conditions, a widely used graphical method is used which employs these numerical solutions. This is seen on the following page as Figure 12 and is reproduced from Hughes's (5) figure 12.5a.

Along with the depiction of numerical solutions to variations of simply supported and clamped boundary conditions, the simply, simply supported curve and Euler curve is also seen in this figure for continuity. The same equation is employed for P_{cr} as for the closed form solution obtainable with simply, simply supported boundary conditions. All of the simple plate (and some stiffened panel, as will be discussed later) analytical calculations employing other-than simply, simply supported boundary condition were completed using graphical data from this figure.

In addition to the development of Figure 12, others have investigated the effect of intermediate boundary conditions that are variably in between simply, simply supported and clamped (5). While these intermediate-type boundary conditions were not explored analytically in this study, a particular variation (noted later in Chapter 5) was used for Finite Element Modeling which best mimicked the boundary conditions that might be seen on a ship's side shell.

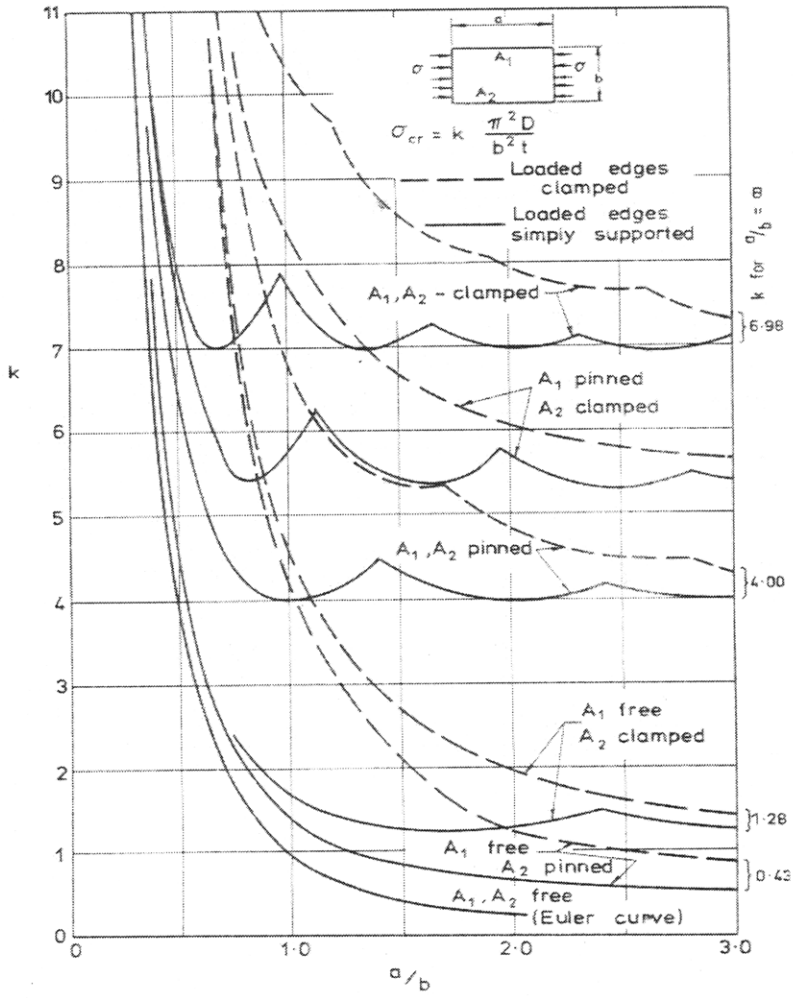

Figure 12: This chart graphically shows the numerical solutions for k_c in the plate buckling equation. This figure is reproduced from figure 12.5a in Reference (5).

A curve similar to Figure 12 which shows numerical solutions for intermediate boundary conditions can be seen in Appendix 3.3.

Plate Design Considerations

While there is no specific point where design-type calculations are completed in this text, the effect of increasing actual (or equivalent, created by doublers) plate thickness quickly becomes understood when buckling and ultimate load data is presented. In design of simple (long) plates, usually a required buckling stress is given over a given $l \times w$ geometry and thickness is varied to satisfy stress. Assuming worst case simply, simply supported boundary condition ($k_c = 4$) and a Poisson's ratio of 0.3, a quick calculation of a required thickness for a given σ_{cr} then can be written as:

$$\sigma_{cr} = 3.62E\left(\frac{h}{b}\right)^2 \quad [32]$$

Here, h is equal to plate thickness. Although Equation 32 can be useful in the design of simple structures and is obviously a threshold that shouldn't be crossed, exceptionally stiff plates and panels tend to yield prior to buckling and therefore render the actual buckling point inconsequential. Consequently, in limit state design, the ultimate load of a structure is often more interesting because it defines the point (similar to the collapse point in a column) where the structure simply cannot carry any more load (5).

3.1.3 Buckling Theory of Stiffened Panels

While closed form solutions for simple plate theory tend to exist for simple boundary condition scenarios and all fail in generally the same manner, analytical modeling of the buckling of stiffened panels greatly depends on the mode of failure. The mode of failure, in turn, greatly depends on material conditions and geometry. As such, prior to discussing analytical approaches to calculating approximations for failure, each possible failure mode is briefly discussed.

Failure Modes

Failure modes can be generally broken up into two categories: overall panel failure and local failure. While overall failure generally occurs when stiffeners are small or weak, local failure develops when plate stiffeners are strong and subsequently the plating between the stiffeners fail. Very rarely in the design of stiffened paneled structures (such as a ship) will one see overall panel buckling, because it is indicative of large scale instability in the overall structure. A more likely scenario is the development of local buckling of the intermediate plates followed closely by stiffener tripping. A stiffened panel has five types of buckling modes (31). They are as follows:

- Mode I: Overall collapse of the plate-stiffener combination as one.
- Mode II: Collapse due to mostly transverse compression (not considered in this study).
- Mode III: Beam-Column type collapse by yield at mid-span.
- Mode IV: Buckling of the stiffener web.
- Mode V: Collapse caused by tripping of the stiffener

These modes are not necessarily independent of one another or mutually exclusive events. In some cases, progressive collapse indicates several local failure modes which can occur nearly simultaneously. An additional mode, Mode VI, indicates a gross yield where neither overall nor

local buckling occurs (usually reserved for relatively stocky plates). In stiffened panel design, it has been found useful to separate each mode of failure and develop an independent strength analysis of each for comparison (32). Each mode is seen below, as well as additional applicable information related to each failure mode. The figures are reproduced from Reference (28).

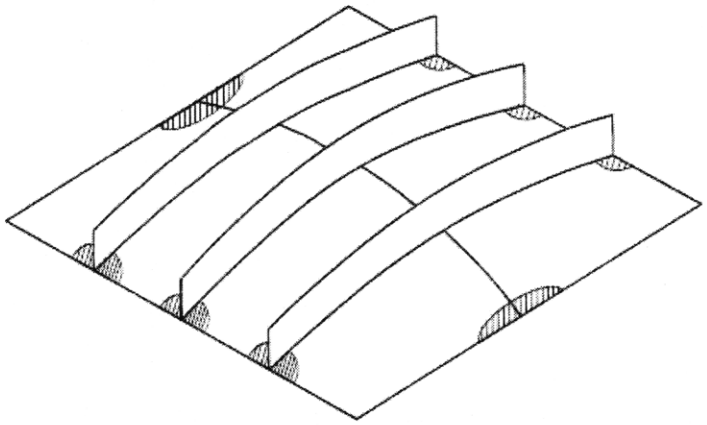

Figure 13: Mode I: Overall panel failure

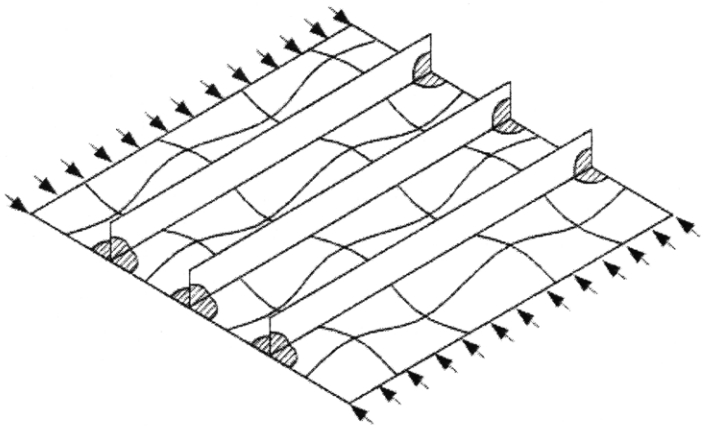

Figure 14: Mode II: Failure due to mostly transverse loading

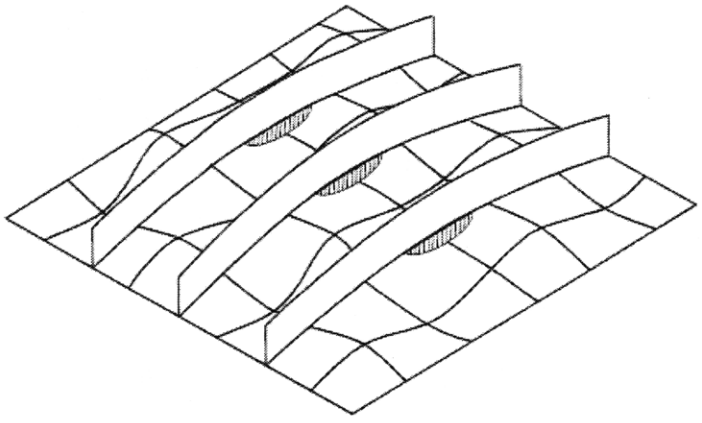

Figure 15: Mode III: Failure due to yielding at mid-span.

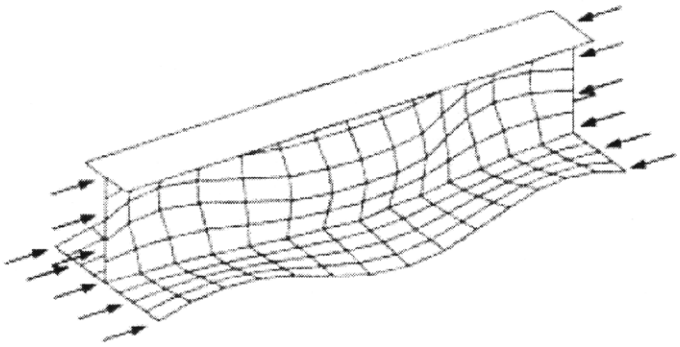

Figure 16: Mode IV: Failure due to local buckling of the stiffener web.

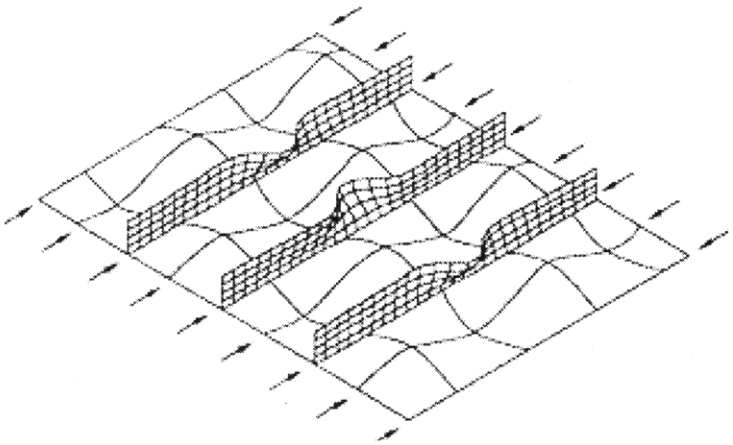

Figure 17: Mode V: Failure due to stiffener web tripping.

Mode I failure is self explanatory and generally does not occur first (as previously stated) in plate stiffener combinations that are designed parts of steel structures. Of all the modes, Mode III seems to be the most interesting in terms of ship structural design. In fact, Mode I collapse is often initiated by this type of failure. Mode III failure generally occurs when stiffeners are of intermediate strength. Mode IV and V failure generally occurs first if stiffeners are inadequately designed for the given load and have a large web height-to-thickness ratio (28). Mode VI generally takes place when the panel is very stocky (i.e. the slenderness ratio is very small) or it is subjected to tensile loads.

Methods of Analysis

Two different methods of analytically approximating stiffened panels were used in this study. Each assumes a different mode of failure. Results based on this stiffened panel analysis and their comparison to finite element methods are shown and discussed in Chapter 5.

The worst case failure mode for a stiffened panel is by far Mode I failure. As mentioned previously, Mode I failure leads to serious overall instability of the structure and therefore was accounted for in this study. Paik et al. (28) and Hughes (5) both agree that the behavior of an

ideal stiffened panel in overall buckling can be approximated using ideal Euler column theory, as each plate stiffener combination essentially acts as an independent column. Ideal Euler column theory is discussed in Section 3.1.1. The applicable column cross section becomes the area of the stiffer and a to-be-determined effective width of the plating on either side of the stiffener, usually referred to as the "effective width" (28). A diagram reproduced from reference (28), showing the applicable cross section (modified to show the section geometry seen in this study), can be seen below as Figure 18:

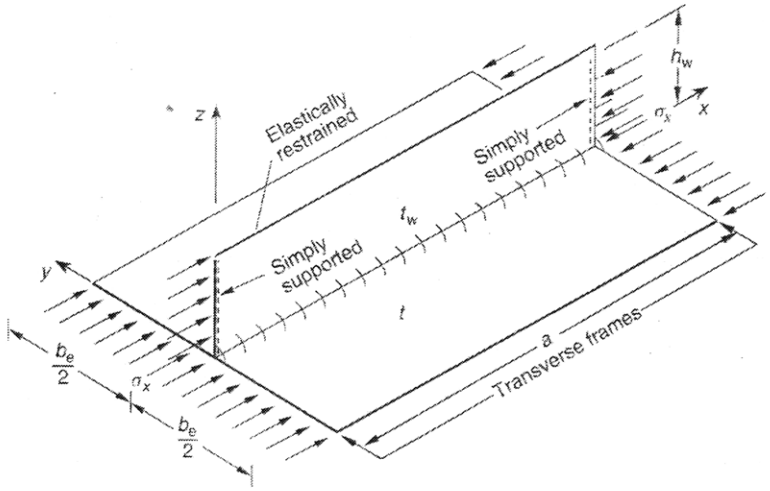

Figure 18: Plate-Stiffener Combination. In overall (Mode I) buckling, this combination is modeled as a Euler Column.

Because the plate-stiffener combination can be modeled as a type of Euler column, the boundary conditions of the unloaded sides are inconsequential because of the relative magnitude of the buckling load under these conditions. This is further validated by calculations which will be seen as part of Chapter 5.

The other method of analysis is based on the Von Karman method. Von Karman is best known for his work relating post buckling to ultimate load using a prescribed effective width. This method will be described in the next section. His method of stiffened panel analysis assumes that failure will initiate from local plate buckling between each stiffener, and simplifies the beam-column method, which is another, more in depth technique of modeling Mode III failure.

This method allows for independent calculation of the buckling load using Equation 31 for each individual sub-panel between each stiffener (30). In his analysis, Von Karman assumed a worst case simply, simply supported boundary condition. The distance between each stiffener is assumed to be *s*.

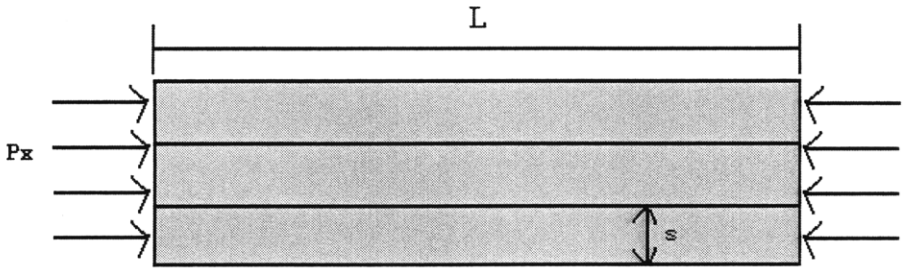

Figure 19: Simply, Simply supported panel with two equidistant stiffeners Von Karman used for his analysis (30).

Since the stiffener spacing is equidistant and the boundary conditions are simply supported, the buckling load per unit length can be written as:

$$(N_x)_{cr} = \frac{4\pi^2 D}{s^2}$$

[33]

Multiplying through by the entire width of the plate ($b = 3s$), the critical buckling load is then written as:

$$P_{cr} = \frac{12\pi^2 D}{s}$$

[34]

A variation of Von Karman's approach can be shown by supposing s is not uniform across the whole panel or different boundary conditions exist (prompting k_c to be different), Equation 34 can then be written as a summation:

$$(P_{cr})_{tot} = \frac{k_{c1}\pi^2 D}{s_1} + \frac{k_{c2}\pi^2 D}{s_2} + \frac{k_{c3}\pi^2 D}{s_3}$$

[35]

It should be noted that in this scenario, the stiffeners act as simply supported boundary conditions but the coefficient is not necessarily $k_c = 4$, it still depends on the wavelength parameter and the new geometry of the subpanel.

3.2 Ultimate Strength Theory of Plates and Panels

In pre-buckling of a plate, the curve of the load to displacement is directly related to Young's Modulus given by Hooke's law, the cross sectional area of the loaded edge, and plate geometry. The slope of this linear line can be defined by some variable "K". Unlike columns which can carry no more strength, plates and panels often can tolerate a subsequent load during the strain hardening phase, as the structure continues to deform with a slope "K/2" until ultimate load is reached. Collapse follows. Due to imperfections, residual stresses, initial deformation, and sometimes first yield, in actual applications there is never a hard "knuckle" where the critical buckling load is reached, rendering the exact buckling load value inconsequential. For this

reason, a dotted line has been drawn in showing the actual path of the curve of the plate. This is shown in Figure 20 below:

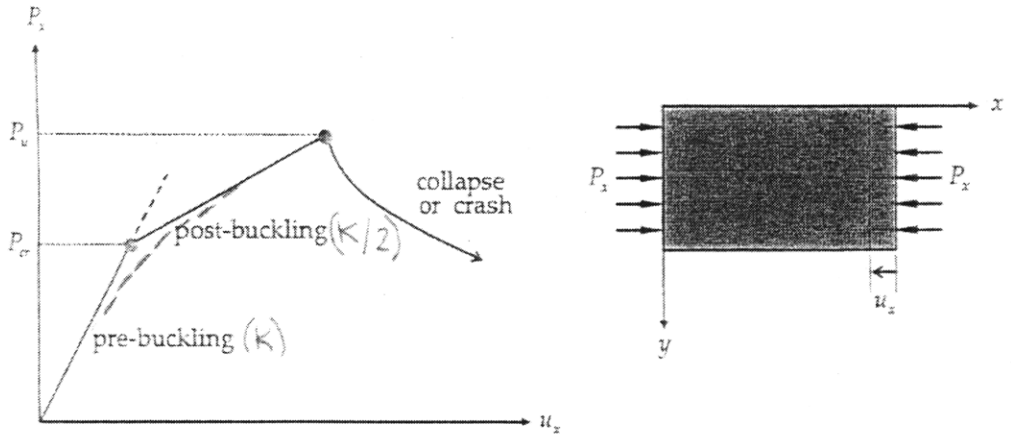

Figure 20: Load Displacement Diagram of Pre- and Post-Buckling through ultimate load. This figure is reproduced from (30).

As computer technology has advanced, determination of the elastic-plastic load-displacement curve of a structure along with its exact ultimate load is now possible through finite element modeling (FEM) whereas before, inexact experimental tests and analytical approximations were the only methods available.

There have been many theories put forth over the last 100 years as to the behavior of plates and panels during post buckling which then are applied to analytically determine ultimate load. Some assume that buckling takes place before first yield, while some assume the opposite. In some structures, yield takes place very nearly when buckling occurs. One of the widely accepted methods of analytically calculating ultimate loads of plates is based upon Von Karman's effective width theory and then modified by the author for subsequent application to panels.

Von Karman Theory of Effective Width

The theory of effective width rests upon relationships between normalized critical buckling stress, ultimate stress, and geometrical parameters with respect to material-dependent yield stress. It operates on the premise that along b in post-buckling, all of the axial stress of a given plate is re-distributed to a smaller width parameter, defined by b_{eff}, with a greater proportion of the load taken by the edge areas, each with a length of $b_{eff}/2$. Von Karman assumed the center area to be stress free (30).

To normalize the buckling stress, Von Karman again assumes a worst-case simply, simply supported plate. The buckling load is then given by Equation 30, substituting 4 for k_c. The corresponding buckling stress then becomes (when D is written out):

$$\sigma_{cr} = \frac{\pi^2 E}{3(1-v^2)}\left(\frac{h}{b}\right)^2$$

[36]

Normalizing by the yield stress and multiplying the constants through assuming Poisson's ratio to be 0.3, Equation 36 becomes:

$$\frac{\sigma_{cr}}{\sigma_y} = \left(\frac{1.9}{\beta}\right)^2$$

[37]

$$\beta = \sqrt{\frac{\sigma_y}{E}}\frac{b}{h}$$

[38]

Here, ß defines the slenderness ratio of the panel that is used in part to determine the mode of buckling of the panels within this study.

Once ß is calculated, an arbitrary $b_{effective}$ variable is substituted for the original *b* and a b_{eff} is solved assuming the edge zones of the plate are at yield during bucking, allowing $\frac{\sigma_{cr}}{\sigma_y} = 1$.

$$b_{eff} = 1.9h\sqrt{\frac{E}{\sigma_y}}$$

[39]

Assuming that b_{eff} carries the entire load until ultimate load is reached; the total average ultimate stress can then be written as:

$$\sigma_u = \frac{P}{bh} = \sigma_y A$$

[40]

$$A = b_{eff}h$$

[41]

Using Equation 40, the ultimate stress can be normalized by the yield stress, by dividing both sides by σ_y. Simplifying and re-applying Equation 38, results in the following relationship:

$$\frac{\sigma_u}{\sigma_y} = \frac{1.9}{\beta}$$

[42]

Using the function established by Equation 40, it is possible to modify Von Karman's formula for *A* (Equation 41) to include stiffener area by smearing it into *h*. Alternatively, the Von Karman modified ultimate load for a stiffened panel with two web-only stiffeners can be written as:

$$P_{ult} = \sigma_y 2\Big(\big(b_{eff}h\big) + \big(h_w t_w\big)\Big)$$

[43]

In order to determine under which realm failure occurs, it is useful to compare the spectrum of ultimate and buckling load solutions across a large range of slenderness ratios (ß). In Von Karman's case, this comparison is seen below:

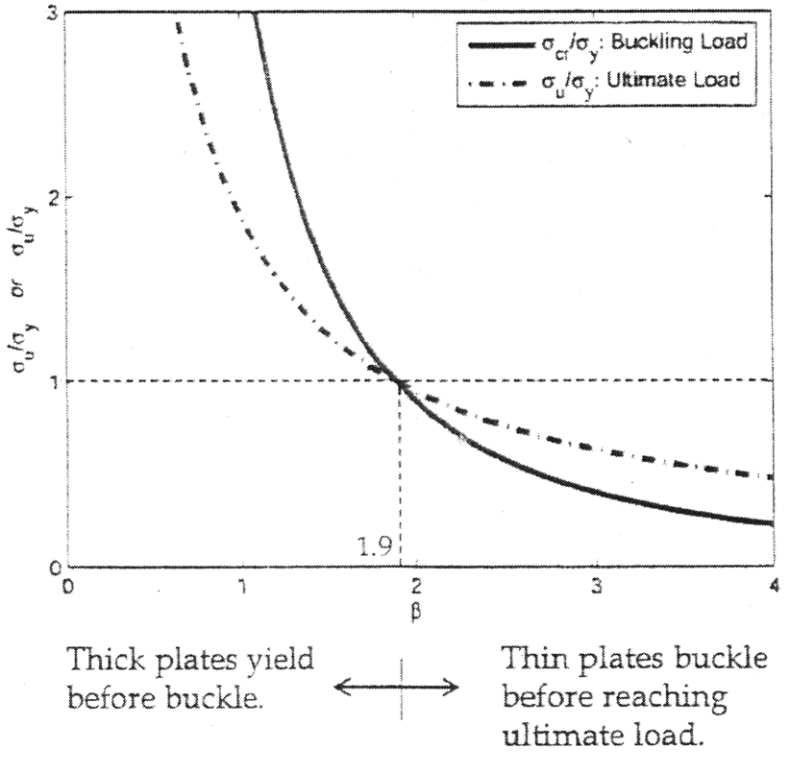

Figure 21: Comparison of Critical Buckling and Ultimate Stress Normalized by Yield Stress reproduced from (30).

In Von Karman's version of the figure above, the slenderness ratio where the transition mode-of-failure occurs is 1.9. This is the solution to Equations 37 and 42 assuming unity for each normalized ratio. For the simple plate buckling on which Von Karman worked, Figure 21 above accurately quantifies the buckling and ultimate loads based on his approximation. When these results are extrapolated to be used for more complex geometric shapes such as panels, the graph presents more qualitative analysis. This shows under which circumstances the panel will fail and can ultimately help predict the failure mode for subsequent analysis under different theory.

3.3 Fracture Mechanics Theory

Although fracture of ductile steel is a very real concern in the ultimate limit state design of a complex steel structure such as a ship, it is not a predominate subject within this study. Regardless, the result of fracture due to excessive fatigue, buckling, or extreme loads can play an

important part in the progressive structural failure of a ship. Therefore, some discussion of fracture mechanics and its shipboard applications must be included.

3.3.1 Fracture Fundamentals of Ductile Steel

Fracture of ductile steel generally falls into one of two groups. Fracture is either caused by a geometric non-linearity associated with buckling and large deflection, or a material non-linearity due to yielding or plastic deformation. Fatigue fracture, buckling induced fracture, and extreme loading fracture all fit into this category. Ductile materials in fracture generally show slow, steady crack growth with a large amount of plastic deformation. In all, this type of fracture spans four regimes once a crack tip forms:

- Blunting of the Initial Crack Tip
- Initial Crack Growth
- Stable Crack Growth
- Unstable Crack Propagation

If the last regime is left untouched, catastrophic failure has the potential to occur (28).

Fatigue induced fractures form cracks that are usually the result of imperfections in usual stress concentration areas of a structure. These cracks develop over time due to repeated cyclic loading. These cracks however, are not necessarily indicative that there was a failure in preliminary design strength calculations of a particular structure. It merely means the structure may be coming to the end of its service life. With careful observation, these cracks can be repaired with no significant degradation of structural integrity. However if the cracks are left untouched and the structure is then subjected to extreme loading, catastrophic failure could potentially occur (28). Buckling induced fracture causes cracks to form after buckling occurs. In steel plated structures, fracture usually occurs after ultimate load where no more strength is retained. Fracture due to large scale loading is the extreme end of fracture due to buckling (and usually yielding that either precedes or follows buckling). In extreme loading scenarios, large-scale fracture can signify the onset of catastrophic failure if cracks propagate out of control (28).

3.3.2 Shipboard Applications

To determine the effects of fracture on steel structures such as in shipboard applications, Paik et al. (28) suggests it is usually more appropriate to assess the residual strength of the structure, taking into account cracks that have already formed over time. Discussion continues to cover the different types of fracture associated with cracks and note that ductile fracture is essentially an intermediary between brittle fracture (seen in the Liberty Ship debacle) and rupture. As noted earlier, most often these cracks are a result of either a typical stress

concentration developed over time due to cyclic fatigue loading or a weakness in structural strength resulting in buckling induced cracks.

On a ship (and in general), three methods for cracking exist. These are opening, sliding, and tearing. To analyze fracture mechanics, several basic methods have been introduced, including the energy method and the stress intensity method. Both operate on the premise that fracture will occur if the energy or intensity level of the given specimen surpasses a critical level defined by mathematical formulation (28).

In terms of this study, the reduction in tensile strength of a stiffened panel due to an existing, non-propagating crack of certain location and size is of particular interest. While mathematical formulation of this concept can be seen later in Chapter 5, it is important to realize that cracking in strength members causes static and dynamic loads to be re-distributed within other strength members. This may in turn cause unsafe stress levels in the structure causing full scale hull girder failure.

3.4 Hull Girder Failure Fundamentals

The overall, catastrophic failure of the hull girder is not a likely scenario given the design standards and the quality of steel production and welding techniques available to the ship building market today. Later in this study it will be well established that even after elastic-plastic (local) buckling of stiffened hull plating, the structure is still able to carry additional load before ultimate load and fracture. Still, this kind of overall, disastrous failure has been known to occur in rare circumstances. Sometimes, human error is a significant factor in the cause if ships (cargo) are improperly loaded in port. Other times, it is a result of progressive collapse behavior after a single strength member experienced a load larger than that for which it was designed (28).

3.4.1 Progressive Collapse Behavior of Ships

The progressive collapse behavior of ships rests upon the theory that shipboard loading is of a magnitude that surpasses the design load. In compression, this will lead to buckling and/or yielding. If the ship is subjected to further loads, the most effected member will then collapse or even offer negative strength characteristics as the load is then re-distributed throughout the hull girder. Buckling of more strength members will continue until the ultimate strength of the hull girder is reached (28).

After the initial buckling event of a hull, it is obvious that some quantity of its original design strength is lost (of course, this depends on the severity of the buckling). Qualitatively, strength loss can be modeled through the use of a partially effective section that is modified to

describe the portions of the cross section that have been affected by the event. For buckling scenarios caused by collision or grounding events, the effective section is more difficult to model and usually computer aided calculators are employed. More information on partially effective sections and the involvement of the classification societies in such events can be seen in Reference (28).

3.4.2 Assessment of Structural Safety

The preceding sections of this Chapter have explored the engineering theory of local and global failure of a ship's hull at many different levels. In assessing the structural safety of a ship, (or any structure for that matter), it is first important to decide the threshold of the acceptable probability of failure. Whether this is determined by moral or economical methods, history and statistical theory has provided a standard probability of 1% that a once-in-a-lifetime wave encounter will create a scenario where a ship is loaded beyond its means. Assuming a ship encounters a certain (extremely large) number of wave encounters throughout its designed lifecycle, this 1% chance extrapolates to a one chance in about 10 million (17).

Governing bodies assess structural safety through a statistical comparative method, but it is still very much an inexact science. As discussed in Chapter 2, there is no accurate way to quantify all of the structural imperfections, deflections, corrosion, and residual stresses present at any given time on any given ship. Therefore, governing bodies usually accomplish this task by building probability density functions using Raleigh or Gaussian methods and applying a certain platform- and mission-dependent safety factor (17). Whatever the method for accomplishing this task, the goal is the same: Construct a ship which will keep both the structure and the crew safe throughout its lifetime. Chapter 4 discusses and analyzes two cases where this goal was not sufficiently met.

This Page Intentionally Left Blank

Chapter 4: Application and Global Analysis

After a shipboard accident or series of accidents, determining "why" is usually the greatest single question. This question often needs to be answered to place blame for further litigation and in some scenarios, so that the event can be avoided in the future. There is another reason, however, that is often overlooked. Academias, particularly research institutions, use experimental methods to try and reproduce actual events to not try and find out why the event occurred, but to understand how failure occurred. These institutions cherish the opportunity to learn from discovering these answers, which are are then passed on to those who might design ships in the future.

While the preceding chapters of this thesis focus on the theory behind ship structural design, modes of failure, and what occurs when excessive loading is present, this chapter creates a connection between real world examples of ship failure and academic research. It serves as the basis for an understanding of the methods used to determine local strength and failure characteristics of plates and panels as it applies to naval patrol craft. This is best completed by presenting a broad spectrum, engineering analysis of failure, along with a history and basic structural data from each platform.

4.1 Platform Backgrounds

The two ships that are examined in this study are the United States Coast Guard 123' (110') Island Class cutter and the U.S. Navy/ U.S. Coast Guard 179' (170') WPC Tornado Class Patrol Craft. Each vessel is different in its own right but they share some unique characteristics and ultimately provide a valuable and unique form of comparison when it comes to structural integrity of naval vessels.

4.1.1 United States Coast Guard Cutter Patrol Boat (WPB) 110'/123'

The U.S. Coast Guard 123' Island Class Cutter was originally born more than 20 years ago as the Coast Guard's new patrol boat workhorse to replace an aging 82' and 95' patrol fleet. After various setbacks in the contract award due to "irregularities in the procurement process", the contracts for all 49 of the existing patrol boats were awarded to Bollinger Shipyards in Lockport, Louisiana (33). Based on a trusted and extremely successful original British design, the 110's were valued at approximately $7 Million each and were commissioned between 1985 and 1992. Missions of the 110' include:

- Maritime Interdiction Operations
- Search and Rescue

- Port Security
- Fisheries Law Enforcement
- Defense Readiness

Of the 49 original cutters, 41 are still in service across the United States and overseas in the Persian Gulf. The remaining eight (now de-active) were transformed into the upgraded 123' (34).

The birth of the 123' was a formulation grounded in the U.S. Coast Guard's Deepwater Program. This name refers to more than a dozen projects in Coast Guard acquisitions ranging from short small boats, to unmanned aerial vehicles, to the largest U.S. Coast Guard cutters ever built. Until 2007, this entire entity was run by a single, multi-faceted acquisition program under the name Integrated Deepwater Systems (33). Figure 22, seen below shows the various acquisition programs involved in Deepwater:

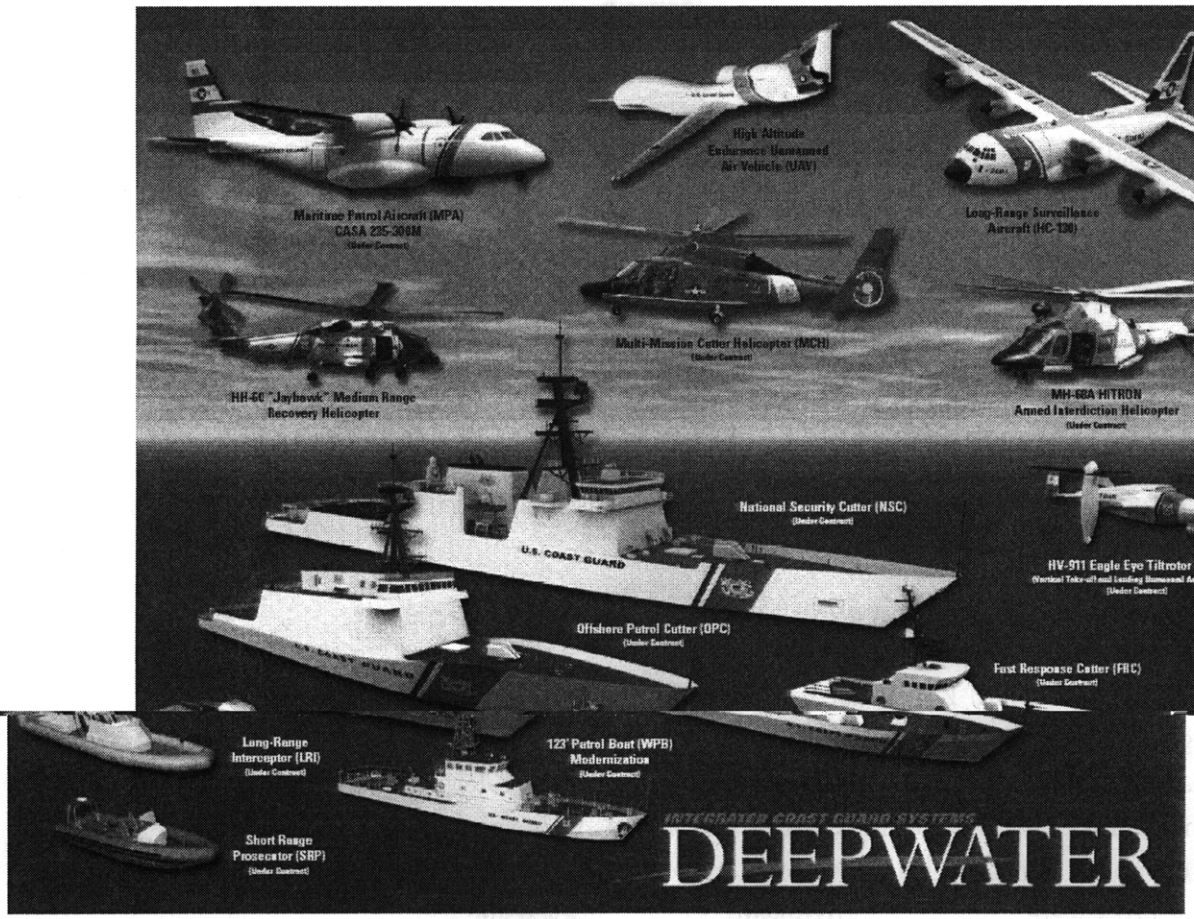

Figure 22: U.S. Coast Guard's Deepwater Assets (34).

One of the first projects to be undertaken as part of the deepwater project was the 110'-123' conversion program. The premise of the acquisition was to upgrade and refurbish the hulls of the existing 110' and extend the service life another 15 years. This program was centered on

three main areas of upgrade, namely the extension of the stern to include a stern launch and recovery system for the Coast Guard's short-range prosecutor, an upgraded communications suite, and a new superstructure with updated bridge views and habitability. A diagram detailing all the upgraded capabilities of the 123' can be seen as part of Appendix 4.1. In addition, it was thought that the hull would have upgraded seakeeping characteristics with the addition of 13' (35). The conversion process began in 2002, with plans to upgrade all 49 cutters. The principle characteristics of the 123' are as follows, seen below in Table 2.

WPB 123' Characteristics		
Length	123' (orig. 110')	ft
Beam	21	ft
Draft	7.3	ft
Block Coeff (C_b)	0.508	
Displacement (FL)	175	LT
Speed	28	Knots
Propulsion	2X 3,325 Paxman	HP
Propulsors	2X5 Bladed	Prop
Endurance	3200	NM
Crew	16	ppl
Armament	MK 38 25mm Cannon, 2X.50 Caliber Guns	

Table 2: 123' General Characteristics (33) (36).

During sea trials of the first upgraded 123' (Matagorda), mid ship failure occurred where stress levels exceeded yield levels of the structural steel used in construction (35). This prompted a structural upgrade of all 8 cutters, either completed or under construction, to include several longitudinal doubler straps (seen in (37), the 123'midship section drawing) to increase the overall section modulus of the cutter in an effort to curb any further damage from occurring.

Figure 23: The 5' stern section of the Matagorda at the shipyards in Lockport, LA soon after it was cut as part of the upgrade.

After other major structural issues (to be discussed in detail in the next sections) were noted on additional cutters, the operating profile was restricted based on crew safety concerns.

The decision was made in June 2005 for the Coast Guard to stop the conversion process at 8 cutters. After noting increased plastic deformation on the majority of the hulls, regardless of the limited operating profiles and numerous measures to increase structural strength, Commandant Admiral Thad Allen suspended all 123' operations effective November 30th, 2006 (13).

After 2007, amidst continuous criticism from outside sources and both houses of Congress who instituted various oversight legislatures, the Deepwater Program split its various acquisition programs into independent entities with the Coast Guard as the chief integrator. This split came on the heels of the decision to deactivate the fleet of eight 123' for reasons discussed later in this chapter. On April 18th 2007, a report was released that the Justice Department was conducting an investigation into the Deepwater Program and specifically focusing on (among other things) the 110' to 123' conversion project issues. As of this publication, the results of this investigation have not yet been made public and the Department of Justice has asked both Integrated Deepwater Systems (IDS) and the U.S. Coast Guard to retain documentation pertaining to the program (13).

4.1.2 United States Navy Patrol Craft (PC) 170'/179'

The 179' was originally designed as a replacement for the 65ft MK III patrol boat in use by U.S. Navy Special Forces Command. They were originally designed to be classified as a "boat" in Navy terms but later classified as a ship. Bollinger Shipyard in Lockport, LA, was awarded the contract to begin work on the ships in 1990. Originally built as a 170' Patrol, Coastal (PC), the ship was based on the Vosper Thorneycroft patrol boat design, a ship that complied with ABS rules at the time of original design. The original contract with the United States Navy was built for and funded by the U.S. Special Forces Command. Initially, the Bollinger contract called for eight ships to be built, but a contract was quickly completed in 1991, guaranteeing an additional five ships. A final ship was placed under contract in 1997 for a total of 14 ships (19).

Commissioned between 1993 and 2000 as the Cyclone class, the PC's fulfilled their planned missions. These included but were not limited to:

- Maritime interdiction operations
- Escort operations
- Noncombatant evacuation
- Foreign internal defense
- Tactical swimmer operations
- Reconnaissance & intelligence collection

The principle characteristics of the ship are as follows, seen below in Table 3.

WPC 170'/179' Characteristics		
Length	170/179	ft
Beam	25	ft
Draft	5.8, 8.5 Nav.	ft
Block Coeff (C_b)	0.4	
Displacement (FL)	380/410	LT
Speed	35	Knots
Propulsion	4X3600 Paxman	HP
Propulsors	4 X 6 Bladed	Prop
Endurance	2000	NM
Crew	26	
Armament	2XMK 38 25mm Cannon, 6X.50 Cal Guns	

Table 3: 170' (179') General Characteristics (19) (38).

Due to their role in U.S. special operations, the maneuverability and speed characteristics of the vessel were unprecedented for its time. Operational capabilities included reaching flank speed in less than 180 seconds and decelerating and moving to full astern in an additional 60 seconds (19).

In 2002, the Navy designated the ships for regular U.S. Naval service, effectively ending their tour as special operations ships. Shortly afterwards (and after structural upgrades), a ship extension program commenced which increased the length from 170' to 179'. Figure 24 below shows a split screen of one of the PC's and after the transformation:

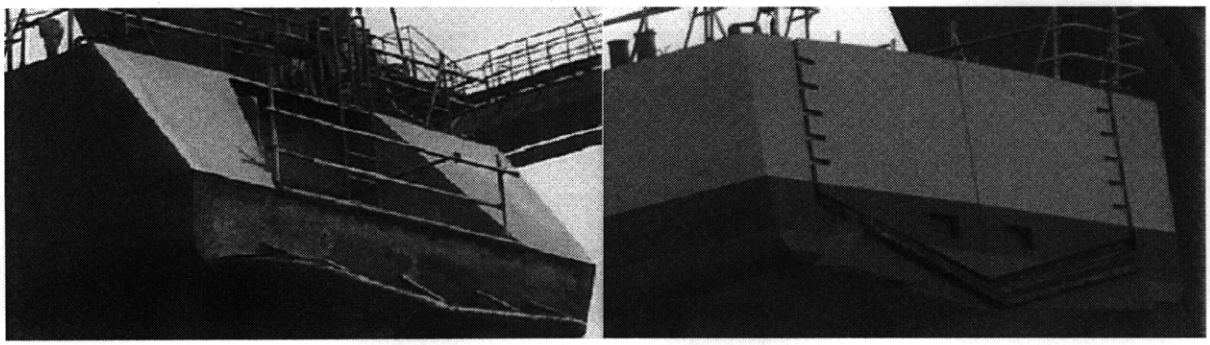

Figure 24: U.S. Navy Patrol Craft before and after conversion. Note the large stern flap on the 170' pre-conversion while on the 179' post conversion it is nearly non-existent.

This project was completed in 2006 for 10 of the 14 original ships. The extension program included a stern launch and recovery system as well as an updated communications suite. In 2004, PC 1 (USS Cyclone) was decommissioned and transferred to the Philippine Navy and

PC's 2, 4, 8, 13, and 14 were transferred to the U.S. Coast Guard to work in maritime safety and security operations. These missions included:

- Homeland defense
- Alien migrant interdiction operations (AMIO)
- Law enforcement, particularly in illegal narcotics trafficking
- Search and rescue (SAR)

All of the ships transferred to the U.S. Coast Guard are the 179' extended version (38). To account for the extra weight and to fix structural problems that will be discussed in the next section, (4.1.2) structural enhancements were made to the deck structure which effectively increased the section modulus to satisfactory levels. In addition to the extension, extra fuel tanks were created in void spaces to increase endurance, giving the PC's the ability to travel with deployed battle groups. In 2005, the Navy originally made plans to decommission 8 of the PC's, and transfer all of the remaining extended versions of the class to the Coast Guard (38). Figure 25 below shows the USCGC Tornado (WPC 14) just before its commissioning as a Coast Guard Cutter:

Figure 25: USCGC Tornado (formerly USS TORNADO) just before its commissioning ceremony to formally transfer custody of the ship to the U.S. Coast Guard.

Although the PC's were scheduled to be returned from the Coast Guard back into Navy Service as early as September 2008, these plans were scrapped. As of the spring of 2009, the 13 remaining PC's are scheduled to remain in service pending funding through fiscal year 2012.

4.1.3 Platform Failure Overview

The 123' Patrol Boat experienced its first taste of structural failure during sea trials of the very first converted cutter, the Matagorda. The significant failures seen with this class of cutter were mainly limited to this cutter and the Nunivak, however six of the eight experienced alignment problems and other significant structural issues discussed which ultimately led to their removal from service.

Matagorda & Nunivak

While underway during sea trials, Matagorda experienced failure amidships during sea trials while transiting at 22 knots in seas of 4'-6' (sea state 4) (35). Buckling of both the side shell panels and deck along frames 22-24 was significant enough to be seen without any difficulty. Figures 26 (a,b &c) seen below, document the side shell failure in official pictures taken by the Coast Guard.

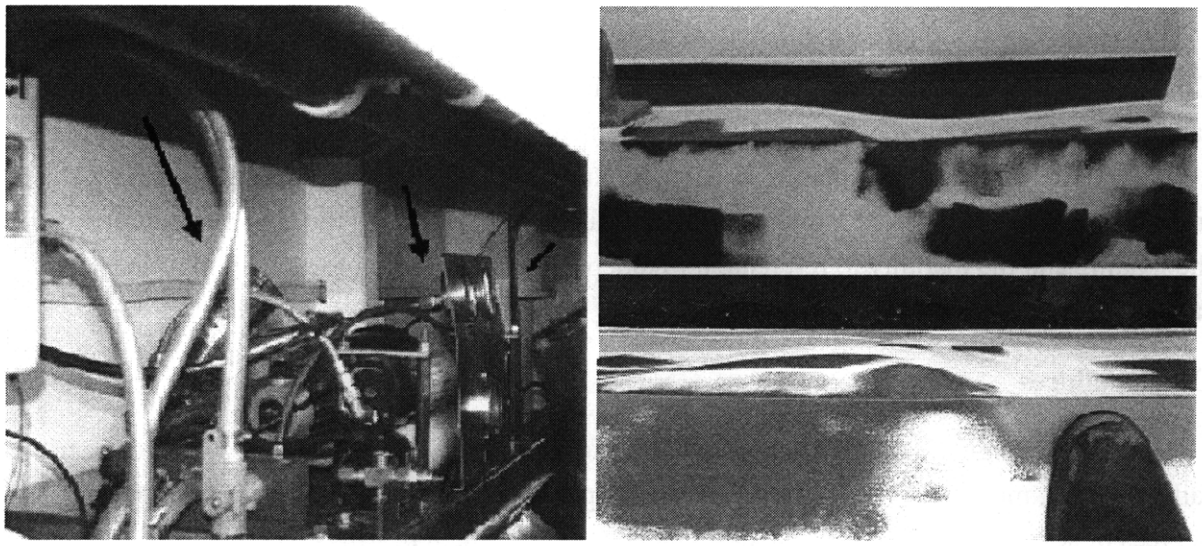

Figure 26: (a, b, c) Buckling Failure pictures taken by the Coast Guard. This failure was aft of midships at frame 24-25 (2).

When the matter was investigated, the contractor indicated that there were errors made in the initial structural calculations and local resistance to buckling was limited, especially due to dynamic loading in high seas (2). To remedy this obviously serious issue, structural upgrades included the addition of 7 ½ inch, # 10.2 Plate doubler straps (discussed in section 4.1.1) proposed by IDS and lengthened by the Coast Guard for additional robustness (2) (18).

Much like Matagorda, Nunivak experienced significant failure due to excessive loading, but the location and type of failure was significantly different. While underway conducting operations in 8'-10' seas, the cutter reported hull deformation one hundred and ten feet aft of the forward perpendicular along the side shell in the area directly forward of the stern launch. The

damage consisted of diagonal indentations and Coast Guard defined "chevrons" (2). This damage occurred in an area previously upgraded due to lessons learned from the Matagorda failure. A figure of the damage and its location can be seen on the following page, reproduced from the June 2006 brief to Congress on Deepwater issues:

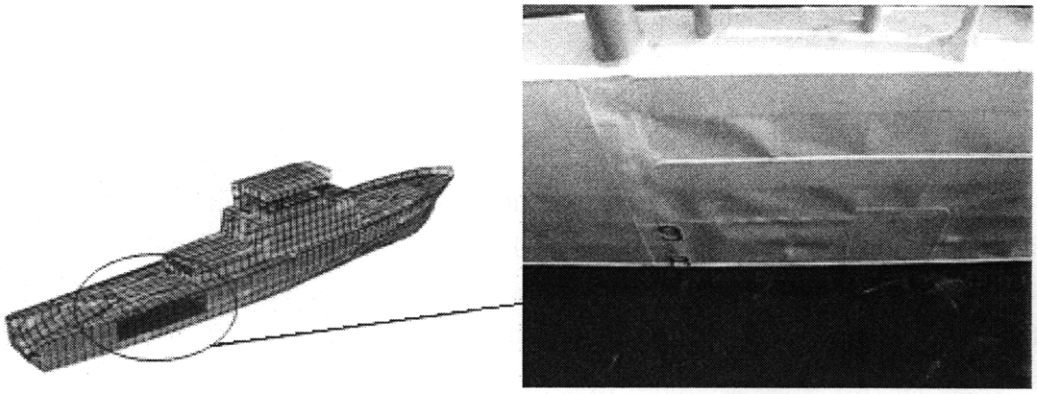

Figure 27: The Location and Extent of the Damage on board Nunivak.

Unlike Matagorda, an independent study conducted by D&P (discussed further in Chapter 5) found that the structure should have withstood plastic deformation through the entire range of predicted sea states and headings. To remedy the problem, the Coast Guard installed 100 square foot of additional plating to augment the relative sturdiness of the section and welded intermittent deck stiffeners to provide additional support (18). Due to the apparent complexity of the loading and the inability to re-create it in independent analysis, an examination of local failure was not conducted.

Other Failures

Another sign of structural integrity issues for the WPB 123's came in the form of bearing failure. In all, more than two thirds of the fleet experienced bearing issues varying in their degrees of severity. In each of these cases, shaft seals and main bearings were overheating during normal operation, some at significantly lower RPM's than would be normally expected. After determining all other possibilities for bearing failure, such as lack of cooling or incorrect sizing, it was determined that the bearings were failing due to shaft miss-alignment and possible lack of adequate cooling. Upon further inspection into the alignment problem, it was discovered that different degrees of apparent buckling deformation existed in the hull section around frame 28. To remedy the alignment problem, Coast Guard engineers had to repeatedly remove the main bearing mounts and remount them consecutively lower and lower, to the point where they could not be lowered any further (35). This essentially indicated the entire hull was slowly, plastically deforming.

Due to all of these significant failures, every cutter in the 123' fleet experienced cracking along the deck up forward on the foc'sle, back aft along the sides of the stern launch, and along each side of the superstructure. There is no clear timeline of the appearance of the cracks (pre-or post buckling and hull deformation). Appendix 4.1 shows a diagram outlining the different failures seen on the 123'.

Cyclone Class Failure

For the 170' Cyclone Class, structural problems started becoming apparent just a few years after delivery. This differs significantly from the 123' case because failure occurred *pre-conversion* (3). In terms of specifics regarding the dynamic loading conditions when each failure was noticed and/or occurred, no data is available, although it is plausible to assume that some moderate to severe dynamic loading (seen in higher sea states) was present. Significant failures included hull cracking and buckling observed on the deck girders and side shell. These failures were not limited to one or two vessels in the class, they were seen class-wide and considered mission-jeopardizing failures, much as the 123' failures were. Not every failure was seen on every single vessel, however. The Navy classified these failures as types I-III damage, noting each with increased severity and each indicative of a progressive failure (39). Damage seen included the following:

- Stage I Damage: Cracking of centerline girder at mid-ship
- Stage II Damage: Cracking of outboard edges of raised engine casing
- State III Damage: Buckling in various longitudinal stiffeners along the deck and side shell

This damage is seen below in Figure 28 (a&b), and on the next page in Figure 29 (a&b), which shows damage that occurred prior to the structural upgrade:

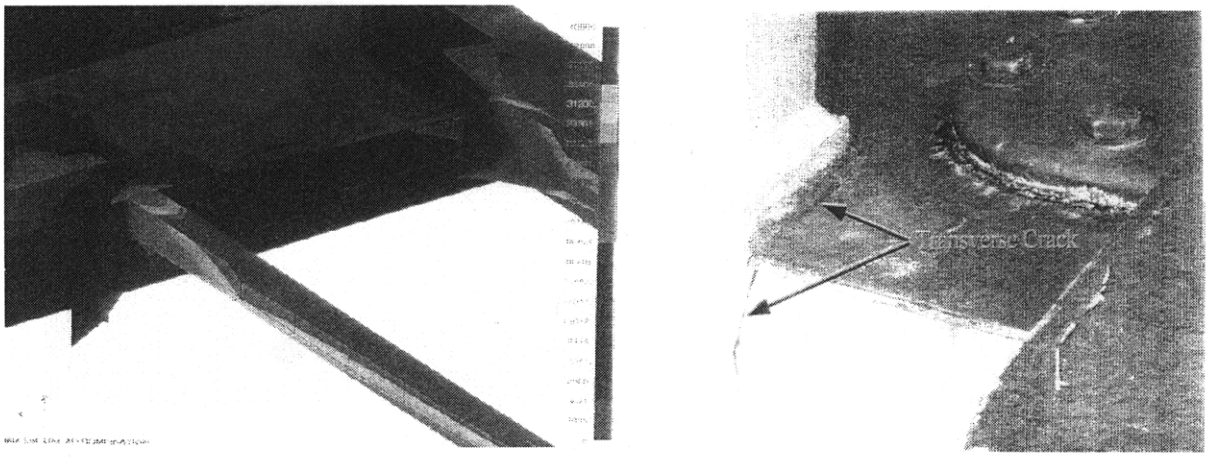

Figure 28: (a & b) Stage I and Stage II Damage seen on the Cyclone class. Figure 4-7 (a) shows a crude FEA analysis with the centerline girder past yield strength in a sagging condition. Figure 4-7 (b) shows stage II cracking on the raised engine casing. A synopsis of ship's drawings can be seen in Reference (40).

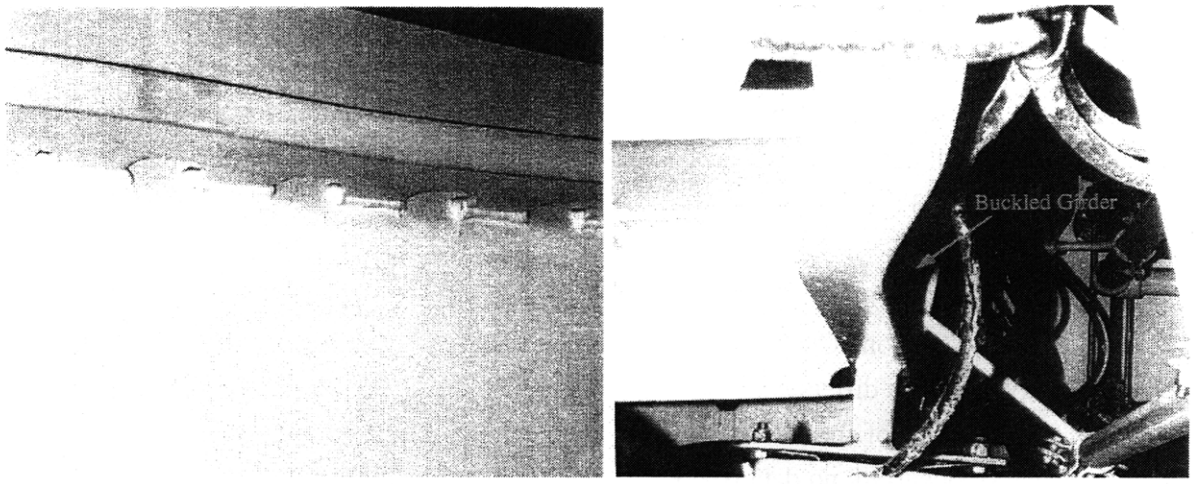

Figure 29: (a & b) Stage III Damage just aft of Frame 30 detailing a buckled side shell stiffener (a) and a buckled deck stiffener (b). These pictures were taken by the Navy on board PC-2 (39).

A diagram detailing the extent of the Stage I-III damage on board the Cyclone Class patrol craft seen in the vicinity of the mid ship section can be seen in Appendix 4.2, while a matrix detailing the extent of damage for each specific ship along with additional images can be seen in Reference (39).

To remedy the extensive problem of severe structural failure, a feasibility study was completed by Puget Sound Naval Station Detachment-Boston in conjunction with NAVSEA to perform a structural analysis and come up with a solution to strengthen the hull. The design finally implemented involved strengthening the deck section modulus nearly 70% by adding almost 4.5 LT of additional material (39). The crude drawings of the original and improvements can be seen below as Figure 30:

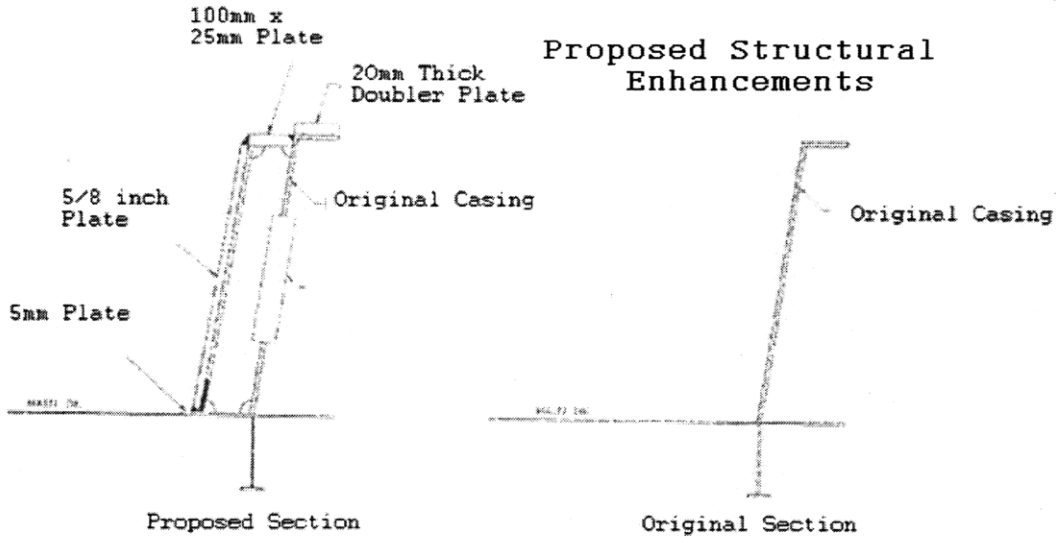

Figure 30: Proposed enhancements of the Cyclone Class Patrol Boat. This image is reproduced from Reference (39).

Improvements seen in Figure 30 include a 5/8" plate outboard of the original casing, two doubler plates, and "piping" to encase the original engine room casing. The proposal for improvements was approved through the U.S. Naval chain of command and the work was completed. At the time of the proposal, the structural improvements were also determined to be strong enough to allow a 9' extension and extra fuel tanks, briefly discussed in Section 4.1.1. Similar to several failures seen on the 123' (including Nunivak failure and shaft alignment problems), no in depth analysis was completed on the local fracture or buckling failure seen on the 170'-179' conversion as part of this study.

The lack of analysis in these sectors was largely due to the complexity of loading and changes in stress concentrations upon fracture, and also the lack of in depth information on the structure itself. Regardless, to have an overall understanding of the primary hull girder loading experienced by each of these two patrol boats, stress calculations were completed detailing pre- and post structural upgrade scenarios and subsequent error margins examined for continuity as seen in the next several sections of this Chapter.

4.2 Stress Calculations

Since the 123' case and the 179' share similarities with mid ship strength, stress calculations were completed in accordance with traditionally practiced naval architecture methods on both platforms. These include primary, secondary, and tertiary stress calculations where applicable. Initially, Equations 3-5 from Chapter 1 were used to determine the maximum bending moment under still water, hogging and sagging conditions. Still-water structural integrity calculations are relatively simple and are based on the shape of the buoyancy curve. However, predictions involving the unique and unpredictable nature of ocean waves provided a much more daunting task to naval architects. Due to the relative importance of wave induced loading and the extreme difficulty in predicting ocean spectra to measure the effects of wave induced loads, the naval architecture community typically employs a quasi-static representation of the probabilistic spectra of waves (41). This was done purely for the analysis of ship structural strength. The trochoidal wave's shape is designed to have a wavelength equal to the length of the ship and a wave height (two times amplitude) seen below as Equation 44:

$$h_w = 1.1\sqrt{L} \qquad [44]$$

In this case, L equals the length overall (LOA) of the ship. The trochoidal wave is described by the pair of the parametric equations seen on the next page:

$$x = L\frac{\theta}{2\pi} + h_w\frac{sin\theta}{2} \quad [45]$$

$$y = h_w\frac{1 - cos\theta}{2} \quad [46]$$

In this case, θ ranges from 0 to 2π and the origin is adjusted as to create both a worst case hogging and sagging scenario as shown in Figure 6. It is usually one of these two scenarios which set the limitations for the beginnings of shipboard structural design (14).

Although this quasi-static wave is created to quickly determine reasonable worst case structural scenarios, it falls incredibly short of predicting the seakeeping characteristics of the ship. Seakeeping can be defined as the ship's ability to continue to be mission effective in adverse sea conditions. To predict seakeeping characteristics requires a full seakeeping analysis which involves application of extremely complex probability theory and spectra analysis, something that will not be touched on in this study.

4.2.1 110' to 123' Conversion Case

The 123' WPB primary stress analysis is based on midship section modulus calculations performed by the Coast Guard technical authority (35). The 123' WPB mid ship section is shown in U.S. Coast Guard Drawing 085-031, seen in Appendix 4.3. Using Equation 6, the maximum primary bending stress associated with the hull can be determined for a calculated bending moment (in a hogging or sagging or still water scenario) and section modulus at any position along the hull. In the case of the 123', the "worst" case scenario for bending moment was determined to be just aft of amidships, where the engine room soft patches are installed in the sagging profile. The section modulus (SM) and moment of inertia (MOI) values for several key locations (summarized from ELC Excel spreadsheet calculations) can be seen below in Table 4. The Coast Guard's Engineering Logistics Center (ELC) 024 Branch took the lead on the section modulus calculations

123' Section Modulus (SM) and Moment of Inertia (MOI) Summary							
Frame Number	123' with Stern Ramp - Post Retrofit in accordance with Deepwater			123' Post Structural Upgrade - Doubler's & Sponsons added for extra structural support			Comparison
Spacing is 46"	Deck SM	Keel SM	X Section MOI	Deck SM	Keel SM	X Section MOI	MOI % Difference
23	3,152	4,302	266,662	5,747	5,330	405,280	52.0%
25	3,798	5,133	317,507	6,237	6,287	455,404	43.4%
27	2,570	3,394	216,760	4,886	4,450	345,127	59.2%

Table 4: This table shows a summary of Section Modulus and Moment of Inertia calculations in accordance with Coast Guard Technical Authority. All units are multiples of inches (S.M is inches^3 and Moment of Inertia is inches^4)

The distance to the neutral axis is calculated by simple division in accordance with Equation 7. Unit conversions were completed as necessary. It is important to note that the midship section (typically where the bending moment is the largest) is at frame 23.5 and the damage on the Matagorda occurred at frame 24-25 in accordance with section 4.1.2. Table 4 represents both the ship as it was before the doubler plates were added to strengthen the section modulus and also after the modification took place. Copies of the Excel spreadsheet calculations completed by ELC can be seen in Appendix 4.4 (42).

Examining the trend of the values of the section modulus found in Table 4 and applying it to Equations 6 and 7, it is easy to see that maximum stress areas will likely occur where section modulus values are at their least-value point. This is illustrated by the relationship between stress, bending moment, and section modulus, seen below:

$$\sigma_{Primary} = \frac{M_{sagging}}{Z_{min,deck}} \quad [47]$$

Applying Equation 47, the absolute worst case primary stress is equal to 16,473 psi, if $M_{sagging}$= 1,575 LT-ft and $Z_{min,\ deck}$=2570 in^3. One long ton (LT) is equal to 2,240 pounds. The maximum bending moment (for a trochoidal quasi-wave 13ft versus 12.1ft) was determined to be in sagging with head on waves in a minimum operating condition. Although the wave is 0.9 feet higher than commonly considered, this particular class of Coast Guard ship was known to operate in seas with significant wave heights at least this high (35). The min-op loading condition for the 123' is noted in the ship's Damage Control book and will not be discussed (18).

This result for primary bending stress is, as mentioned before, a worst case scenario; where the damage occurred the section modulus was a little bit larger. This is reflected in charts showing how the section modulus changes across a variable x-distance from the forward perpendicular. In this vicinity, primary stress was determined to be 13,431 psi based on a section modulus of 3152 in^3. Table 5, seen on the following page, shows the overall distribution of stresses based on the relevant section modulus values previously seen.

123' Primary Stress Based on S.M Calculations (Min - Op Condition)						
Frame #	Worst Case 123' with Stern Ramp, Post Retro (psi)		Worst Case 123' Post Upgrade (psi)		Upgrade Comparison	New Safety Factor: SDS 100-1
Spacing is 46"	11.9' Wave	13' Wave	11.9' Wave	13' Wave	% Diff. at 13'	Max P. Stress = 16.8 ksi
23	12732.2	13431.5	6983.1	7366.6	45.2	2.3
25	10566.6	11146.9	6434.5	6787.9	39.1	2.5
27	15615.5	16473.2	8213.6	8664.8	47.4	1.9

Table 5: Primary Stress calculations in a minimum operating condition for the 123'. These calculations are based on a Worst-Case Bending Moment Calculated by U.S. Coast Guard technical consultants D&P and are verified against SDS 100-1 (43).

The 123's section modulus calculations (prior to the modification to increase it) were nearly identical to those of the original 110' prior to the conversion project. Worst case primary stresses calculated for the original 110' were found to be 9955 psi. This is 6,518.2 psi lower (39.5%) for worst case scenario or 1,191.5 psi lower (10.7 %) for the damage location at frame 25.

In this case, it is obvious that the maximum primary bending stress alone does not reach the yield point of the steel plating that was found to be buckled (type BS 4360 grade steel as reported by USCG technical authority and confirmed in ship's drawings) (35). However, this data does not examine how secondary and tertiary stresses were affected by the conversion. The original ELC 123' WPB graphical depictions of weight, buoyancy, and other curves can be seen in Appendix 4.5 (44).

Secondary stress calculations were deemed to be nearly nonexistent on the area of the hull in question because they assume a lateral force or pressure against the face of the stiffened panel (like hydrostatic pressure seen on the hull due to the force of buoyancy). Secondary stresses can be likened to any initial deflections that existed due to wear and tear or hull maintenance over the course of the cutter's life. FEA analysis will later show that small initial deflections, unless exceedingly large, are not of particularly large concern on a macro scale. Tertiary stresses in this case are much more prevalent.

In 1988, a comprehensive structural review was completed for the then 110' patrol boat, which focused on the inadequacies of the thickness and strength of bottom hull plating. This paper was published in the 96th Volume of SNAME Transactions (8). Although this paper focused on forward hull plating, a brief longitudinal strength analysis was completed, including a tertiary stress analysis. In order to perform the tertiary stress analysis, the Heller-Jasper method was used, as discussed briefly in Chapter 1. Keeping in mind that prior to the post-retrofit hull strength upgrade the shell plating on the 110' and 123' were identical, it has to be assumed that the tertiary stresses experienced by the stiffened panel are at least those of what the 110' experienced. Tertiary stresses in the 110' case were determined to be 27,687 psi. Inputs included breadth and thickness values, a "k" factor based on boundary conditions (k = 0.75 for a simply, simply supported assumption), a multiplier, and panel design pressure (8). Once these inputs were determined it was safe to say that this calculation pre-retrofit is nearly identical for the 123'.

To determine overall combined stresses seen in the plating structure, it is suitable to use the method of superposition which allows for the simple addition of stresses to take place. Adding the two stresses (if secondary stresses are assumed to be neglected) it is found that total 123' stresses were 44,160.2 psi for worst case scenario and 38,833.9 psi at the point of failure.

Given a standard yield stress of 40,000 psi for BS 4360 steel, it is easy to see that in a worst case scenario, the yield stress is surpassed by 10.4% and at the failure point for a 13' wave, the safety factor is a mere 1.03. This factor obviously allows next to no room for environmental issues, unexpected severe loading, initial deformations, residual stresses, or any other type of factors that could cause hull failure, and also assumes that the buckling point of the side shell is greater than the yield point.

4.2.2 170' to 179' Conversion Case

By comparison, overall less information is known about the 170'-179' conversion hull, but it provides one very important point of comparison: Although this design failed in a very similar fashion to the 123' project, the ships were able to be fixed and be used in a full operational spectrum (45).

Similar to the 123', the primary stress analysis starts with determining the location of the maximum bending moment and examining the concurrent section modulus to calculate the resultant primary bending stress. The relevant section was determined to be midships and the cross section with the overlaid neutral axis (along with damage locations) can be seen in Appendix 4.2. A somewhat smaller, 12' trochoidal wave is used (using Equation 44 yields a required wave height of 14.7ft) in this case. The maximum bending moment is seen in a sagging condition at 3788 LT-ft. The weight-buoyancy curve and the resultant load curves are below:

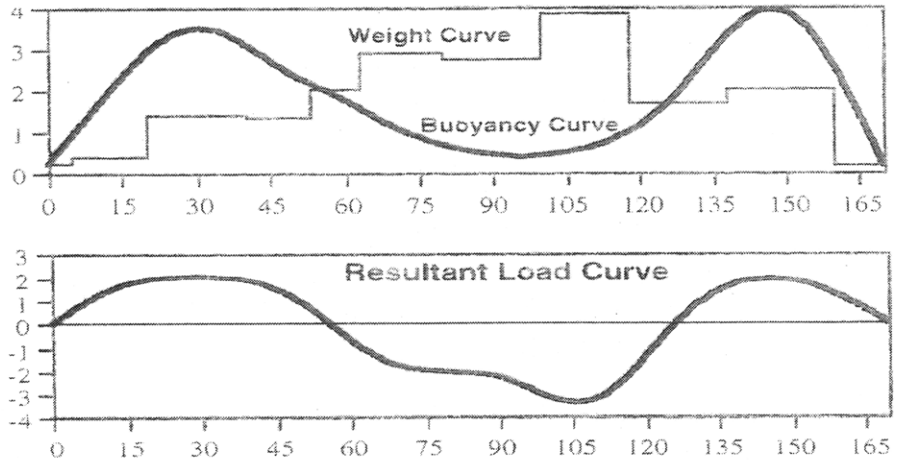

Figure 31: Weight-Buoyancy and resulting Load Curve for the pre-conversion 170'. It is reproduced from Reference (39). The "x" axis represents feet aft of the forward perpendicular and the "y" axis represents Long Tons (LT).

The resultant primary stress calculation based on the double integration of the load curve seen above in concurrence with Equations 3-5 can be seen below as Equation 48:

$$\sigma_{primary} = \frac{3788.6\ LT \cdot ft}{663\ in^2 \cdot ft} \qquad [48]$$

With appropriate unit conversions primary stress based on Figure 38 and Equation 48 is calculated to be 12,800 psi. It should be noted that this value for primary stress is less than what the traditional trochoidal wave calculation (given by Equations 44-46) presents. Regardless of these solutions, the 170' structural enhancement feasibility study conducted by NAVSEA engineers developed a more accurate absolute worst case scenario bending moment considering dynamic forces to be present, rather than just a quasi-static wave. It was determined that the worst case bending moment occurred at a displacement of 360 LT with a maximum primary bending moment of 9,346 LT-ft. This is significantly higher bending moment than was calculated by the 12' foot or traditional quasi-static wave scenario.

Calculations were completed by NAVSEA Carderock Division. Similar to the 123' case, section modulus and resulting primary bending stress calculations were completed at various strategic locations along the hull for pre and post strength upgrade hulls. Section moduli for the critical frames along midships (fr. 27-32) are depicted below in Table 6. The complete section moduli throughout the hull can be seen as part of Reference (46), NAVSEA Drawing 5106697.

170'-179' Section Modulus (SM) and Moment of Inertia (MOI) Summary							
Frame Number	170' As Built by Bollinger			170' or 179 Post Structural Upgrade: Doublers and Pipe Fittings			Compare
Spacing is 43.1"	Deck SM (in^3)	Keel SM (in^3)	X Section MOI (in^4)	Deck SM (in^3)	Keel SM (in^3)	X Section MOI (in^4)	MOI % Difference
27	9,576	10,500	926,352	13,056	12,276	1,237,968	33.64%
29.5	8,892	10,380	969,984	14,064	12,276	1,328,400	36.95%
30	7,956	10,224	906,768	14,016	12,612	1,345,248	48.36%
32	7,932	10,824	927,792	12,672	13,008	1,300,896	40.21%

Table 6: This table shows a summary of Section Modulus and Moment of Inertia calculations in accordance with NAVSEA. Note the increase in Moment of Inertia values with the addition of the structural upgrade.

The table above shows data from before and after scenarios of the failed 170' hull and the retrofit 179'. It is important to keep in mind that the hull extension project took place after the structural enhancements were completed and no more major structural issues have been noted post enhancement on this class of ship. Corresponding to the data seen above in Table 6, the primary stress distribution pre-and post upgrade can then be calculated using known and assumed maximum bending stresses for sagging conditions.

The data below, seen in Table 7, shows the differences in primary stresses due to the structural enhancements that were completed prior to (or in some later cases) along the same time frame as the extension. In addition to this tabular data, a graphical analysis of the data showing trends due to change in x-location can be seen in Appendix 4.6.

170' Primary Stress Based on S.M Calculations (360 LT Condition)						
Frame #	As Built 170' by Bollinger Yard (psi)		170' Post Structural Upgrade (psi)		Upgrade Comparison	New Safety Factor Based on Rules (DnV)
Spacing is 43.1"	12' Wave	Worst Case	12' Wave	Worst Case	% Diff. at Worst Case	Max Permissible Stress = 25.39ksi
27	10,633.0	24,238.6	7,798.8	17,777.9	26.7%	1.43
29.5	11,450.9	27,321.3	7,239.9	17,274.0	36.8%	1.47
30	13,404.6	33,072.7	7,264.7	17,923.8	45.8%	1.42
32	12,836.8	30,804.2	8,035.2	19,281.8	37.4%	1.32

Table 7: Primary Stress calculations for the 170' with a displacement of 360LT. These calculations are based on the 12' quasi-static wave loading condition which is smaller than the typical derived size for a vessel this large. The worst case scenario is based upon calculations done by NAVSEA which include dynamic loading that can be seen as part of Reference (46).

Because the calculation of maximum bending moments for ships are extremely sensitive to the displacement and loading condition of the hull, only the 12' wave and worst case loading conditions for the pre-retrofit baseline PC hull are shown. The bending moment partially involves dynamic loading as calculated by NAVSEA. Therefore, the safety factor examined is a rules based factor for maximum permissible bending stress which is the ratio of the maximum allowable bending stress and minimum section modulus for a given design and loading condition. The formulas used in the rules are based on empirical data (discussed in Chapter 1). Further discussion of rules based margins can be seen in Section 4.5.3.

Secondary and tertiary stress calculations were not completed for the 179' (170') due to the nature and the severity of the failure seen, and limited information on the local structure of the hull. A plausible way to verify secondary and tertiary stresses do not cause the overall stress of the hull to surpass the yield strength of the steel, a rules based approach can be taken. Therefore, primary stress calculations were verified to be within limits using two classification societies (ABS, DnV). This was done as part of the feasibility study conducted by NAVSEA (46).

4.3 Engineering Analysis of Failure Types

The engineering analysis of failure provides an excellent bridge between real life failures and an academic understanding of the factors that affect hull failure at both the global and local levels. This is accomplished by understanding how failure occurred and discussing this reasoning in conjunction with known causes for strength degradation, rather than speculating on the uncertainties of why it occurred.

Referring back to section 4.1.1 which discusses the timeline of each vessel, as well as section 4.1.2, which discusses where each failure occurred in detail, it is easy to walk through the

engineering side of failure seen at each significant location. This can be broken down into the two classes of ship and then broken down further by damage location and type of damage. Some relevant pictures of the damage are also seen in section 4.1 and the entire collection is seen in References (2) and (39).

4.3.1 United States Coast Guard Cutter Patrol Boat (WPB) 123'

- Midship side shell buckling at frames 22-24: At this location, a 1.5" amplitude buckling wave over an entire period of 5 feet developed due to loading conditions described in section 4.1.2. It was described as buckling in the "overall mode" by Coast Guard engineers (35), as a result of excessive primary stress. In a sense, these assessments are correct: This failure is undoubtedly due to global failure of the hull girder caused by yield, not the collapse of an Euler-type column. Locally, the failure of the side shell panel can be accurately described initially as Mode III failure in accordance with stiffened panel theory discussed in Chapter 3, though other modes of failure are present after t=0. In mode III, the initial yield point of the plate-stiffener combination is reached as failure occurs at mid-span.
- Side shell deformation aft at frames 32-33: This "chevron" type and diagonal deformation was most likely caused by a combination of primary bending stresses and associated shear stresses due to an excessive wave load. This deformation is shown below.

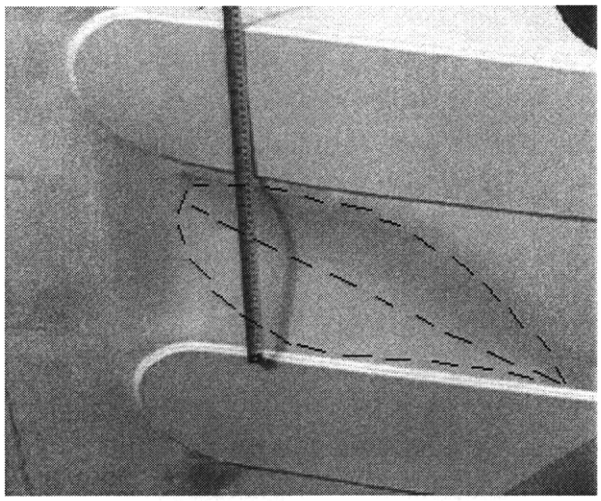

Figure 32: Close up of the side shell damage seen at frame 32-33 with dotted lines marking the deformation (2).

The 45° wedge shape deformation is a classic sign of yielding in shear with a biaxial load consisting of both types of stress. This failure occurred in an area where primary stresses would tend to increase dramatically with a relatively small change in forces. Here, the section modulus decreases dramatically as the doubler additions end. Unfortunately this

failure could not be reproduced in FEA. A potential reason might be that the loading condition was an anomaly due to a rare combination of forces and is nearly impossible to reproduce.

- Hull deformation underneath the MDE's and associated shaft alignment problems: This hull deformation was discovered upon several reoccurring failures of shaft seal and main bearings for the main propulsion system. Five separate cutters showed sinusoidal buckling with an amplitude of 0.75 inches over a 2-3 foot period. Bearing casualties were experienced on at least two-thirds of the cutters and variation of the deformation was present on all. Uncorrected shaft-misalignments were determined to be up to .167" with a normal allowance of .002-.005" (35). The 15" cutlass bearing used on the 123' can be seen below:

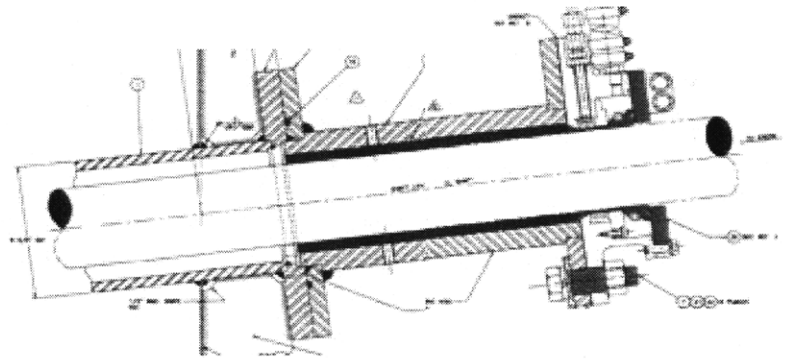

Figure 33: 123' Cutlass Bearing and Seal configuration. The bearing is seen in blue and the seal is in red. Ideally, seawater moves directly through the seal to cool the bearing. This figure is reproduced from Reference (2).

Consequently, the approximate amplitude of the actual deformation was .75 inches over a distance of 3-5 feet. Like the side shell deformation associated with failure at midships, this type of failure can also be categorized as Mode III due to the characteristics presented for analysis.

- Cracking and fracture of the main deck: These failures were a result of the overall flexing of the hull and the relatively weak, non marine-grade aluminum deck material. It was determined that "stress corrosion cracking" was primarily at fault and nearly all the cracks ran longitudinally over all areas of the main deck on all 8 platforms (35).

4.3.2 United States Navy Patrol Craft (PC) 170'

In contrast to the particular WPB class failures which presented two single, large scale failures and smaller associated failure, the PC 170' followed more closely the classic

"progressive failure" model. The stages of this progressive collapse as it relates to this particular patrol craft are noted below:

- Stage I failure of main deck hull girder at frame 30: This was most likely caused by an initial yield of the girder in the sagging mode, which caused a material non-linearity that then created a crack tip in ductile fracture. Aided by the environment (sea spray) and cyclic loading and unloading of the hull while in the seaway, initial crack growth (in accordance with fracture mechanics discussion in Chapter 3) occurred relative to the properties of BS 4360 steel. This then progressed into stable crack growth where ship's force was able to halt it using artificial means (39). Once the crack formed, the ship's ability to withstand both large, dynamic hogging and sagging loads was diminished as more load was placed on other parts of the cross section near the deck. This is what led to Stage II failure.

- Stage II failure of the outer portions of the engine casing at frame 30: In accordance with Stage I failure, when the main deck hull girder could no longer hold sufficient load, it was redistributed to the outer portions of the engine casing. The casing itself is not sturdy enough to hold the additional load and the same chain of events took place. Subsequent yield caused material non-linearity, causing a crack tip that eventually, through environmental impacts and cyclic loading, led to stable crack growth. Once these sections were no longer able to be loaded to full capacity, major structural issues began to form in the form of stage III failure (39).

- Stage III failure consisting of deck and side shell buckling and subsequent cracking: The failure seen in Stage III was caused by excessive axial loading and a reduced effective section modulus, which caused mode III buckling and mode VI gross yielding of stiffened panels in several locations in the vicinity of frame 30 (39).

4.4 Global Strength Reduction Factors

The calculation of primary bending stresses based on the equations discussed in Chapter 1 and the detailed explanation of failure locations do not tell the whole story of failure by themselves. Section 3 of Chapter 2 discusses various causes for strength reduction due to construction, loading, and time-based problems. Globally, there are two main areas of interest that can cause a reduction in strength sufficient enough to cause pre-mature buckling. These are vibrations effects (including slamming) and global corrosion considerations. The others described in Section 2.3, will be discussed in a local bucking analysis that is conducted in Chapter 5. Due to the availability of information about present hull degradation and conditions

surrounding the actual failures, the strength reduction factors discussed in the following sections and conclusions following this application are mostly applied to the 123' case study.

4.4.1 Slamming and the Effect of Excessive Vibration

The effects of slamming, particularly on smaller, faster ships with thinner hulls can be devastating to the structural integrity of a hull if a skipper does not stay within appropriate operating realms of the ship. The operating profile, detailing specifics about speed and wave height tolerances is a critical part of managing the slamming phenomenon. As discussed in Chapter 2, the hull girder vibratory response occurs primarily in the first mode of natural frequency but smaller responses are noted in the second and third vertical modes. This response, if coinciding with forced vibrations (i.e. machinery, propeller blade passage), could cause resonance that degrades the integrity of the ship at a much faster rate than would be seen in normal shipboard operations.

In order to quantify the effects of slamming, natural vibration and potential coinciding forced vibrations on the 123', the numerical natural frequency of the ship is calculated in a pre-structural upgrade condition using Equation 15. This equation is based on work by Shlick with a modification proposed by Liddel to account for added mass (24). Using this formula and 156,850 for φ (determined empirically for ships with fine lines), the first mode natural frequency of the 123' is found to be 3.66 hertz.

Slamming (usually in excess) has been reported to increase the primary hull bending stress by upwards of 30% (21), however the overall severity of any given slamming event depends on a multitude of different factors. The figure below shows a Coast Guard Cutter (not the 123') just after the moment of impact during a slamming event.

Figure 34: U.S. Coast Guard Cutter SPENCER (WMEC-905) just after a slamming event with green water over the bow. The image was taken by the author in the Northern Atlantic Ocean in December 2005.

The overall intensity of the event is in direct correlation with the relative velocity of the hull and the water at the moment of impact. This assessment of the overall strength does not even necessarily take into account the local lateral stresses seen on the hull bottom plating where actual impact occurred.

In their work, Mansour and d'Oliveira (21) provide a numerical assessment of the magnitude of the time varying bending moment (occurring over the natural frequency of a ship) due to slamming. This can be scaled to give an order-of-magnitude assessment of the forces that may have affected the 123' fleet during operation. Further verification comes from essentially comparing the solution to that of the known jump in bending moment due to dynamic forces assessed on the 179' fleet by NAVSEA in Reference (46).

Using Reference (21) as a guide, the increase in bending moment due to reasonable dynamic slamming forces at the given sea state were calculated to be 1002 LT-ft (based on a previously determined worst case baseline moment of 1575 LT-ft), while the relative increase of the bending moment for the 179' was determined to be 5,558 LT-ft. This correlates to a 63% increase from the 123' and a 146% increase for the 179' (Though other, unknown factors may be present in the case of the 179'). These calculations were completed for similar state loading conditions, are considered worst case, and may actually be much larger values than operationally encountered. While this correlation might not be quantitatively absolutely correct and does not necessarily prove anything, qualitatively it shows that there absolutely must be a consideration for slamming events, particularly in a smaller ship with fine lines. The calculation methodology for the 123' result is discussed further in Appendix 4.7.

Coast Guard Authorities have stipulated that at the time of the midships failure on the Matagorda, the cutter was underway at approximately 22 knots in 4-6 foot seas (35). This correlates to an approximate engine RPM rate of 1200 (20rps) and a correlated shaft RPM (based on a reduction ratio of 1:1.625) of 740 (12.3rps) (47). The first mode natural frequency calculated by the Shlick-Liddel method does not coincide with any pronounced forced frequencies that may have been seen on the ship at the point of failure causing resonance. However, the third order vertical natural frequency of the cutter (calculated to be 11.74 hz) does closely coincide with the shaft RPM's encounter frequency and could have created some undue resonance but it cannot be asserted that this was a direct cause of the failure. It is plausible, however, that this was one of many events that may have played a role, especially if existing cracks were affected. Experts say that to significantly degrade steel (more than is seen in regular fatigue loading), the resonance characteristics of a vibrating structure have to exceed 20mmps for a prolonged period of time (25). This did not necessarily occur by any means on the 123'.

The formulation of the effect of slamming on a cutter such as the 123' makes one important distinction – in this analysis the hull is made of ideal steel and considerations for both normal and unique fatigue loads are not fully developed. It is easy to speculate, given the original life expectancy of the cutter and the associated fatigue of the hull after 20 years of service, that the material properties were in effect "modified" to the point where excess dynamic forces, including slamming characteristics with some resonance could have amplified the degree of magnitude of the failure.

4.4.2 Corrosion Considerations

Over the course of the investigation of structural integrity issues of the 123', it was determined that some of the cutters had corrosion far greater than had been previously assumed (35). This may have been caused by three flaws in the 110' original design, noted below:

- There was no corrosion allowance built into the design of the 110' (35).
- The aluminum used for the 110' deck was not marine grade (35).
- Some hull plating was not to ABS standards (8).

When several of the 110's, after approximately 20 years of service, came into dry dock to begin the retrofit process, a significant amount of hull and deck plating was replaced at additional cost to ensure the continued structural integrity of the cutter (35).

Unfortunately, there is no real way to quantify how much corrosion affects the strength of the ship because it depends on a multitude of different factors. In fact, in the case of the 123', corrosion is discussed as being as closely related to crack formation as some of the stresses. Upon investigation by Coast Guard members of the Deepwater staff, it was determined that deck cracking, appearing on all eight cutters, was caused by chloride-induced stress corrosion cracking Independent testing later confirmed that many of the aluminum deck samples taken from various 110's and 123's showed susceptibility to intergranular corrosion above normal levels, although it was noted that susceptibility could vary based on sample location on board the ship (48).

4.5 Discussion

Examination of the structural failure of an extremely complex structure with time dependent loads and boundary conditions that are defined based on individual assumptions can certainly be a daunting task. Interestingly enough, there was no "overall" grillage buckling in either the 123' case or the 170' case that was discernable. It is plausible that some form of overall loading condition caused local buckling but in the sense of stiffened panel failure this

cannot be classified as the overall buckling mode. Ultimately, this is a good thing because stiffened panels are not designed to fail in the overall mode before local panel buckling and or stiffener tripping occurs. With a good understanding of the material properties of the steel and the strength characteristics of the geometry of the stiffened panel, it is still difficult to determine at the global level if yield or buckling occurred first in the case of panel failure on the 123'. In reality, this is the epitome of the uncertainty in ship structural design and analysis. It is reasonable however, based on the nature of the failure and the forces present, to assume that both yielding and buckling were factors in failure as gross yield combined with several modes of buckling.

4.5.1 Platform Comparison

An overall comparison of the two platforms and over global failure yields fairly interesting results. One ship failed post production using original plans while the other failed post upgrade and extension. Once the structural upgrades were complete, the PC was not only strong enough to support its load but an extension and extra fuel tanks were added and no problems have been reported. Conversely, the 123' suffered continual and worsening debilitating issues which eventually led to the disbandment of the entire class of cutter. This brief yet important comparison shows that some structures are inherently flawed no matter what upgrades are completed, while some are genuinely fixable. The problem isn't identifying flaws once failure occurs. The difficulty rests on the sometimes completely intuitive, human-driven design process that, through enough careful time and effort, can potentially eliminate them all.

4.5.2 Validation

Validating the calculation and the consideration for the discussed strength reduction factors is relatively simple at a global level. Could it be reasonable to assume that failure was caused by a combination of corrosion of the hull, stress corrosion and strength degradation of the deck, resonance of natural and forced vibrations due to slamming and machinery, residual stresses, shearing, initial imperfections, and initial deflection? Maybe. But it is impossible to prove or disprove any direct theory of this magnitude which could have serious consequences. In reality, there are so many potential variables and combinations of internal factors, loading, conditions, and operator intuitiveness that it is often impossible to be able to say "this event occurred like this because of X, Y, and Z." It is still important, however, to note all of the potential causes for strength degradation (away from what is determined in design) on all levels, as was either done or introduced in this Chapter, and then verify a specific version of that design by examining safety margins put in place by governing bodies such as ABS.

4.5.3 Rules-Based Design Margins

The rules based design margins for the 170' and 179' strength upgrade and conversion can be found in Reference (46), a comprehensive NAVSEA drawing that details the differences in section modulus, bending moment, and primary static and dynamic stresses for the ship. Rules based margins are calculated in this reference for minimum section modulus, maximum bending moment and the resulting nominal permissible bending stress according to empirical formulas generated by two different governing bodies, ABS and DnV. Due to this available information, it is suitable to say that even though they are not required to by law, the 170' and 179' structurally upgraded editions satisfy all major structural requirements by satisfactory margins that are available in the reference.

Regardless of the noted post-retrofit failures that occurred on the 123', it is still plausible to say that all three major structural categories (min. section modulus, max. bending moment and nominal permissible bending stress) may be satisfied under ABS rules. United States Coast Guard Engineers working out of the USCG Deepwater office have verified that post structural upgrade, (doublers, sponsons, and extra plates added as discussed in this Chapter) the 123' does in fact meet these structural requirements as set forth by ABS (35).

4.5.4 Conclusions and Application to Local Analysis

It is difficult to pinpoint the succession of events that led to failure and ultimately the question of why failure occurred in the first place. This is best left to boards of inquiry and investigation. However, the vital connection between real world problems and engineering analysis at large and small levels of ship structures, along with the understanding of the "how" question, is critical for ship designers and builders of the future to cut costs while improving design methods and safety.

Figure 35: The idle fleet of 123' WPB's. This is the unfortunate result of the uncertainty of ship structural design and analysis.

This task, imposed on ship designers of the future, once again proves the need to understand the connection and transformation methods between the calculation methods of large, Naval Architecture associated problems and local, structural mechanics driven analysis.

The successful transformation of real-world primary bending stress data to continue analysis at a local level depends on certain assumptions that will be discussed in detail in the next Chapter. The process for this is relatively simple: Assume a uniform worst case axial stress exists over a particular shell edge effective area for a given stiffened panel and with simple calculations the load supported by that panel can be determined. Chapter 5 uses this premise to examine different proven methods of analysis of a replica stiffened side shell panel from the 123' and then validate associated experimental and operational results.

Chapter 5: Local Analysis of 123' Side Shell Paneling

The previous chapter of this thesis focused on the analysis of the design for the 123' and the 179' conversion as a whole, and the failures seen on board each vessel. Furthermore, it compared each of the failure modes based on visual clues provided in photographs and good engineering practice. This chapter will take that analysis one step further just for the 123' conversion, bridging the gap between real life failure and mechanics theory by examining localized response at the panel level due to the excessive loading seen throughout the ship.

5.1 The Local Response –Axially Loaded Panel

The 123' is a primarily longitudinally stiffened vessel with three inch longitudinal stiffeners spaced 18 inches apart supported by transverse frames 46 inches apart. Upon construction, the ship met all requirements for bulkhead placement and compartment standards based upon requirements set forth by the United States Coast Guard construction contract. After the ship experienced significant structural failure, as described in the narrative at the beginning of Chapter 4, the ship's structural integrity was reexamined and additional tests were done to try to understand what had gone wrong. These included a full ship FEA analysis which tried to recreate failure under the same set of parameters, laboratory crush testing of a "test panel" nearly identical to a panel found on frame 23-24 of the Matagorda where failure occurred, and re-(hand)-calculation of strength information amidships. The test panel isometric drawing submitted by the Coast Guard to the U.S. Naval Academy for testing can be seen in as Figure 7.

In order to validate the way the local response actually occurs in a particular mode of testing, it is important to examine how large scale shipboard loading due to static conditions and those found in a sea way can be related to a single panel. As discussed before, the cross section of a ship can be likened to a beam, and therefore as the beam is subjected to a bending moment, compression and tension develops. In heavy seas, there are torsional and horizontal moment forces acting on a hull, but these moments are usually orders of magnitude less than the calculated vertical bending moments (5). If the beam is in effect "smiling" as in the shipboard sagging scenario, a positive moment is applied. This creates increasing compression above the neutral axis and tension below the neutral axis. In the actual events, each ship failed at the deck level also at the top of the side shell along the freeboard amidships. This is the farthest location from the neutral axis and keeps with the results of the stress Equation 6, which uses the distance from the neutral axis in the numerator while maintaining a constant, geometry driven denominator. This correlation allows a piece of shell plating of a sagging hull to be modeled as a stiffened panel subjected to a constant, uniform axial load. In reality, as the distance to the

neutral axis shrinks, the stress (and therefore the axial load) also decreases, leading to linear distributed axial shell loads.

In addition to axial load seen on the panel, shearing is also present. This type of shear is only the result of planar bending. The shear stress formula is noted as Equation 8 in Chapter 1 and has requirements under the "rules" (11). Inverse to axial or normal stress, shear stress is negligible or zero at the farthest distance from the neutral axis along the centerline of the vessel and increases as the distance decreases to a maximum at the neutral axis. In order to conduct worst-case axial stress scenarios under a variety of conditions and parameters, a constant edge axial load in FEA and theoretical work was applied to simplify the process. In experimental testing of panels with b/t ratios similar to those examined in this study, shearing of this nature had very little effect on the overall strength and can therefore be essentially neglected (5).

5.2 Panel Analysis

Using the information and testing already completed by the United States Coast Guard and its subcontractors on panel sections in question in the 123', it is of particular interest to look at similarities between actual testing completed, computer-generated FEA analysis (in buckling and ultimate load) and theoretical calculations based on proven plate and stiffened panel theory.

Material Properties

The plate in question is made of BS 4360 Steel. BS 4360 is classified as mild steel and is of British origin. It is a well known structural steel that is used extensively due to its superior weldability. Construction applications include:

- Ships
- Rolling stock
- Petroleum storage tanks
- Containers

A brief description of the material properties and chemical composition are below in Table 8:

BS 4360 Grade Structural Steel Properties & Chemical Composition			
Material Properties		**Chemical Composition (Max %)**	
Thickness Considered	#5 Plate (.112 in)	C	22
Young's Modulus	2.96E+07	Si	50
Poisson's Ratio	0.3	Mn	1.6
Yield Stress	40,000 psi	P	0.05
Ultimate Strength	58,000 psi	S	0.05

Table 8: BS 4360 grade steel material properties, and basic chemical composition.

This type of steel is a common in construction and has performed well in a variety of different marine and land based applications. A more detailed review of BS 4360's material properties can be seen as part of Reference (49).

5.2.1 Boundary Conditions

When examining boundary conditions on any kind of analysis it is important to not only keep in perspective what is trying to be accomplished but also if the boundary conditions make sense under given circumstances. Boundary conditions can dictate enormous differences in both theoretical calculations and finite element approaches and usually cannot be absolutely accurately re-created in experimental scenarios. All of this aside, what boundary condition scenarios are correct in the instance of the 123' side shell panel? The boundaries are obviously not free but are they clamped, simply, simply supported, or a combination of the two? To rationalize how the answer can differ based boundary conditions alone, it is easy to use the theoretical load calculation for a plate under compressive load. In this case, the critical load equation (seen in Chapter 3 as Equation 31) is identical except for changes in the k_c factor based on boundary conditions. This factor, when used in conjunction with Figure 12, denotes extreme differences in buckling load simply based on what boundary conditions are introduced. The introduction of stiffeners and other complexities under different boundary conditions only adds to the different load carrying capacities and provides the need for accurate assessment that much more.

Boundary Conditions on the 123' side shell

The "test" panel piece submitted by the Coast Guard is a 32" x 94" orthogonally stiffened panel. In some instances (with regards to this study) it was modified to slightly smaller (reasoning to be subsequently discussed) dimensions of a 32" x 46" longitudinally stiffened panel with appropriate boundary conditions to account for removed transverse stiffeners. In either case, there are two distinct sides. These sides are comprised of the loaded edges, which are the vertical edges along the vertical frame edges and the horizontal edges, which run along the length of the ship between the transverse frames. The top horizontal edge comes relatively close to the aluminum-steel explosion weld which attaches the side shell and deck edge to the aluminum deck. In this case, the boundary condition would fall somewhere in the simply supported realm. The edge is clearly not clamped down but it also is clearly not rotationally restricted in every direction or simply pinned to limit its range of motion. Similarly, the bottom horizontal edge's nearest longitudinal stiffener is 11 inches away and there are no other stiffener systems in the vicinity. Therefore, it is plausible to say that this edge falls in a variation of simply supported. Tables 9 and 10, seen on the following page, give the best possible boundary condition scenario using engineering knowledge of the ship system, named condition "Alpha."

Condition Alpha Loaded	
Ux	Free (to be loaded)
Uy	Pinned
Uz	Pinned
Rx	Pinned
Ry	Free
Rz	Free

Table 9: Loaded Edge Profile

Condition Alpha Unloaded	
Ux	Pinned
Uy	Pinned
Uz	Pinned
Rx	Pinned
Ry	Free
Rz	Free

Table 10: Unloaded Edge Profile

In this case, U is displacement and R is rotation. The x-direction is the direction along length of the hull, the y direction defines the breadth, and the z-direction quantifies the depth of the hull. It must be noted that this is a slight deviation from what is commonly used in stiffened panel theory, but it is intended to apply in this situation only where a portion of plating with stiffeners is examined. When dealing with a simple plate that is bounded on all four sides with longitudinal and transverse stiffeners and loaded axially it is commonly accepted to assume a simply, simply supported specimen. When applicable, the "Alpha" boundary condition will be used but in certain cases, (especially in the analytical analysis) a simply, simply supported or simply supported, free boundary condition is used for simplification purposes.

5.2.2 Methods of Analysis

The three methods of analysis to be examined are all very different but provide some clue as to not only how strong each panel or plate is but the mode of failure and how failure strength and mode can change based on analysis methods and boundary conditions.

Experimental Analysis

Due to limitations of money and material, no large scale experimental testing could take place for this study. Instead, the actual experimental part of this study will focus on the experiment already done and how the test panel relates to theoretical work and Finite Element Analysis of similar variations of the test panel. The test panel is made up of the same type of steel and has nearly identical geometric shape of a panel seen on the 123' built in the Bollinger shipyard. Of course the residual stresses due to forming and construction or other strength reductions due to eccentricity are different and dynamic loading is not considered.

The experimentation was completed (as previously mentioned) in the mechanics lab at the United States Naval Academy in Annapolis, MD. The testing was supervised by Dr. Jeffrey W. Stettler, USN and Mr. Paul H. Miller, Associate Professors in the Department of Engineering. The test took place in July 2006 (7).

The experimental setup included the test panel given to the Naval Academy from the United States Coast Guard. The panel's construction follows the U.S. Coast Guard drawing # 123-WPB-TEST-PANEL. This drawing can be below as Figure 36:

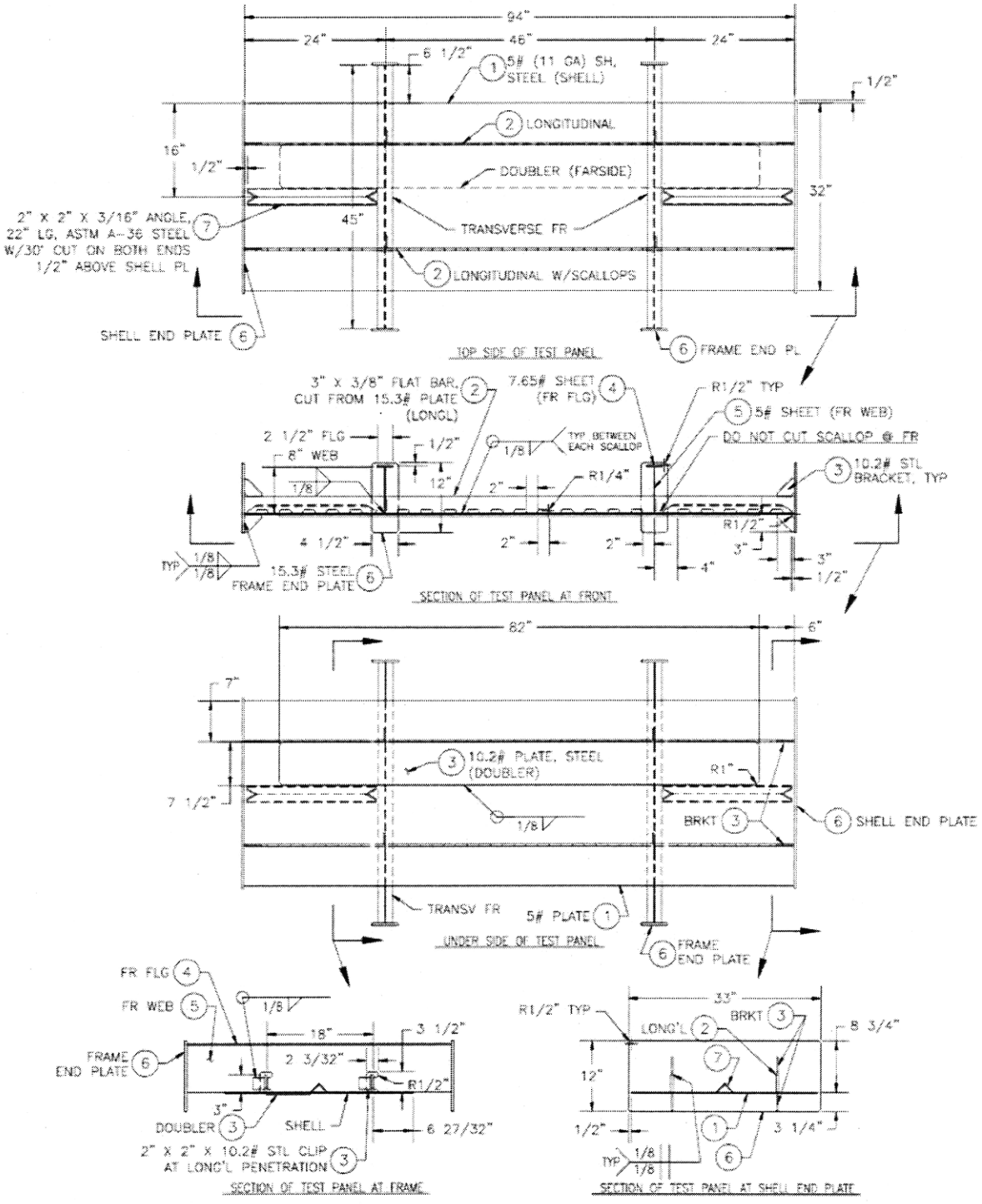

Figure 36: U.S. Coast Guard Construction drawing of the Test Panel used in the July 2006 U.S. Naval Academy Test

The test panel is not identical in every aspect to that seen on the cutter. There were several modifications made by the Coast Guard for testing purposes in hopes that the test would cause buckling to occur in the middle of the test panel along the 18" x 46", 0.112 inch thick plate. This was accomplished by adding angle pieces in both end bays and triangle brackets connecting the pressure plates to the longitudinal stiffeners. The experimental setup was rather simple, using a compression loading frame provided by the Naval Academy. The loaded sides were bolted to the test apparatus in a type of "simply supported" setup while the unloaded edges were essentially free, although there were stabilizers seen on the ends of the transverse frames. The transverse frame spacing (with measurements shown in Figure 36) is 46" while the spacing between longitudinal stiffeners is 18". In addition, strain gauges were added at strategic locations to determine local stress at specific locations. Figure 37 below shows the experimental setup:

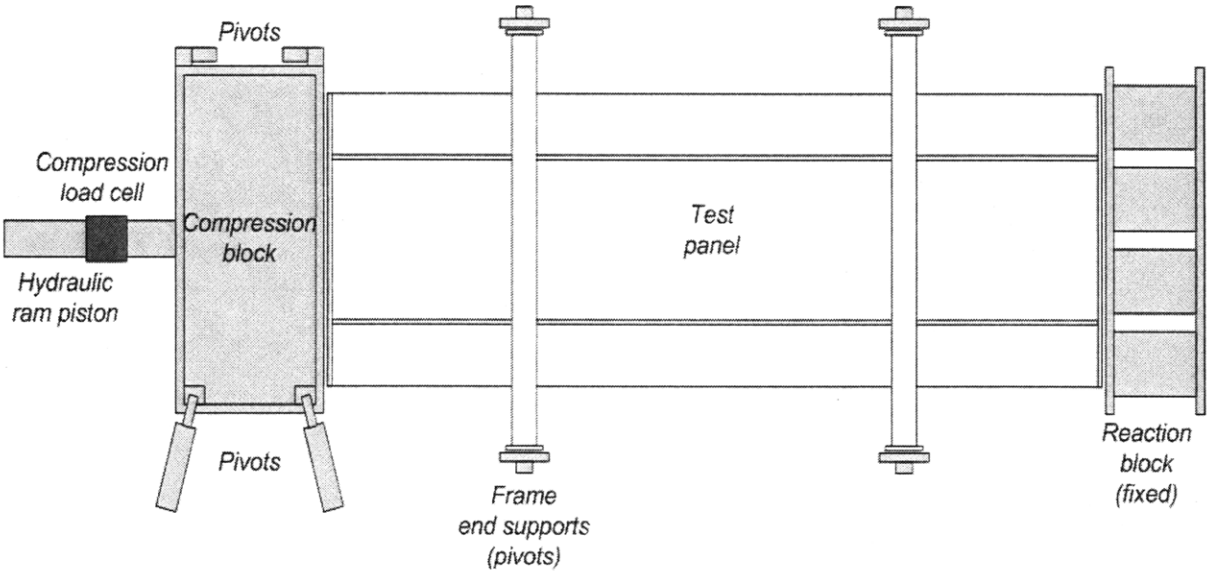

Figure 37: Test configuration as drawn by the U.S. Naval Academy testing team.

The experiment was conducted in two phases. The United States Coast Guard speculated through their own, independent FEA analysis, that the panel could withstand approximately 66,000 lbs of compression force before failing. Due to this prediction, initially the panel was loaded to 47,000 lbs and held to ensure plate integrity. Following the initial test, the panel was re-loaded to failure at a 0.01 in/sec rate of strain. The test resulted in the panel failing after local stress concentrations caused welds to fail in one of the end bays. This occurred at approximately 176,000 lbs of force. This was significantly more than was predicted by the Coast Guard for a simply supported - free condition but it must be noted that the boundary conditions seen were by no means ideal (7), nor was loading entirely symmetric due to the doubler. The boundary conditions can better be described as a simply supported – free modified condition where each of the frame end supports is simply supported and the edges are left free.

In the end, the experimental testing was successful, although it did not buckle in the center bay where the Coast Guard desired. Instead, it failed in one of the end bays due to stress concentrations and weld failure as compression took place. Furthermore, inconsistencies were noted in the strain gauges and displacement potentiometers, even while the panel was in pure axial compression with simply supported loaded edges. The report furnished to the Coast Guard discusses this may have been the result of the design-based decision to place the doubler plate away from the panel centerline and initial imperfections and deflections in the material during the construction phase, all unquantifiable uncertainties at the time of the experiment (7). Due to the imperfections and the relative resistance to compression loading at the doubler region as compared to the rest of the panel, the panel may have experienced load eccentricity resulting in a bending moment induced by the simply supported loaded edge.

Regardless of these results and the attempts of the Coast Guard to induce failure in the center bay, the experimental testing of the mock side shell plate was successful for the means of this comparison study. Its results give the approximate magnitude of the ultimate load, where failure occurred, a glimpse into the failure modes, and an idea of how boundary conditions can significantly change experiment outcomes with very little variation. The additionally relevant strain gauge and potentiometer curves with commentary can be seen as part of Appendix 5.1.

Finite Element Analysis

The purpose of the detailed finite element analysis (FEA) of the stiffened panel in axial compression was to provide a contribution to the analysis of the 123' structural issues by an independent source. Furthermore, it was to create an academic examination of the trends of steel stiffened panels used in ship construction in an elastic-plastic environment subjected to axial compression with initial imperfections.

It should be noted that a full finite element model of the 123' was created by BMT Design and Planners for the Coast Guard Technical Authority in order to try and recreate failures seen on a global level and to propose global-level solutions to the issues outlined in section 4.4. The study was headed by Dr. Pradeep Sensharma and supervised by the D&P Director of Engineering, Dr. Malcolm Willis. Although the report submitted did discuss the buckling characteristics due to static and wave loads of the ship and larger panel sections, they did not explicitly look at the test element or complete any comparison analysis. The report is noted as Reference (18).

To provide a better platform for a parametric study of design, only a portion of the FEA analysis actually used a geometrical replica of the test panel the U.S. Coast Guard built for testing. Other facets of the FEA analysis essentially used cropped versions of the plate section

and included only one transverse frame length with longitudinal stiffeners. This cropping allowed for smaller modifications to have a larger overall effect and provide a more viable study. ABAQUS/CAE Version 6.8 was used to conduct all of the model analysis, however the software programs Rhinoceros 4.0 and Hypermesh 8.0 were also used to build and modify some of the models, respectively. The series of three screenshots show the model built in Rhinoceros, modified in Hypermesh, and the resulting imported meshed geometry in ABAQUS for testing.

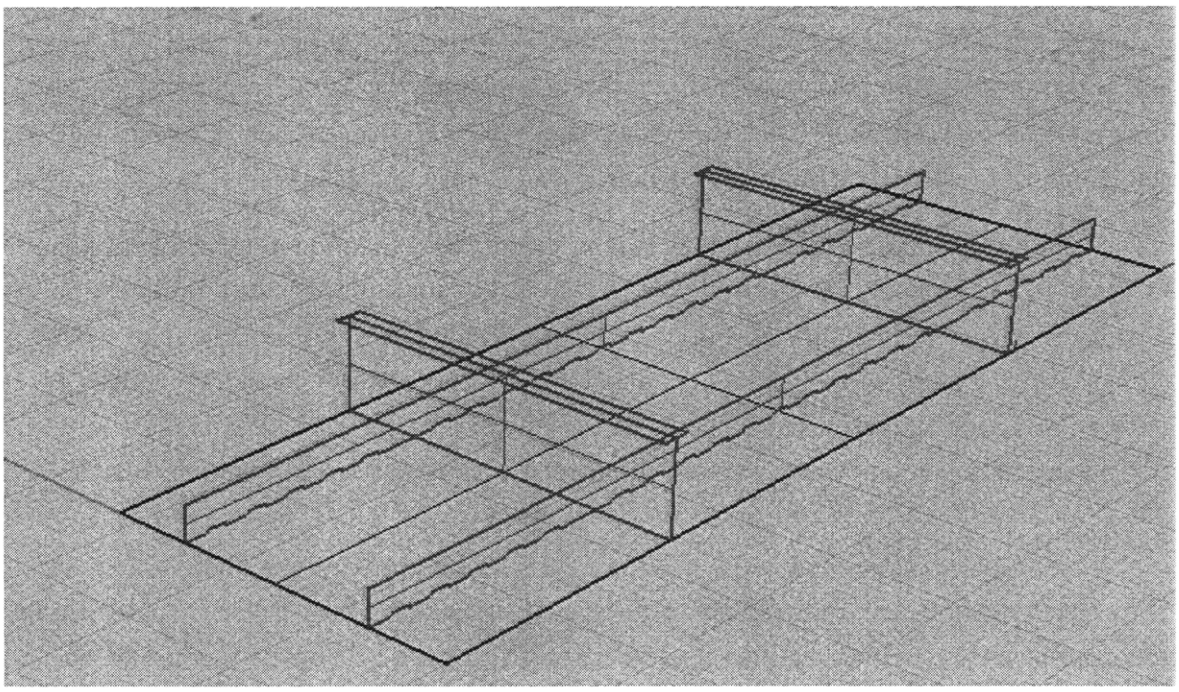

Figure 38: Rhinoceros screenshot of the experimental plate shortly after the modeling was complete.

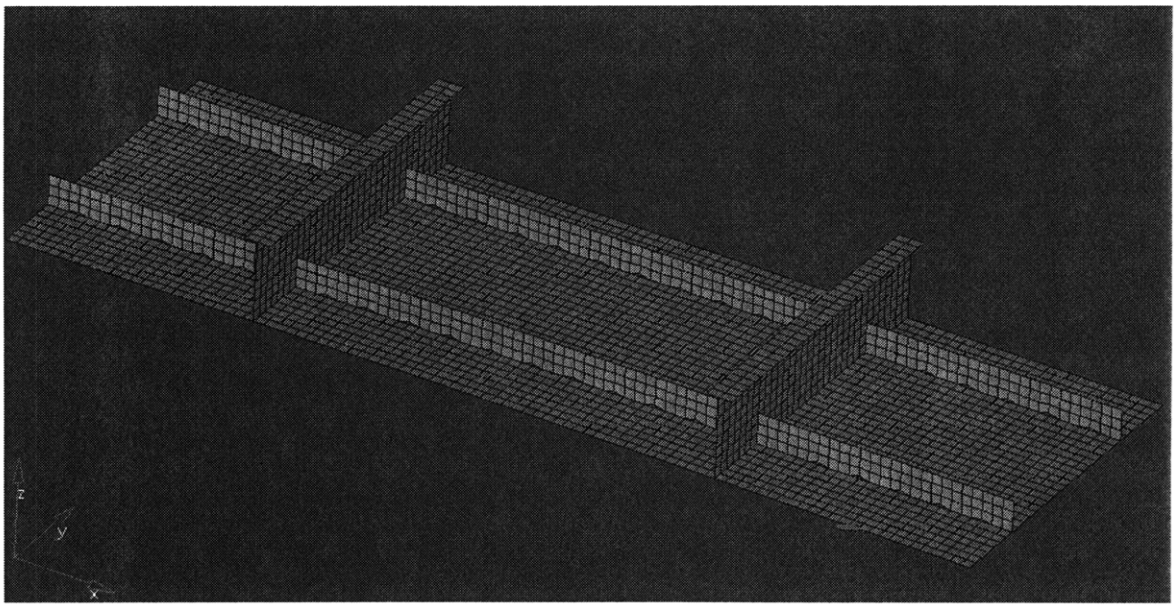

Figure 39: The mesh was created and nodes brought together within tolerance as seen in this screenshot from Hypermesh.

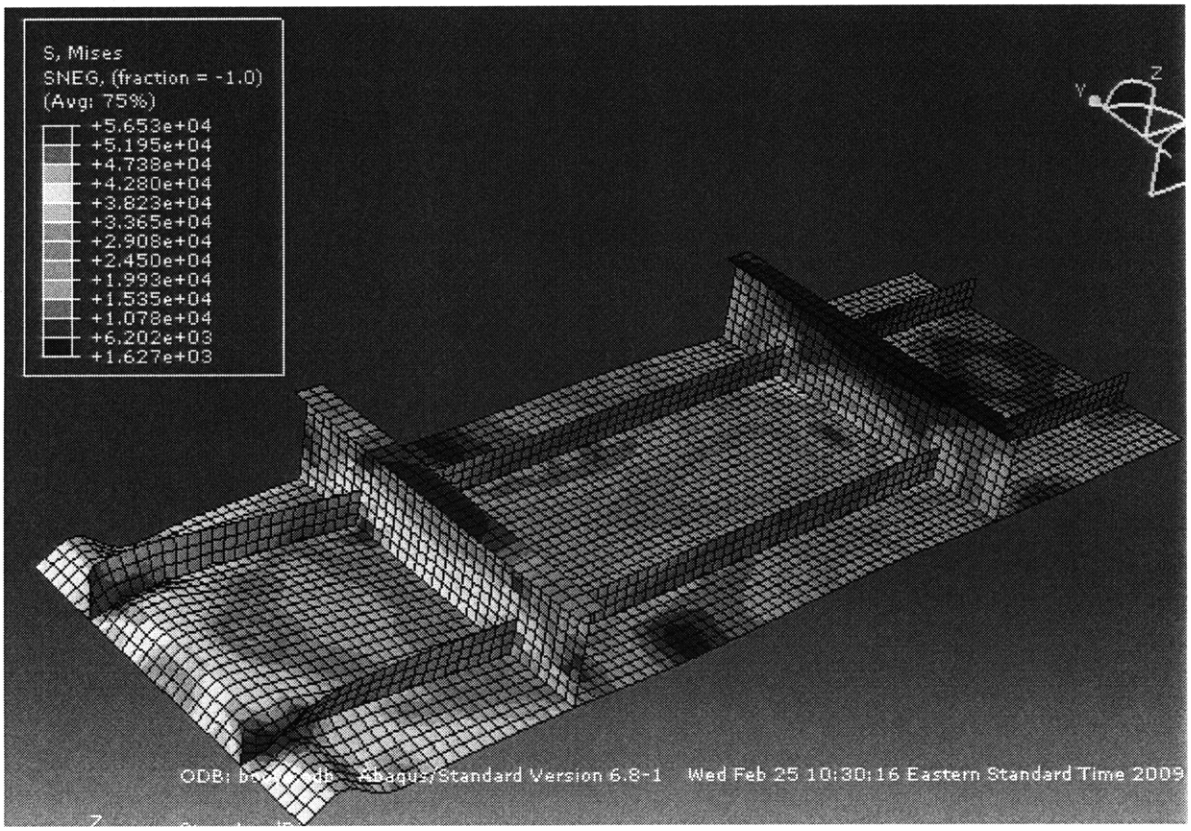

Figure 40: Screenshot of ABAQUS results an axial loading scenario with a displacement of 1.1 inches. Note this FEA solution has striking similarities as compared to the pictures seen of experimental results later on.

The figures above show a representation of the parametric study. As discussed, both cropped plates and full length models were used. The study examined both combinations, number of stiffeners and thickness adjustments. Unlike design, the original placement of the longitudinal and transverse stiffeners and their relative size had to remain because they already exist in place. A change in plate thickness in certain areas, addition of doubler plates (the addition of doubler plates are discussed in section 4.2 pertaining to hull history) or addition of extra stiffeners over a certain portion of the hull would potentially be the only viable solution.

Once the geometry was entered into the ABAQUS solver either from Hypermesh or from the programs own sketching software, inputs were applied to run each test case. The inputs for the stiffened panel buckling module included the following:

- Import part geometry using any/all available drawings and sketcher.
- Identify the appropriate material for use (in this case BS4360 steel) and input elastic and plastic characteristics.
- Define and assign different sections of the shell geometry and assign thickness as per the study.

- Create a test "instance" in order to prepare the program to create a mathematical mesh and a testing scenario.
- Mesh the model using 1" square structured meshes.
- Create a test "step" which defined the type of module to use in testing.
- Assign boundary conditions as per testing criteria.
- Assign shell edge load as per testing criteria.
- Create a job and submit it for analysis.

Initially, the different combinations of panels and plates based on the experimentally tested model and actual 123' side shell were tested using the ABAQUS Buckle module in a purely elastic mode. Different combinations of boundary conditions were used, including the most probable for a side shell piece that is part of a hull, as noted in section 5.2.1. Due to the large amount of raw data collected using this module within ABAQUS, the complete set can be seen in Appendix 5.4.

Once the elastic buckling loads, buckling modes and comparison data was accumulated, it was important to examine load-displacement characteristics of the different plate and boundary conditions based on the elastic-plastic characteristics of the BS 4360 steel. The data collection procedure for the FEA analysis was very similar to that of the buckling analysis, however a different "step" module was used (Static, General and Static, Riks instead of Buckle) and specific node "sets" were defined in order to follow specific displacement and force pathways. The fundamental difference between the Static, General module and the Static, Riks module is in the way that the mesh calculations are completed. While Static, General uses time as the step increment, Static, Riks uses an arc measurement as the step increment and as a result has more potential variance which allows for extremely complex meshes to be computed. ABAQUS/CAE Documentation provides a thorough explanation of how FEA analysis is completed, and will not be repeated here (50). Further information on this topic can be seen in Appendix 5.2. As a general check and to prove the effectiveness of both load-displacement methods, a comparison between Static, General and Static, Riks was completed and any differences noted.

The load to displacement data was collected by requesting History Outputs from ABAQUS/CAE. A single node was selected to represent the history of displacement in the U1 (x) direction while the sum of the force exerted on the edge nodes represented the load in the RF1 (x) direction. All of the Static, General outputs were created with Time (seconds) as the dependent variable and load (lbs) and displacement (inches) as the independent variables. To mimic the experimental setup, an edge load was applied to only one of the two longitudinal edges while the opposing edge was pinned in the U1, U2, and U3 directions but left free to rotate. These ABAQUS/CAE outputs were transferred to internally created report files as data

arrays and time was eliminated to create the load-displacement curves. As before, all the transformations occurred within Excel due to ease of comparison and further discussion.

After "perfect" (i.e. modeled with no blemishes in FEA) stiffened panel's load-displacement curves were compared and strengths assessed, a simulation of potential initial deflections was completed by providing a sinusoidal lateral pressure load creating a out of plane displacement which would be equivalent to 1% of the thickness on an 18" x 46" inch simple plate. This was repeated for a displacement equaling 10% of the thickness and then an estimated load was extrapolated out based on ultimate load for the actual stiffened panel used in the experimentation process for a simply supported case.

Analytical Analysis

The calculations performed by hand are in accordance with the plate and stiffened panel theory discussed in the appropriate sections of Chapter 3. The analytical calculations were completed to not only try and prove consistency with the FEA analysis, but also to relate classroom governing-equation theory to real life situations. Simple plate theory calculations cover not only the critical buckling load but it also it defines the appropriate number of wave responses based on the length to width relationship, which can have a profound effect on the load it can take. Below is a representation of the wave response for each plate size and the corresponding k_c factor for several boundary conditions in the analytical realm, including variations of clamped conditions for comparison purposes.

Wavelength Number & Kc Response: Analytical Theory					
Boundary Condition		18" x 46" Wave		32" x 46" Wave	
Loaded	Unloaded	Response	Kc Factor	Response	Kc Factor
S. S.	Free	1	0.2	1	0.4
S. S.	S. S.	3	4.1	2	4.45
C. C.	C. C.	3	7.7	2	8.75

Table 11: Wavelength Number and Critical Value Response generated using analytical methodology. It is important to note that a change in the number of waves under given boundary conditions can significantly affect the buckling strength of the plate. Using an inexact (though highly accurate) method such as FEA might present such an issue as seen later on.

Using these correlations as a guide, simple plate buckling calculations were completed for 18"x46" and a 32"x46" simple mild steel (BS 4360) plate using the non-smear drawing thickness of 0.112 inches. These plates were analyzed under a variety of applicable boundary conditions in accordance with analytical equations discussed in Section 3.1.2. For plates with any number of clamped boundary conditions, it is impossible to achieve a closed analytical solution and therefore Figure 12 in Chapter 3 is used as widely accepted analytical solution tool.

Boundary Conditions		Analytical Calculations based on Plate Buckling Theory			
Loaded	Unloaded	18"x46" (h=0.112)	18"x46" (h=0.212)	32"x46" (h=0.112)	32"x46" (h=0.168)
S. S.	Free	296.5	2,010.9	528.5	1,783.9
S. S.	S. S.	8,569.0	58,114.2	5,229.5	17,649.0
S. S.	C. C.	14,512.3	98,421.2	8,221.9	27,748.8
C. C.	S. S.	9,292.0	63,017.9	6,342.6	21,406.2
C. C.	C. C.	16,078.3	10,9042.2	10,277.4	34,686.0

Table 12: Analytical Results from Plate Buckling Theory. All values are expressed in Pounds

In addition to the baseline thickness of the plate prescribed by the drawing, the buckling strength of the plates was compared to plates with the doubler plate smeared. These new thicknesses amounted to 0.211 and 0.168 inches for the 18"x46' plate and 32"x46" plate, respectively. The calculations are detailed in Appendix 5.6.

Although simple plate theory provides a good stepping stone into stiffened panel theory it is still important to move to the more complicated stiffened panel analytical approach. The stiffened panel used in the analytical analysis is a representation of the 32"x46" panel with two longitudinal stiffeners, representing the experimental panel between the transverse stiffeners. Per discussion of stiffened panel theory in Chapter 3, only one applicable boundary condition was examined as Hughes (5) and Paik et al. (28) report Euler column buckling theory to be an acceptable approximation method to determine (and rule out) buckling in the overall mode. Using Euler ideal column buckling theory of a plate-stiffener combination, the buckling values were calculated to be as follows for a baseline 32"x46", longitudinally stiffened panel and variations:

Euler Buckling Load: Basic Column Theory		
# Stiffeners	Plate thickness = 0.112	Plate Thickness = 0.168
2 Stiffeners	584,479	584,479
3 Stiffeners	876,719	1,014,824

Table 13: Results Based on Ideal Column Theory. All units are in Pounds.

Right away it is clear that the buckling loads are extremely high (in fact, it will be shown that these loads are higher than the ultimate load of the stiffened plate). The simply supported edge, where the transverse stiffeners would exist, is a widely accepted approximation in the structures community. Analytically, the plate-stiffener combination method is modeled assuming elastic buckling occurs in the overall mode.

Using this analytical approach to calculate stiffened panel buckling load clearly does not yield results within acceptable parameters. This is verified by FEA representation of the panel,

shown in pure elastic buckling. In this representation, it is clear that the panel first experiences local sub-plate buckling between the longitudinal stiffeners, seen below in Figure 41

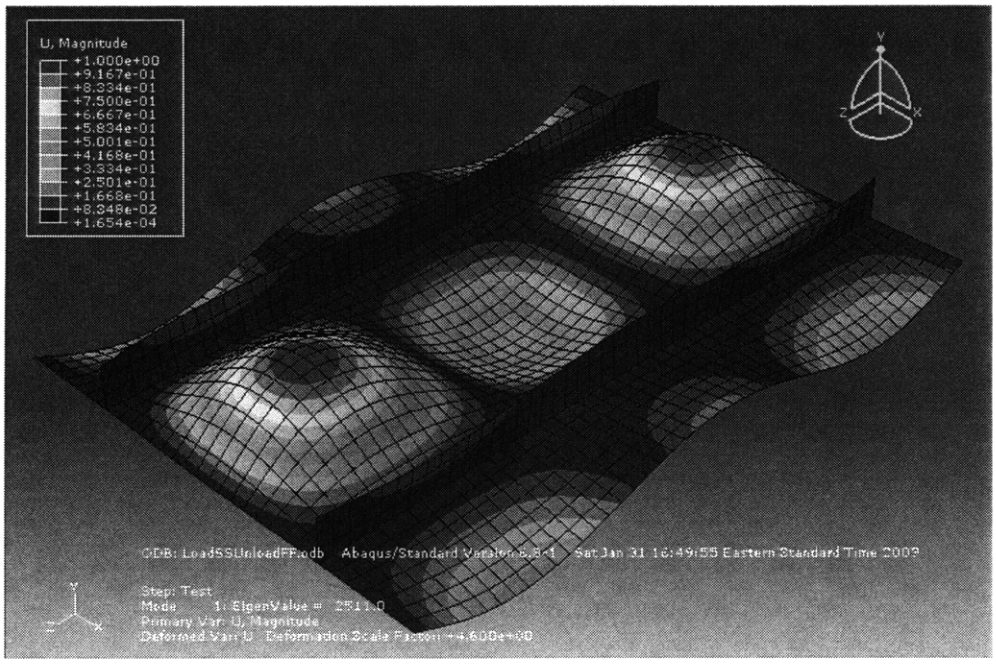

Figure 41: FEA Analysis of the 32" x 46" stiffened panel buckling showing buckling occurring due to plate failure. This is indicative that overall buckling will take place post overall first mode failure which is desirable in stiffened panel design. The FEA also shows that the plate will most likely behave as a combination of three smaller plates as it buckles in a 3 wave mode.

Here, the stiffened panel is better modeled by applying simple plate buckling theory to the three smaller plate sections and adding the resultant buckling load. By splitting the plates, the resultant plate dimensions include one 18"x46" center plate, and two 7"x 46" edge plates. This method is explored for a stiffened panel simply supported on four sides and a panel with free unloaded edges based on the boundary conditions seen in experimentation. k_c for the center plate is always calculated assuming simply-simply supported boundary conditions based on accepted practices. The results are seen below in Table 14:

Stiffened Panel Buckling Analytical Data: Von Karman's Approach		
Boundary Condition: Four Sides Simply Supported		
# Stiffeners	Plate thickness = 0.112 in	Plate Thickness = .168 in
2 Stiffeners	51,522	173,888
3 Stiffeners	76,364	257,730
Boundary Condition: Loaded Edges SS, Unloaded Edges FR		
# Stiffeners	Plate thickness = 0.112 in	Plate Thickness = .168 in
2 Stiffeners	13,185	44,499
3 Stiffeners	38,027	128,341

Table 14: Stiffened panel buckling results based on Von Karman's plate addition method. All results are in pounds.

The calculations for these values were completed in spreadsheet form and can be seen, along with methodology, in Appendix 5.7. The solutions above are much more reasonable than the values calculated using overall mode column buckling theory, and can be compared more readily to simple plate analysis, experimentation, and FEA results.

To better understand how the addition of stiffeners affect the elastic buckling load, the chart below shows the change in buckling load across simple plate and stiffened panel varieties with applicable boundary conditions for original and smeared plates. The chart also shows the relative increase in buckling strength of the stiffened panel variations due to the addition of the doubler plate. The stiffened panel results are based on simple plate and Von Karman's approach. The values seen in Figure 42 only show results for the simply, simply supported plate and panel and the simply supported, free (Euler) plate and panels. In some cases, the calculated buckling load exceeds the approximate ultimate load (and obviously the yield point) but these values are still shown for consistency.

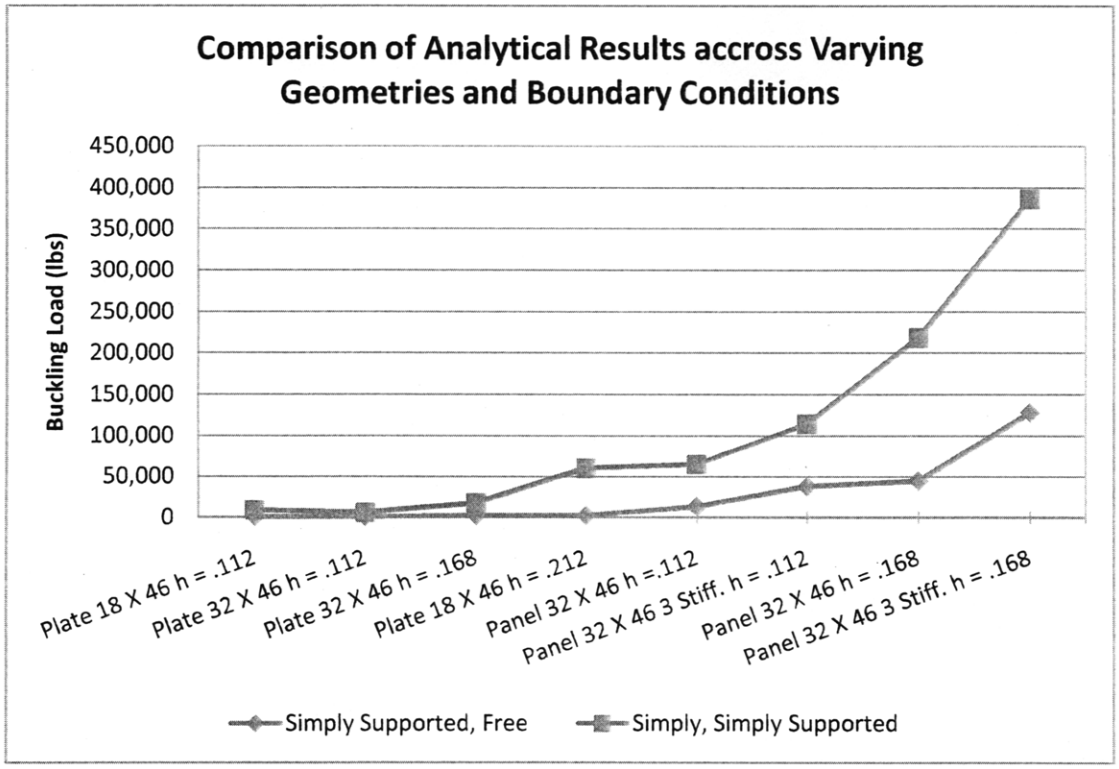

Figure 42: Comparison chart for analytical calculations completed using simple plate theory and Von Karman's approach. In the last four entries is particularly obvious how much the addition of the doubler plates helps overall plate strength.

Using simple plate theory and subsequent stiffened panel theory, it is possible now to extrapolate these results in the context of the Coast Guard's experimental plate with transverse and longitudinal stiffeners. Transverse stiffeners in this role must have a minimum rigidity to provide near non-defecting support to the stiffeners and plate as a whole to prevent grillage

buckling. In this case, structural engineers Timoshenko and Gere (50) developed specialized solutions to ensure proper transverse stiffener rigidity to prevent failure for various numbers of longitudinal supports. This calculation verifies that the transverse stiffeners on board the 123's meet the necessary criteria. This is further validated by experimental results and actual damage on the ship (overall grillage buckling did not occur in either case).

Once all the buckling load calculations were completed, an analytical solution was developed for ultimate load using BS 4360 material data and Von Karman's effective width theory. The effective width of the plate in the combination was calculated based on this method, discussed in Section 3.2. The effective width theory was applied assuming two different size base plates to examine the relative differences and to uncover which assumed size best portrayed the actual plate behavior. 32"x46" and 18"x46" size plate specimens were used under the guise that the smaller plate would represent local plate buckling occurring first. Additionally, the thickness was varied to simulate a pre and post-doubler smear.

Once effective breadth was determined for each plate combination, the resulting ultimate stress for the stiffened panel was calculated by first determining the overall cross sectional area of the plate stiffener combination using only the effective width of the plate and the standard stiffener and applying it to Equation 43. This is diagramed below in Figure 43.

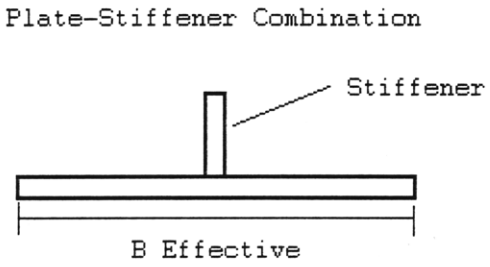

Figure 43: A sketch of the plate stiffener combination used for determining the Ultimate Load using Von Karman's method. The sketch is not to scale.

Even though Figure 43 is not to scale, it is easy to see that the extra area of the stiffener enables the plate to carry more of a load. For two stiffeners, this area is multiplied by two and ultimate load is determined. The results for effective width and its corresponding ultimate load can be seen on the following page in Table 15. Effective width was calculated using Equation 39 and the corresponding ultimate load using Equation 43, seen in Chapter 3. The ultimate loads calculated using this method are on the same order of magnitude as experimental results. Although limited FEA load-displacement work was completed using the "cropped" plate stiffener combination, a simple, one sample comparison of ultimate load was examined for continuity purposes.

Analytical Calculations of Ultimate Load (Von Karman)		
Geometry: 32"x46" Plate		
Calculation	No Doubler Smear: h = 0.112 in	Doubler Smear: h = 0.168 in
Effective Width	6.11 inches	9.16 inches
Ultimate Load	144,745 Lbs	213,110 Lbs
Geometry: 18"x46" Plate		
Calculation	No Doubler Smear: h = 0.112 in	Doubler Smear: h = 0.168 in
Effective Width	5.87 inches	8.8 inches
Ultimate Load	142,595 Lbs	208,272 Lbs

Table 15: Ultimate Load based on Von Karman's effective width theory is seen above. Note that both geometry and thickness is varied to provide a basis for comparison and validation.

The complete collection of analytical calculations can be seen in Appendices 5.6 through 5.8 and are completed in spreadsheet form. All of the results are incorporated into the graphical comparison representations that are summarized and shown in the discussion section or in the previously mentioned Appendices relating to this chapter.

5.3 FEA Results

The finite element results encompass three stages of review. These include simple Eigen-value buckling load calculations to get an idea of the order of magnitude and mode of buckling in each case, an extensive load displacement curve analysis using plausible boundary conditions as described earlier, and an elementary look at the effect of initial deflection when applied in an FEA environment.

5.3.1 Buckling

The initial finite element analysis of the buckling characteristics of the plates in question turned out as expected with a few interesting outlying points of interest. Figure 44, seen below, shows the basic geometry of a simple plate:

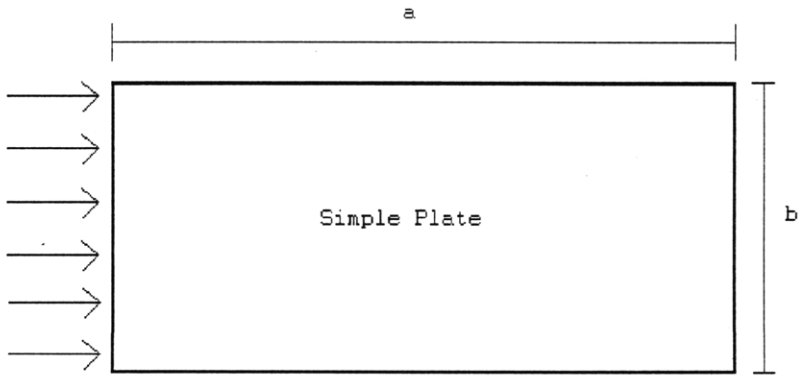

Figure 44: A sketch of a simple plate with a uniform axial edge load along the *b* edge.

In terms of Finite Element Analysis where instability dictates the lowest Eigen-value buckling load, it doesn't matter if the plate is loaded from both sides or only from one side, as seen on the previous page. The introduction of FEA helps to alleviate the issues that develop when more and more complex structures are analyzed. The graph below represents how the boundary conditions and variation of plate affect the critical buckling load within FEA. The data covers simple plates all the way to the buckling analysis of the experimental plate furnished by the Coast Guard.

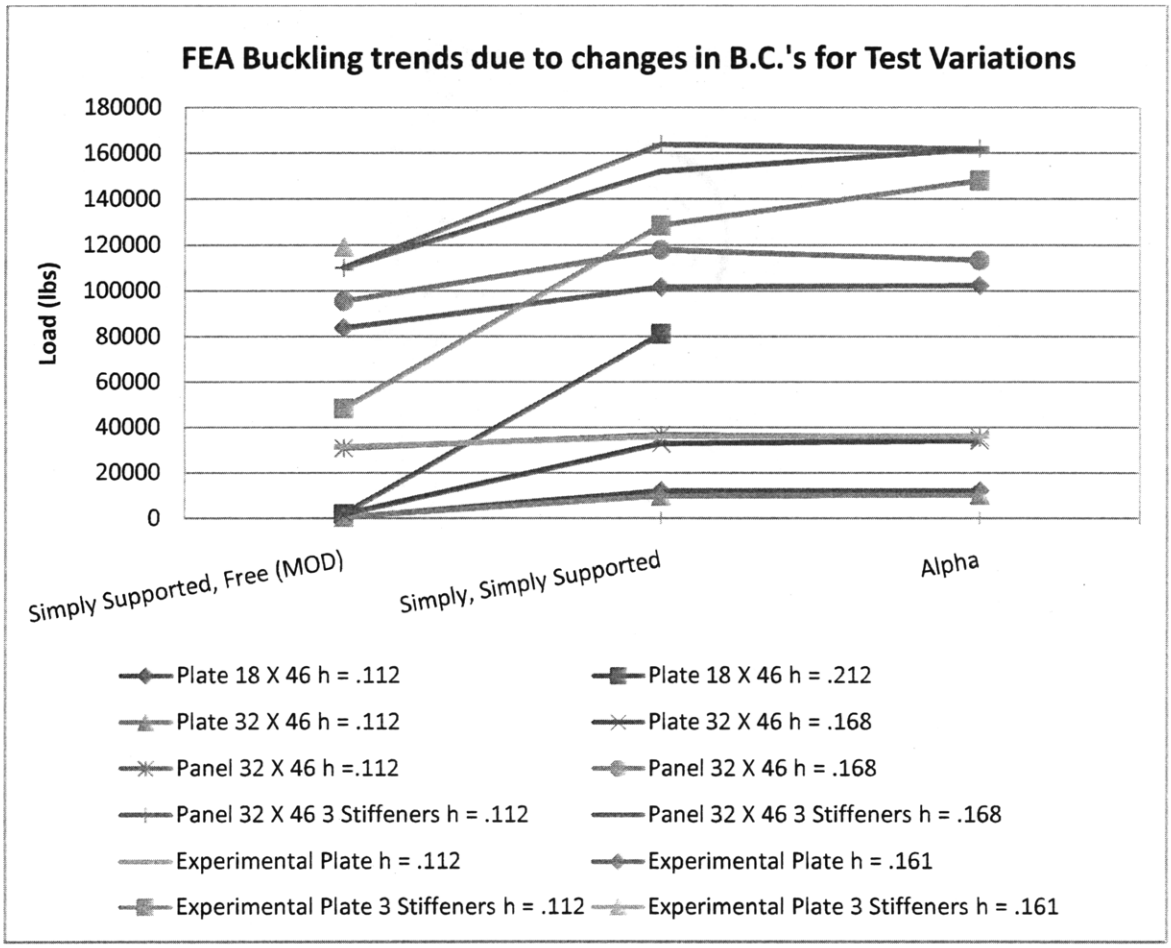

Figure 45: Boundary Condition trends for Finite Element Calculations. In some cases, the buckling load is actually less for boundary condition alpha than the simply, simply supported scenario. This is the case because the mode of buckling changes with the more restrictive boundary condition. In addition, several data points were removed due to outlier conditions.

In Figure 45, note that both the boundary condition trend and magnitude of buckling is nearly identical for the cropped 32"x46" stiffened panel and the actual experimental panel for smear and non-smear variations. This validates the use of the cropped plate for an overall strength analysis. The raw data table, calculations pertaining to how parameters were chosen and accounted for in the study and additional visual results for pure elastic buckling load can be seen in Appendices 5.3 through 5.5. The actual test panel in buckling without the doubler plate smear can be seen below as Figure 46. The boundary conditions in this case were the simply

supported, free (modified) version which best re-creates the boundary conditions seen in the experiment.

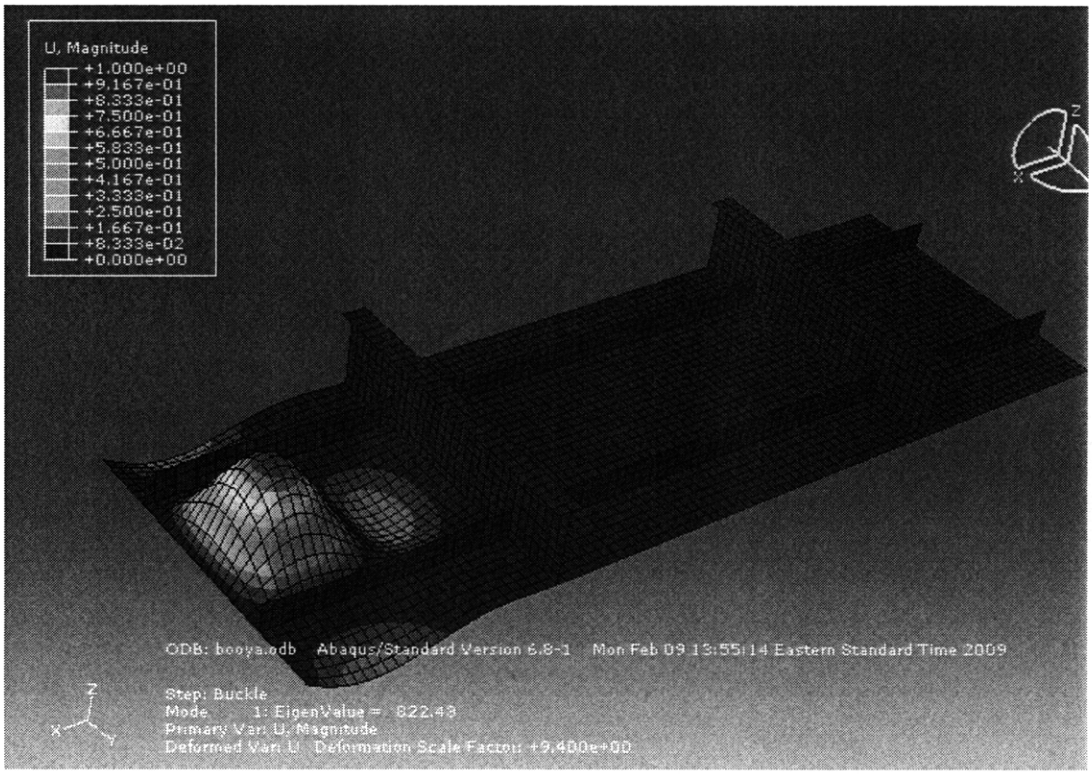

Figure 46: FEA buckling of the experimental plate with Simply Supported, Free Modified Boundary Conditions and no consideration for a smeared doubler. Finite Element Analysis in simple buckling already indicates that buckling and/or failure will occur in the end bay, rather than the center.

In this particular situation, the buckling load was calculated to be 31,252 lbs by FEA analysis. Due to the initial deformations, slack in the testing apparatus, construction inconsistencies, and potentially present residual stresses present in the actual experimental plate structure, the elastic buckling load calculation seen visually here in Figure 46 only serves as a guide to where the slope of the load displacement curve may (depending on yield characteristics) change from "K" to "K/2". For a real panel with this geometry however, this exact point is rather inconsequential because there will never be a hard "knuckle", as discussed in Chapter 3.

5.3.2 Load Displacement

In addition to examining the critical buckling load criteria in FEA, the load displacement curves were examined as noted in the previous section. Results of load-displacement curves were first examined both in the Static, Riks realm and the Static, General realm to ensure consistency. Figure 47, seen on the following page, shows this comparison with the boundary conditions to mimic those seen in the experimentation completed at the Naval Academy.

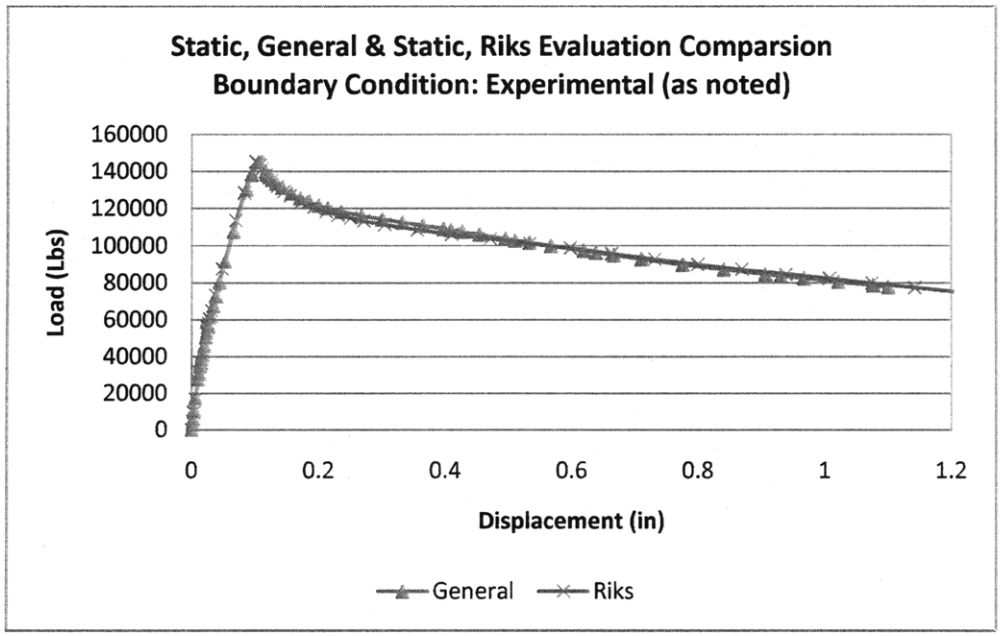

Figure 47: Correlation of Static, Riks and Static, General Mesh Techniques.

Figure 47 above not only proves that both methods are suitable for analysis; it also shows a mild transition from the initial elasticity into plastic deformation. This can be seen below, as the previous figure is blown up for analysis purposes.

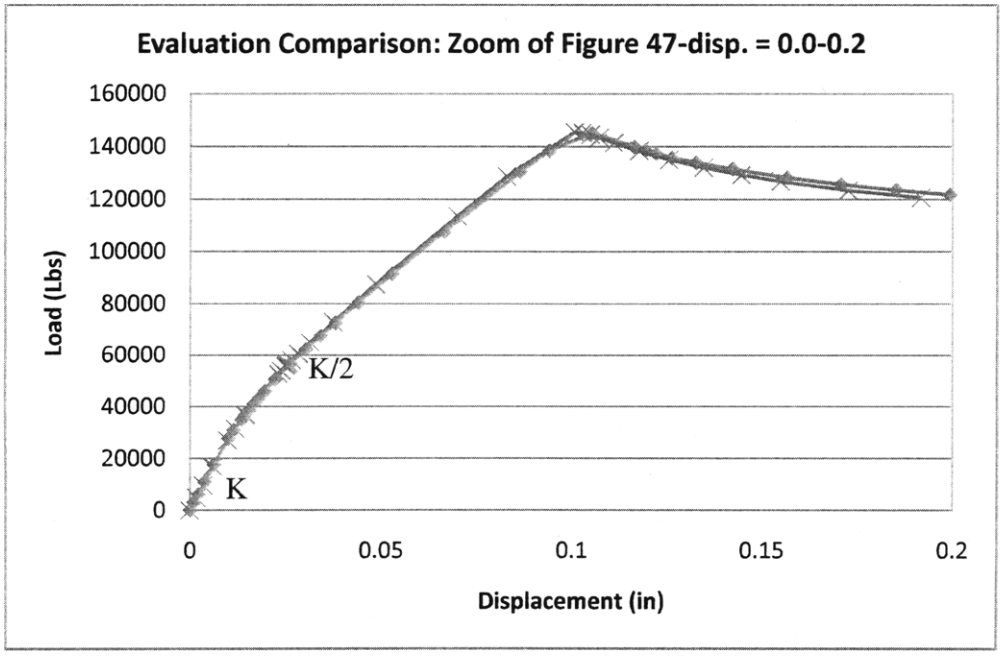

Figure 48: Graphical representation of Elastic-Plastic Plate theory created in FEA.

From the figure above, it is obvious that both methods correlate to each other and are within reasonable limits given the material, plate geometry, and loading conditions. The corresponding

visual depiction of the plate after undergoing the elastic-plastic deformation can be seen below in Figure 49:

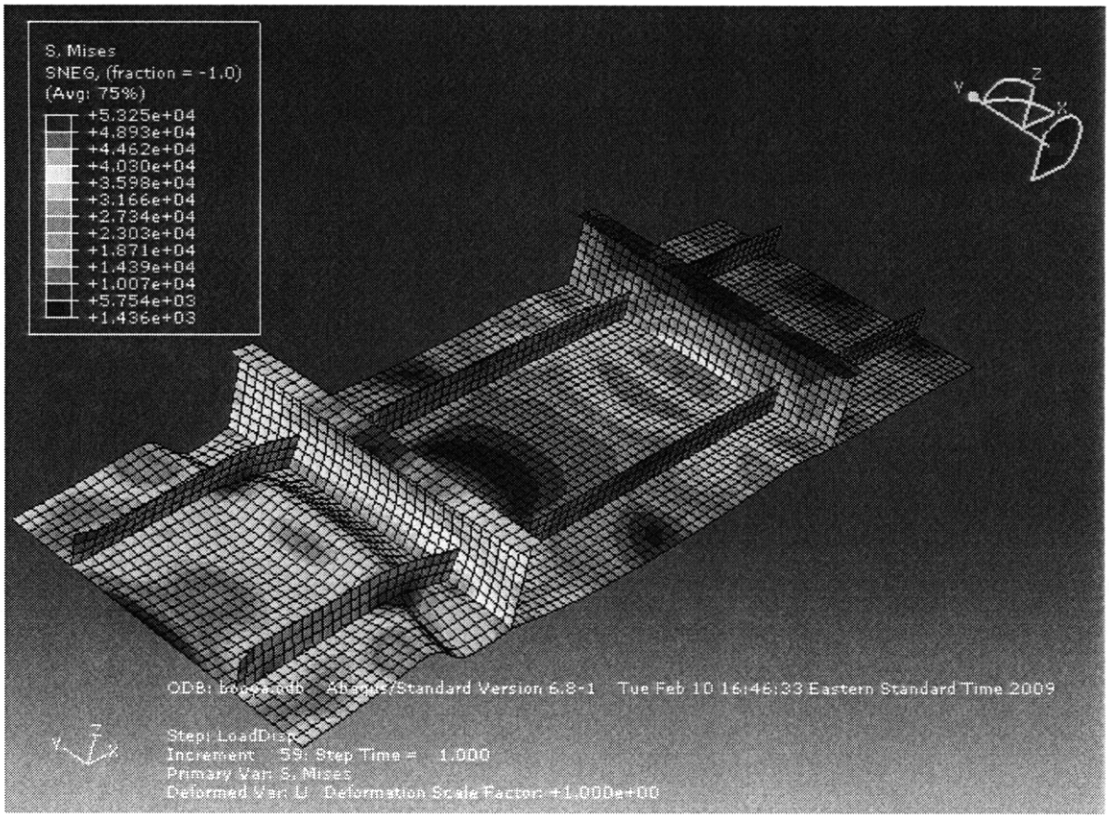

Figure 49: S. Mises Elastic-Plastic Analysis of the experimental plate. Displacement in the U1 Direction was 1.1 inches to correspond approximately with what was conducted experimentally.

The boundary conditions chosen above for the comparison are in accordance with the boundary conditions used in the experimental testing procedures. These are discussed in the first part of section 5.2.2. The colors seen on the figure above describe the distribution of Mises stress. As noted by the table on the upper most left hand corner of the figure, the stresses range from 53,250 psi (red) to 1,436 psi (blue).

Load displacement curves were generated for only three boundary condition scenarios, listed below:

- Experimental testing criteria (loaded edge and opposite edge simply supported)
- Simply supported criteria (all four edges are simply supported by pins with freedom to rotate)
- Condition Alpha (a modification of simply supported to reflect a real shipboard scenario discussed in section 5.2.1)

These boundary condition scenarios carry through each of the geometric modifications as part of the parametric study that follows the same model as the buckling load FEA. A table of testing criteria can be seen below. Keep in mind that these testing criteria were examined at each of the boundary conditions mentioned on the previous page.

No Doubler Smear (h = .112 inches); 2 Longitudinal & 2 Transverse Stiffeners	No Doubler Smear (h = .112 inches); 3 Longitudinal & 2 Transverse Stiffeners
Doubler Smear (h = .161 inches); 2 Longitudinal & 2 Transverse Stiffeners	Doubler Smear (h = .161 inches); 3 Longitudinal & 2 Transverse Stiffeners

Table 16: The study's goemetrical variations based on the experimental side shell panel furnished by the U.S. Coast Guard.

The baseline group best suitable for direct comparison with the experimental results analyzed earlier are the load-displacement curves, which vary boundary conditions while keeping the geometry of the plate fixed and consistent with experimentation. Unfortunately, it is impossible to accurately model the doubler plate in FEA so the doubler was effectively smeared into the plate to account for its added strength. Under ideal conditions, the magnitude of the ultimate load of the curve that shows the experimental setup boundary conditions should be very close to the magnitude of the experimental results with a percentage of experimental error yet to be accounted for in the ideal plate. The Load-displacement group of curves showing baseline-geometry (geometry identical to the experiment) can be seen below as Figure 50.

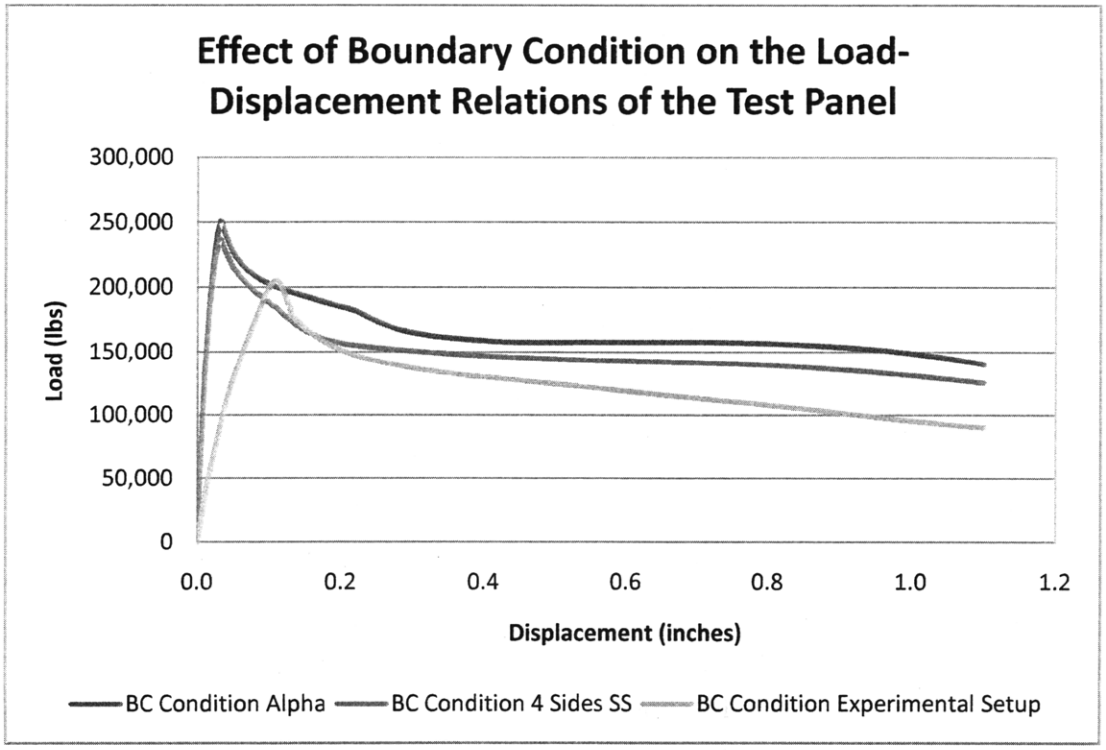

Figure 50: Load-displacement curves for three sets of boundary conditions and their relative effect. Notice that the curve showing experimental boundary conditions collapses at a much larger relative displacement. Also, keep in mind these results are for an ideal plate without any associated strength reduction factors.

In pure comparison, it is immediately apparent that none of these curves match up with the magnitude of the experimental load, which is as expected. These curves are, however, within an order of magnitude of the results and strength reduction factors have yet to be considered. The effect of strength reduction factors will be further discussed in section 5.4.

In order of precedence, it is plausible to say that the magnitudes for each geometry-boundary condition curve, the magnitude of the load is the most important. To better visualize the range of ultimate load magnitudes as they vary through the parametric space, a plot of ultimate loads and their corresponding displacements for several different geometry variations under three boundary conditions can be seen below as Figure 51. The experimental result is also plotted on the figure below to show continuity with experimentation and prove the results are on the same order of magnitude:

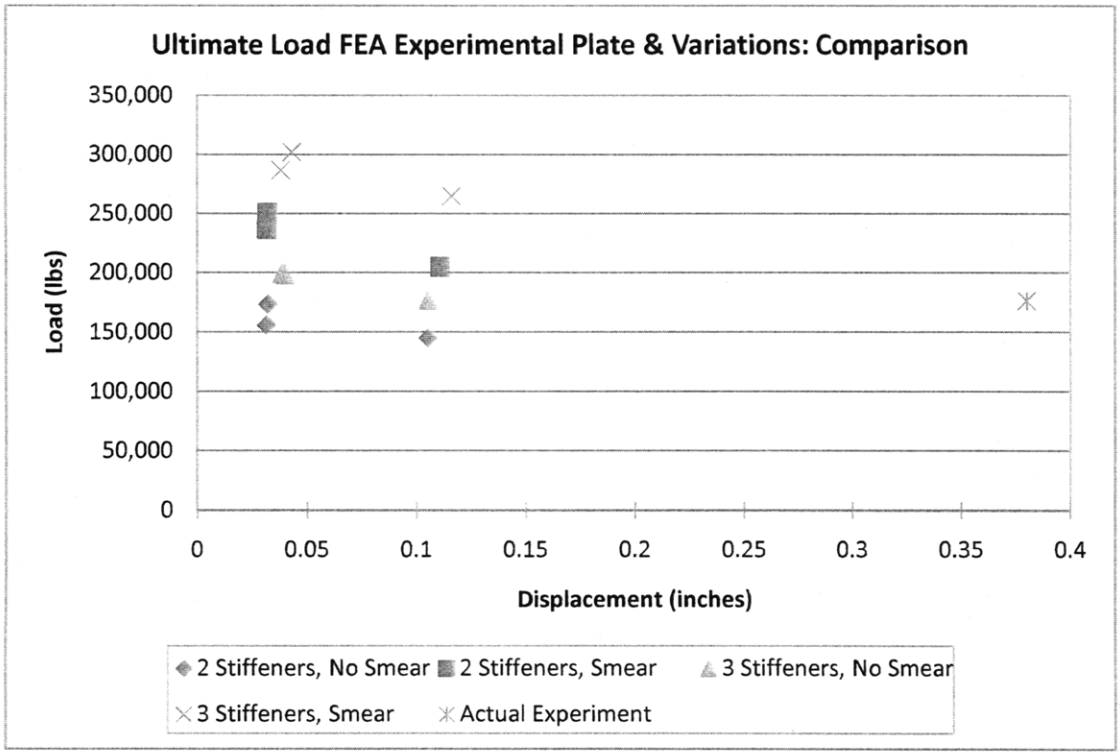

Figure 51: Ultimate load data plotted as single points. The data cluster with approximately 0.03 displacement represents simply, simply supported and Alpha boundary conditions while the data cluster at .1 inches represents experiment B.C's

Load-displacement curves were not generated for every possible boundary condition standard. The reasoning being is that it is acceptable to hypothesize there is no way an actual side shell panel would exhibit conditions constituting it having all four sides clamped or any other variation where no rotation in any direction existed. All of the applicable load displacement curves under various comparison criteria can be seen in Appendix 5.9. The corresponding visual representations can be seen in Appendix 5.10.

5.3.3 Initial Deflection Study in FEA

The discussion of the effect of initial deflections in Chapter 2 presents the basics of strength reduction and outlines several formulas. These formulas use a given magnification factor to determine whether significant initial deflection will prematurely cause failure. In most shipboard cases, initial defections will not be a significant issue if no construction anomalies are present. Outlined in Reference (5), this is fairly easily proved within F.E.A. when examining ultimate strength. To create initial deflection in an FEA model, it is suitable to assume that the largest simple plate area (the 18"x46" center bay within the two longitudinal stiffeners) deflects in the overall mode by some amount w_0 based on an applied sinusoidal pressure load q_0. The deflected plate can be assumed to have a simply, simply supported boundary condition. In this condition, the deflected shape can be suitably modeled by a sin-based function. The boundary conditions are acceptable based on the behavior of stiffeners in a large panel such as shell plating, which has both transverse and longitudinal stiffeners (51). The lateral pressure load is governed by Equation 49.

$$D\nabla^4 w = q(x,y) \tag{49}$$

A simple solution can only be attained for a sinusoidal loading condition, given below as Equation 50:

$$q(x,y) = q_0 sin\frac{\pi x}{a} sin\frac{\pi y}{b} \tag{50}$$

The governing Equation 49 is satisfied with simply, simply supported boundary conditions and a sinusoidal loading condition defined in Equation 50, by Equation 51, seen below:

$$w(x,y) = w_0 sin\frac{\pi x}{a} sin\frac{\pi y}{b} \tag{51}$$

This closed form solution for w_0 can be analyzed for some multiple of the thickness of the plate for comparison analysis. The final form of the deflection equation is written as 1% of the thickness of the plate (10% thickness equivalent pressure was examined as well) and can be seen below (51):

$$w_0 = .01h = \frac{q_0}{\pi^4 D(\frac{1}{a^2} + \frac{1}{b^2})^2} \tag{52)}$$

Using Equation 52 at 1% for a smeared plate, the applied pressure magnitude was calculated to be 6.603 psi assuming the "a" and "b" variables to be 46" and 18", respectively. The results of

the FEA analysis with appropriate initial deflection including comparison data are seen below in Table 17:

FEA Initial Deflection Comparison with Experimentally Similar B.C.							
Thickness %	h (inches)	w_0 (inches)	q_0 (psi)	Associated Disp. (inches)	Associated Load (lbs)	% Defl. Change @ Pult	% Less Pult
1%	0.112	0.00112	1.304	0.1061	145633	0.86	-0.39
10%	0.112	0.0112	13.04	0.1034	143429	-1.71	1.13
1%	0.161	0.00161	6.603	0.1053	200090	-4.96	2.39
10%	0.161	0.0161	55.69	0.1015	191443	-8.39	6.60

Table 17: Initial Deflection data completed within Finite Element Analysis. Additional Graphical outlining the overall effect of Inital Deflection can be seen in the next Section.

The associated load was determined from the results of the FEA analysis and, in this case, there is no single equation that relates the change in buckling load to the initial deflection. In order to provide a condition that creates a situation most clearly like that of the experimental plate for later comparison, half of the data sets were collected considering the doubler to be present. The sets of data points pertaining to the non-smear case provide a bit of an insight into the buckling load and ultimate load of a pre-doubler plate and the relative effects of initial deflection. It is clear right away that the impact of initial deflection is extremely small, so small in fact, some of the data appears to be inconsistent, though extremely close (pre-doubler, 1% pressure load). This inconsistency could be a result of inconsistencies or other problems within the FEA model. Selected local-displacement finite element models with a consideration for initial deflection can be seen in Appendix 5.11.

5.4 Local Plate Strength Reduction Considerations

Up until the previous section, any and all simple plates, longitudinally stiffened panel variations and the replicas of the experimentally tested panel have been analyzed assuming an "ideal" structure. While these ideal plate calculations (both in FEA and analytical) are a good estimate (and are certainly trusted in shipboard structural analysis and design programs to provide good design output for a given compression load) of the load and/or stress seen on a certain plate element, they are by no means perfect. As noted in the previous section, global and local hull strength reduction factors were discussed at length in Chapter 2 and applied to the overall ship structure in chapter four. This section, however, focuses on the effect of some of the remaining quantifiable strength reduction factors at the panel level.

Using the baseline, post-doubler stiffened panel (assuming a free-modified boundary condition to mimic the experimental condition), the different strength reduction factors are

examined from an analytical standpoint. All of the calculations pertaining to the results presented in the following sub-sections can be seen in Appendices 5.12 and 5.13.

5.4.1 Basic Initial Deflection Considerations

Notwithstanding the FEA initial deflection work seen in the previous section, analytically, it is relatively simple to determine if any initial deflection of a stiffened panel will have a significant effect on its strength. Simple empirical equations for maximum permissible initial deflection amplitude were developed by Faulker in 1975 (discussed in Reference (5)) that will easily determine if initial deflections with have a significant detrimental effect to overall strength. These empirical equations are a function of a slenderness ratio, ß and the thickness, *h*. The applicable empirical equation to this study can be seen below as Equation 53:

$$\delta_p \leq 0.12\beta^2 h \qquad [53]$$

The slenderness ratio seen above is the same ratio used as a part of Von Karman effective width theory, discussed in Chapter 3 and applied in Section 5.2.2. Including the doubler smear and the stiffeners, the experimental panel's slenderness ratio is calculated to be 1.56 from Equation 38. Using this value for ß and applying it to Equation 53, the corresponding maximum allowable deflection in the longitudinal direction for the plating between each stiffener is then calculated to be 0.05 inches. This maximum allowable value for deflection is well within the 10% of the thickness deflection considered in the FEA analysis and would most likely not be an issue for trained steelworkers. It should be noted, however, that maximum acceptable deflection decreases for longitudinal stiffeners which are intermittently welded (as in the case of the experimental plate). The reduced magnitude however, will still be within the limits of what would traditionally be seen in the longitudinal direction of the experimental plate (5).

5.4.2 Shear Stress Considerations

At first glance, shear stress considerations seem to be quite crucial when determining the overall strength of a stiffened panel as part of the side shell of a ship. Hughes notes that the only thing that a large amount of shearing causes is a reduction in the ideal yield stress (σ_y) by some factor r_τ. From the Henky-Von Mises yield criteria, this factor can be calculated using the following equation, where τ is the shear stress that is present and σ_y is the yield stress of the panel.

$$\frac{\sigma_a}{\sigma_y} = r_\tau = \sqrt{1 - \left(\frac{\tau}{\sigma_y}\right)^2} \qquad [54]$$

During the initial discussion of shear stress considerations at the beginning of this chapter, it was noted that shearing effects in this particular instance are nearly negligible. This is proven using empirical data provided by Dwight et al, detailed in Reference (5). He states that any present shearing stress that is determined to be less than 17.5% of the yield stress should be generally neglected (5). With the given σ_y, this value amounts to 7000 psi. Applying Equation 8 and assuming a worst case shearing force (due to bending) of approximately 55 LT, the maximum shear stress associated with the panel can be calculated to be on the order of 1500 psi. The relevant shear flow calculation was completed using the approximate mid ship section from the 123', based on Equation 9. When the calculated shear stress is substituted into Equation 54 seen above, r_τ is found to be .998, resulting in a decrease of 70.7 psi in σ_y (based on a 40 ksi yield stress). Extrapolating this strength loss to the stiffened panel yields an overall reduction in P_{ult} of a mere 164 lbs, proving τ is not a significant factor.

5.4.3 Imperfection Considerations

Imperfections occur naturally in the forming and construction of steel structures. There are two kinds of imperfections, or on a broader scale, discontinuities. These are the unintentional kind and the intentional kind. Because the intentional type of discontinuities (hatches, etc) are accounted for in the structural design of a ship, this local analysis focuses on the unintentional type. Unintentional imperfections in steel structures cause stress concentrations and are generally unavoidable, even with excellent craftsmanship. The effect of imperfections decreases the structural strength of a plate or a structure in much the same way as residual stresses do. To account for imperfections, ANSI has come up with a modification to the Von Karman effective width ratio (30). The original ratio, given in Chapter 3's explanation of Von Karman theory as Equation 39, now becomes Equation 55, seen below:

$$b_{effective} = b\sqrt{\frac{\sigma_{cr}}{\sigma_y}}\left(1 - .218\sqrt{\frac{\sigma_{cr}}{\sigma_y}}\right) \qquad [55]$$

Using the above equation and the known values of b, σ_{cr}, and σ_y for the specific piece of paneling and type of steel, $b_{effective}$ becomes 7.88 inches and the corresponding difference (decrease) in P_{ult} is calculated to be 12,393 lbs.

5.4.4 Residual Stress Considerations

Determining the magnitude and distribution of residual stresses in any certain plate is one of the most difficult tasks structural designers must master. Through extensive destructive testing outlined by Masubuchi in Reference (23), and empirical formulae discussed in Hughes

text (5), the magnitude of residual stresses in axially loaded plates are best modeled by a so-called typical distribution. Panels however, as discussed previously, are better defined by Equation 11, noted in section 2.3.1. Unfortunately, it is difficult to use this equation since welding information is not available but residual stresses can be approximated using residual stress plate theory. In either case, the residual stresses in a plate similar to the piece of side shell will rarely be more than 10% of σ_y, or in this case, 4000 psi. Applying either of these methods to the panel would certainly show the residual stress approximations to be far less than this benchmark.

Once it was established that the residual stresses present in the stiffened panel in question did not exceed the benchmark of 10% of yield, calculations were completed in order to determine the approximate strength reduction factor. Using Equation 10, the approximate reduction in P_{ult} due to residual stress is calculated to be 296 lbs. Application of the residual stress equations and discussion of the calculation method can be seen as part of Appendix 5.12.

5.4.5 Crack Considerations

Although cracking of the side shell strength members was not a considerable concern on the 123', it is pertinent to include it in strength reduction factors in the context of a part of stress corrosion cracking and also with regards to the 179'. The 179' experienced extreme cracking which some Navy experts at NSWCCD Combatant Craft Department Code 23, note this could have potentially degraded primary bending stress limits by nearly 70%. Fracture is discussed in detail in Section 3.3, but an efficient mathematical check of the ultimate tensile strength of a stiffened panel with an existing crack based on geometry alone is simplified by (28) using Equation 56, seen below:

$$\sigma_u = \frac{(b - c_p)t\sigma_{Yp} + (h_w - c_s)t_w\sigma_{Ys}}{bt + h_w t_w} \qquad [56]$$

The quantities used in the equation above are based on measurements shown in Figure 52, seen below

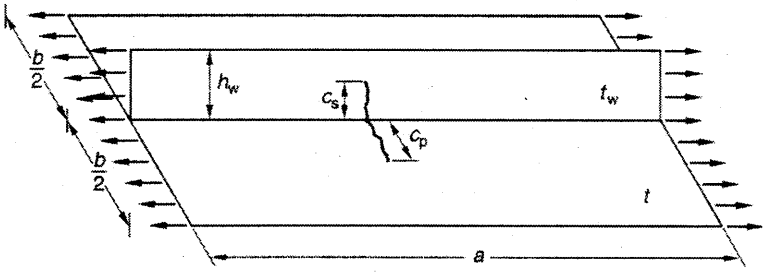

A stiffened steel panel component with existing crack

Figure 52: Model of a plate with existing crack. This figure is reproduced from figure 10.19 in Reference (28).

In this case, *b* is assumed to be $b_{effective}$ as calculated by Von Karman's theory (on the experimental 123' panel) for continuity. Using Figure 52 as a guide and assuming c_s and c_p to be 1.5" and 2.2" respectively, (this amounts to approximately 50% of b/2 and h_w) (56) predicts σ_u to be 25,574 psi and the corresponding P_{ult} to be 130,008 lbs. While this is value is not nearly the 70% strength reduction the Navy worried over, (in fact it is 37%) this is only one specific scenario, and specific cracking seen on the 179' (not analyzed here) could have yielded these results. Regardless, it certainly explains how progressive failure occurred due to strength loss in cracked critical structural members.

5.4.6 Corrosion Considerations

The piece of side shell plating provided to the U.S. Naval Academy testing facility was fabricated for the exclusive purpose of providing experimental results of a plate similar to that seen on the side shell of the 123'. Corrosion, discussed in detail as part of section 2.3.4 and examined from a global-ship standpoint in Chapter 4, is obviously not a factor with the plate sample. Regardless, there is a noted difference between the thickness of the experimentally tested panel base plate and that of the side shell plating seen on the 123's. Coast Guard Drawing WPB-123-085-31 (37), detailing the mid-ship section calls for #6 BS 4360 plating (h = 0.136 inches) while Coast Guard Drawing # 123-WPB-TEST-PANEL detailing the test section calls for #5 BS 4360 plating (h = 0.112 inches), which is 17.6% thinner. In addition, the longitudinal stiffeners present a slightly different geometry and weld pattern, which therefore suggests that some kind of service life degradation through corrosion or other means (no quantifiable amount can suitably be determined) was subtly considered.

5.5 Discussion

In design, where there are limitless combinations and variations of stiffener placement, arrangements, and thicknesses in a quest for optimal strength at minimum cost, there seems to be much more room for error because in most cases, nothing has been built. In post-construction analysis of failure, one usually has to consider what is already in place, try to validate it, and then figure out how to fix it or make it better with manpower, time and cost in mind.

5.5.1 Comparison

Comparing the different methods of analysis is certainly a viable way to not only ensure the theories used are correct for the study's given parameters but also to provide a context for the different variability between those theories. In the analytical world, there is so little room for maneuverability between variations of geometrical design and boundary conditions because of the relative complexity of the structures to be analyzed. This constraint becomes apparent when

analytical results, based on assumptions that may or may not be a good representation of the actual piece, are compared with FEA. While FEA of complex structures has its own set of flaws and (small) rounding errors because it consists of an extremely complex mathematical process, with proper inputs it can provide very detailed results that were not previously available.

The differences in the three methods used to analyze the baseline stiffened panel and its variations in a simple buckling test and ultimate strength produced results discussed in sections 5.2 and 5.3. This provided considerations and sample calculations to account for variables seen in an actual structure. While the application of these strength reduction considerations will be discussed in the next section, the "ideal" plate and panel scenarios are examined here from a graphical approach. Analytical buckling data was only compared with FEA analysis due to lack of experimental testing, however buckling analysis was completed through the entire range of geometries from simple plates all the way to stiffened panels. This comparison is seen below:

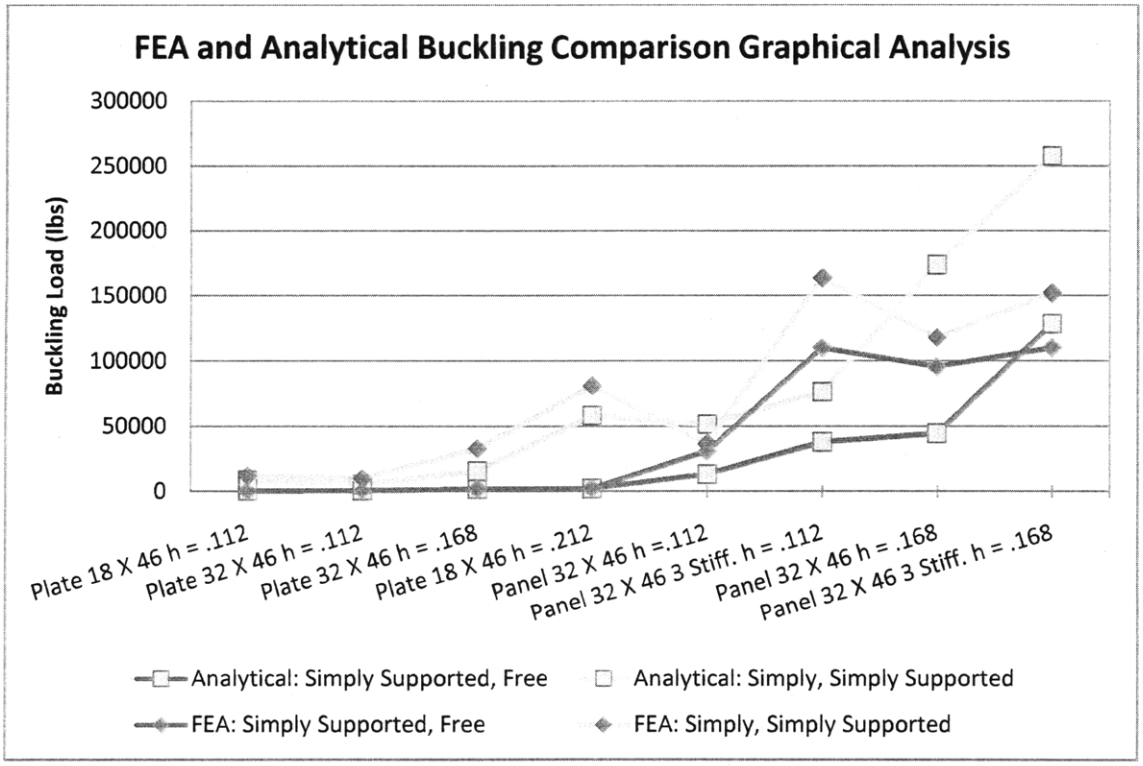

Figure 53: This table shows a graphical representation of the difference in FEA and Analytical Data.

Figure 53, seen on the previous page, provides this comparison for simply, simply supported and simply supported, free boundary conditions. The various data lines have been color coded for ease of interpretation. It is also obvious that in some cases, yield will occur prior to buckling, especially for some of the exceptionally sturdy plates. Additionally, it shows several data points that do not seem to be anywhere near their corresponding values. These variations are

immediately apparent when looking at Table 18 below that shows the analytical error margins depicted in Figure 53 from baseline FEA results.

Error Comparison (% difference)		
Geometry (Measurements in Inches)	Simply Supported, Free	Simply, Simply Supported
Plate 18 X 46 Thickness = .112	-0.4%	28.6%
Plate 18 X 46 Thickness = .212	-0.4%	28.3%
Plate 32 X 46 Thickness = .112	1.3%	46.3%
Plate 32 X 46 Thickness = .168	1.3%	52.6%
Panel 32 X 46 Thickness =.112	57.1%	-40.8%
Panel 32 X 46 Thickness = .168	53.4%	-47.6%
Panel 32 X 46 Extra stiffener h = .112	65.4%	53.4%
Panel 32 X 46 Extra Stiffener h = .168	-16.6%	-69.5%

Table 18: This table shows the Error comparison between Finite Element Analysis results and Analytical solutions. Note FEA is nearly perfect for simple plate geometry with Euler Ideal Wide Column Theory type boundary conditions.

These differences in results could have come from a variety of different realms. While it appears that the simple plate data is nearly seamless for the simply supported, free boundary condition, the simply, simply supported data is consistently 30-40% different. This could be a product of boundary condition mathematical constraints within FEA. In order to successfully execute a buckling module, the pin constraint in the direction of the load cannot be activated, losing the "true" simply, simply supported boundary condition because the analysis tool cannot process the difference between loaded direction and a pinned direction.

As mentioned before, the number of wavelengths in buckling mode plays a large part in its buckling strength. In several cases, the appropriate buckling mode calculated using Figure 61 for a simply, simply supported plate of some specific aspect ratio is different than the one seen from the results of the FEA. Another cause for differentiation is the complexity of analytically analyzing a stiffened panel as a series of separate plates. While the boundary conditions for each set of separate plates are appropriately assumed, error exists because all of the separate plate parts will buckle in the mode of the center plate, but the analytical formula is only completely accurate when it describes the bucking mode prescribed by the aspect ratio. In this case, FEA appropriately predicts a buckling load closer to what might actually be seen.

Other than the magnitude of the error, there does not appear to be any noticeable pattern of error in the different results graphically or otherwise. While the results and visual depictions are helpful to understand how a panel might or will fail, with sturdy, strong structures, there is a very good chance yield will occur before buckling. This was notably the case when using the Euler column global buckling to analytically analyze stiffened panels. These results (Table 13) are outrageously high because one of the principle driving factors (L_{eff}) was only 46 inches. This also proves that the stiffened panels will not fail in mode one (overall mode). Furthermore, this

formula is only valid if global buckling occurs prior to yield, which is not the case in this instance.

After all the different scenarios of buckling were compared and analyzed using the FEA and analytical methods, the experimental data was considered as ultimate load differences were examined. As discussed in sections 5.2 and 5.3, the ultimate loads were calculated using experimentation through axial compression, FEA load-displacement curves in the elastic, plastic realm, and analytically through Von Karman's effective width theory. The graphical comparison of the calculated ultimate loads using all three methods can be seen below in Figure 54. This figure is also partially reproduced as Figure 51 in section 5.2.2.

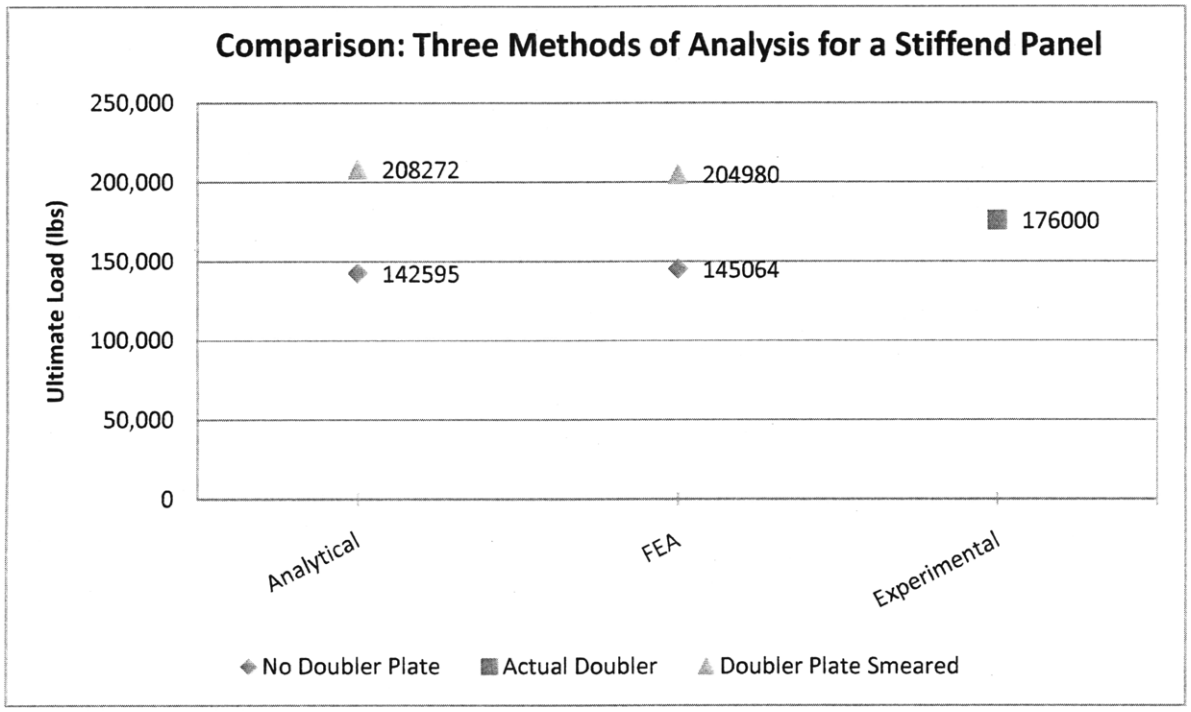

Figure 54: Graphical comparison for the stiffened panel in question, all values are in lbs. Each of the calculated loads is written in next to their respective data points as well. In this case, the boundary conditions in FEA consisted of simply supported, free modified to be consistent with the experiment. The boundary conditions for the analytical calculation were simply, simply supported to accurately capture the effect of the stiffened panels. Analytically, when using effective width theory, the boundary conditions for the unloaded edges outside of the b_{eff} realm have no bearing on the final solution.

The analytical analysis data seen above using Von Karman's effective width theory is actually conducted using the cropped plate rather than the full blown experimental plate. The cropped plate, through all the different phases of testing and boundary conditions, has repeatedly shown nearly identical characteristics as the experimental plate. This phenomenon shows that transverse stiffeners can accurately be modeled using boundary conditions over a variety of specific loading conditions that are included in this study. Unfortunately, in different loading conditions not involving the shell edge or various other loading combinations where transverse stiffening might become a factor, this correlation will not necessarily hold true.

The reasoning behind the differences in the FEA and analytical data sets seen in Figure 54 tends to run along much of the same line as the reasoning for differences in buckling. Particularly, in the case of the experiment, variations in loading condition, machine slippage, and all the reasons discussed in section 5.4 contribute to differences in the ultimate load. Another big reason the data points are generally not perfect is that the effective width was derived using theory that applies more generally to simple plates and was modified to be used for stiffened panels as well. Because there was some variation in the interpretation of the way the stiffened panels behaved under load, effective width was calculated using several different variations of plate theory. For the comparison, the most plausible variation was chosen. These are all discussed in the Von Karman related portion of section 5.2.2.

5.5.2 Validation of Theoretical Results

Using Figure 54 in section 5.5.1 as a guide for the validation of the FEA and analytical calculations as it compares with the experiment is by no means a small task. It is clear from the figure that the experimental results lay where they should be: Less than the ideal plate smear but more than the pre-doubler ultimate load (which unfortunately was never experimentally tested). It is also plainly noticeable that displacement was not a factor of comparison because in terms of ultimate load calculations, it really cannot be justly compared. In fact, the analytical method used to calculate ultimate load does not have an attached displacement. Validation of the displacement seen in the experiment is therefore completed by hypothesizing about the construction of the testing apparatus, the data collection equipment, and the overall "slippage" present in the experimental setup. Although at the point of ultimate load the displacement was almost 0.4 inches, it is still deemed acceptable based on the discussed reasoning.

Validation of the ultimate load carried by the experimental plate can be completed by examining the applicable factors discussed in section 5.4 and their associated results. These include initial deflection, imperfections, residual stresses, and shear considerations. For purposes of pure comparison, corrosion (already accounted for) and cracking (non-existent) are left out. The relative values of each of those applicable strength reduction factors and their summation are listed below in Table 19:

Reduction Cause	Decrease in P_{ult}
Imperfections	12,393 lbs
Residual Stresses	296 lbs
Shear	164 lbs
Initial Deflection @ 10%	13,537 lbs
Sum	26,390 lbs

Table 19: Reduction considerations.

The relative decrease in P_{ult} is calculated in this case from the smeared version of the FEA experimental plate with appropriate simply supported, free modified boundary conditions. This was deemed to be the closest calculation to the actual performance of an ideal plate. In addition, the analytical P_{ult} is within 3,500 pounds of the FEA result and acceptable as an alternative form of the panel solution. Subtracting the sum of the strength reduction factors from the FEA determined value of 204,980 lbs yields a new ultimate strength of 178,590 lbs. This is within 1.5% of the experimental solution. This percent difference could vary due to the unknown coating on the panel itself, partially uneven loading, the smear approximation, or a different percentage of initial deflection, but is extremely close by experimental standards.

5.5.3 Determination of Failure Mode

Overall, the comparison of experimental results through proven analytical and FEA analysis was a success as the ideal panel data, coupled with known sources for strength degradation yielded exceptional results. It is fairly clear from the nearly-realistic comparison to finite element analysis, an understanding of mechanics, and a comprehension of failure modes shown in Figures 13 through 17, that the stocky stiffened panel with relatively strong stiffeners first yielded in Mode VI and then progressively buckled in Modes III, IV, and V in a combination of plate buckling and membrane yield. In the case of this panel, the progression of buckling modes probably occurred nearly simultaneously. Comparison to experimental data beyond this is difficult because the displacement during the test was limited to an overall displacement of 1.1 inches and no intermediate pictures of the test are available. The validation of the failure mode can be further asserted by determining where the stiffened panel lies on a normalized ultimate and buckling stress versus slenderness ratio graph, developed by Von Karman and noted in Chapter 3.

These curves are based on boundary conditions and the geometrical relationships of the plate-stiffener combination. While Von Karman's theory rests on worst-case simply supported basic plates, it can also be applied to a doubler smeared stiffened panel by accounting for changes in several key variables. Figure 55 shows the failure characteristics of the plate-stiffener combination, and can be seen on the following page.

Three points of interest are marked along the curves in addition to the intersection point on this figure. Point "A" shows failure without any consideration of a stiffener for comparison purposes and represents a ß value of 3.94. This point is clearly in the "buckle first" realm (first line intersected moving up from the x-axis). Point "B" essentially takes the stiffeners into consideration by the previously established smear method and represents a ß value of 1.56. This point is in the portion of the chart where yield happens first, correlating with the higher-than-the-yield results from the *purely elastic* buckling analysis. Point "C" represents a slenderness ratio

of 2.04. It illustrates the stiffened panel as it was prior to the doubler addition and characterizes the most likely scenario of failure that occurred on Matagorda. Interestingly enough, it predicts buckling will occur prior to yield.

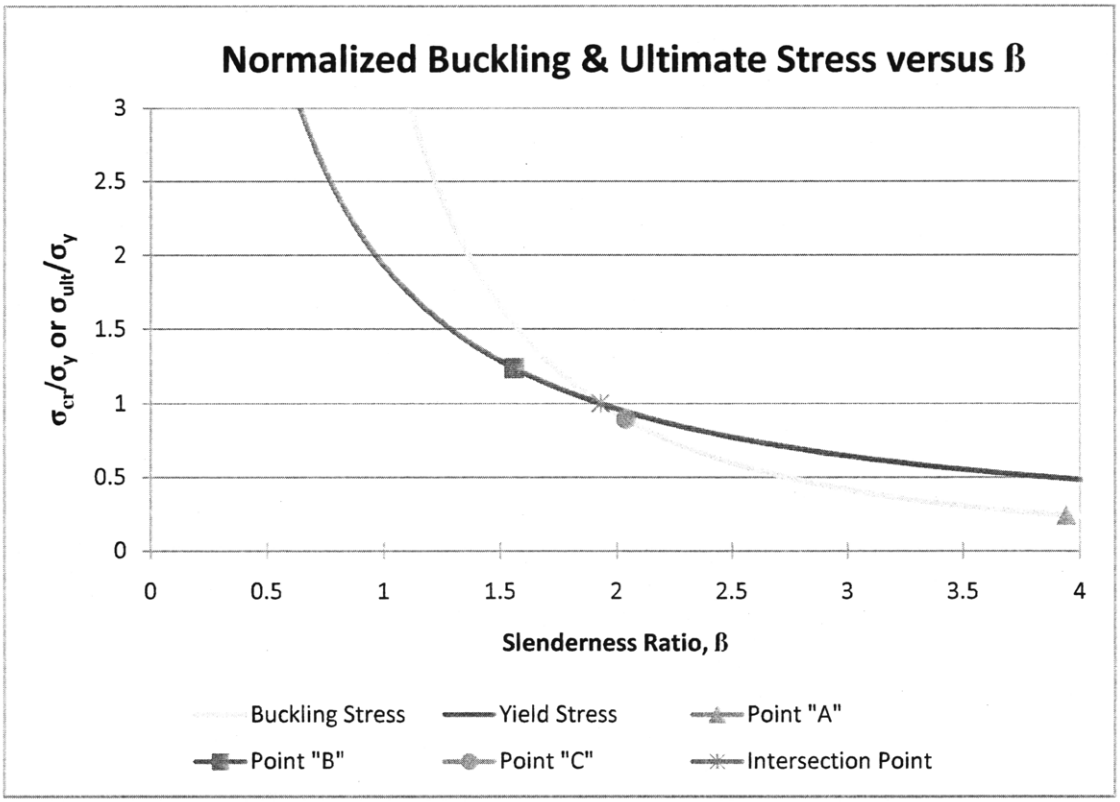

Figure 55: Normalized Buckling & Yield versus slenderness ratio. This graphical analysis solidifies the notion that yield will occur prior to buckling.

Although the FEA and Analytical results of the stiffened panel on which the experiment was conducted are slightly different due to methodology, both either show or indicate that yield occurs first due to the calculated buckling load (larger than yield) and the figure above. The last point marked on the figure is the intersection point of the buckle curve and the yield curve. The intersection point is established by Von Karman Theory: Initially, Equation 30 is used to calculate the relevant k_c factor and then it is plugged it into Equation 31 to determine the appropriate coefficient (1.93). The calculations to support Figure 55 and further discussion of the methods that were used to account for the stiffeners can be seen as part of Appendix 5.13.

5.5.4 Conclusions

Using both the relatively small difference in solution sets and the overall magnitude of the solution for loading, the comparison of each computation method proved to be a success. This is made clear from the nearly-realistic comparison to finite element analysis and failure mode, verified in the previous section. The experimental panel failed approximately where FEA

predicted it would fail and with the doubler smeared, it failed in yield in the end bay. This failure was in defiance of where the Coast Guard desired, who took steps to try and cause failure in the center bay. This is seen below as Figure 56:

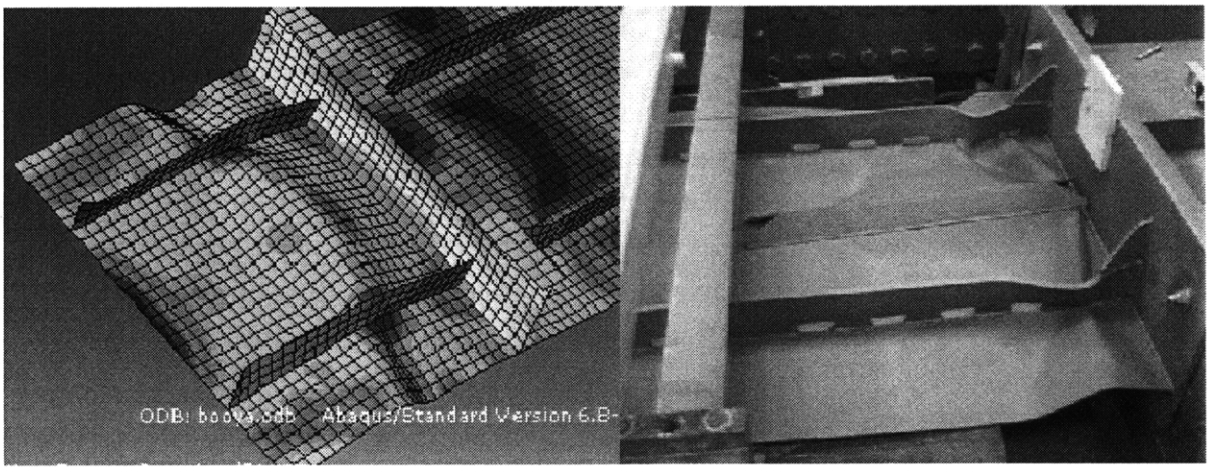

Figure 56: Split screen of Experimental and FEA results. Interestingly, the experimental plate did not fail symmetrically about the x-axis. This is most likely a cause of imperfections. Note the faux "stiffener" which was put in place to try to induce buckling in the center bay. This is seemingly also the cause of the variation in the location of the plastic failure. The FEA variation where initial deflection is considered is an even closer match to what actually occurred.

In addition to the direct comparison of the different methods for analysis, the effect of boundary condition variation and plate thickness variation over a variety of sequentially more complicated geometries was examined and compared as appropriate both within a particular method of analysis or across method boundaries. Through this analysis, there were points which generated interest and also are worth mentioning.

Part of the buckling comparison discussion focused on potential errors in FEA because, in several instances, the plate buckled in the incorrect wavelength mode. Although there was no large-scale attempt to remedy this, a potential solution could have been to increase the fineness of the mesh. Another question with regards to FEA results comes up with the actual experimental plate and the Coast Guard, independently conducted FEA "expected" Eigen-value buckling load. Under nearly identical conditions, the buckling load was determined to be 26% different than what the author determined. This could be due to slightly different boundary condition interpretations and mesh size, and also the inclusion of the "faux" stiffeners which were used to induce buckling in the center bay (which were not included in the author's rendition), or an attempt by Coast Guard authorities to include the doubler, rather than just accounting for it in a smear. Regardless of the "calculated" buckling load for the experiment, it was very difficult to deduce the point of buckling because it almost certainly occurred after yield and, as mentioned in the previous section. No intermediate figures were available detailing the experiment, though potentiometer and strain gauge readouts (seen in Appendix 5.1) do offer hints of this point. Overall however, this point is rather inconsequential because (as seen in

Figure 20), there is no real hard knuckle where transition from K slope to K/2 slope occurs in the load-displacement curve on the way to ultimate load.

Errors in the comparison analysis (between analytical methods and FEA) within both buckling and ultimate load were the result of approximations based on buckling mode. More error might have existed in these realms for multiple reasons. In terms of analytical calculations, it may have been more prudent to model the stiffened panel as two separate beam-columns, (note this is different than a Euler column) rather than as individual plates with simply supported boundary conditions, or under a modification of the Perry-Robertson design formula (31). While FEA analysis clearly shows that local intermediate plate buckling occurs first, Hughes (5) suggests this may be a better method if it is later proven that the lowest buckling mode is Mode III. In terms of ultimate load variation, Von Karman's method is employed by effectively smearing the stiffeners into the effective width of the panel. While this is a good approximation, it will not be exact because a thin plate with a thick stiffener will react differently than a thick plate under axial load.

From these tests and comparison, it is obvious under what conditions and at what load (or stress, if desired) failure occurs due to axial compression of a particular piece of side shell plating of the 123'. While it is impossible to accurately re-create scenarios relating to the actual even given uncertainties and possible unique loading scenarios experienced by the cutter, the magnitude and modes of failure of the paneling described and discussed in this chapter gives a good glimpse into the local mechanics of failure. While Chapter 5 focused on local analysis of a structure, the next chapter discusses applicable conclusions of structural stability and integrity in the context of avoidance during design and construction, and mitigation during operation, and the economics of repair.

Chapter 6: Looking to the Future

As ship design and construction companies and their major clients move into the future, it is highly desireable that they learn from the incidents that have transpired and make necessary adjustments so that problems outlined in the previous several chapters of this thesis can forever be avoided. In the naval warship community, there are two very distinct ways to greatly limit the chances of wide scale structural failure. These are through avoidance techniques during the ship design, construction, and analysis process and mitigation techniques implemented during the subsequent operation of the vessel. These criteria are by no means all inclusive and these techniques (particularly in the design realm) must not stop at the global level. Regardless, there absolutely may be more ways to limit incidents outside of the obvious.

Lastly, if an incident does occur, and it does appear that the problem is fixable, the economics of whether or not to proceed with that repair consists of major decisions, which may include possible budget cuts in other programs and postponement of construction of new assets. In the future, both clients and ship designers must not only develop ways to easily and efficiently assess damage to determine if the cost of repairs will exceed the worth of the ship, but also they must develop safer, more efficient, reliable methods for repair.

6.1 Avoidance Techniques

The task of avoiding structural failure due to excessive loading in a seaway is chiefly the responsibility of the designer. While the "designer" is rarely one person or even a single team of individuals, it is imperative that the global requirements for seakeeping characteristics are clearly outlined based on requirements documentation before the ship's general characteristics are finalized. Subsequently, the dynamic loading limitations can be analyzed during a full structural analysis to ensure the ship can withstand the missions it was created for. This may seem relatively difficult and time consuming at first, but ship design programs of today allow for comparative studies of multiple hulls with little more than general characteristics as inputs.

6.1.1 Global: Ship Design and Construction

Globally, much of the avoidance techniques that can be employed have already been touched upon. Even today, Congress is still criticizing the Navy and Coast Guard on their ship design and construction process. Based on several failures (structural or otherwise) the U.S. Navy has developed a comprehensive guide in the Naval Vessel Rules that governs their ship design standards. This incorporates both mission specific, goal oriented criteria and basic criteria for hull strength and stability. It is easily assumable the U.S. Navy engineers who

developed the rules had in mind the structural failures of the past and implemented additional safety factors and clearly outlined capabilities for given ship types and designs to avoid major incidents in the future.

With regards to avoiding the structural failures that are discussed in this study, it is obvious that the designers did a less than adequate job ensuring that the ships would be structurally sound enough to endure the environment where they were required to operate. The blame for why this happened cannot be placed on any one source (client, designer, construction firm, liaisons, etc) nor should it be, because often times it is impossible to essentially "point the finger". In this particular case, one ship is fixed and operational and the other is scrap. Obviously no more of either ship type will ever be built in the future but if they were, obvious avoidance techniques would include the following:

- Ensure the ship meets all requirements of the Naval Vessel Rules or other governing body
- Ensure construction techniques are strictly adhered to including the use of marine grade structural steel and aluminum (if applicable).
- Ensure allowances are included for ship displacement growth and also for corrosion
- Ensure the client and actual operator is well aware of the limitations of the ship based on design criteria and loading conditions.
- Ensure the client provides the operator with specific limitations should a structural failure event occur.

Of course it is impossible to list everything that needs to be completed on the global level but the idea of these criteria is cemented in place. Avoidance techniques do not stop at the global level however, and stiffened hull, side shell and deck panels that will be subjected to large loads should be analyzed as well.

6.1.2 Local: Stiffened Panel Design and Analysis

Locally, there is also much that can be done to avoid structural failure events. Once an initial design has been completed, the next avoidance technique starts by using good methods to model stiffened panels, ensuring correct strength data can be collected and analyzed. These techniques include the methods used in this study: FEA, experimental, and analytical methodology. It is important that within each of these techniques, the stiffened panels are loaded as closely as possible to realistic loading conditions and considerations are made for strength reduction factors that are seen in real life versus an ideal panel which is typically modeled in FEA. When conducting experiments, choosing boundary is critical in order to mimic conditions seen onboard ship. Condition "Alpha", created as part of this study, created what would

probably be a realistic setting but its unique boundary conditions are hard analyze in an analytical realm. In an ideal situation, creating an uneven, time varying load (given appropriate equipment) might yield much more realistic results for a side shell panel than would otherwise be seen in a basic in-plane compression test, but it would be even more difficult in a comparison scenario, even using FEA methods. When conducting basic analysis analytically, it is equally as critical to model the structure correctly as it is to make the correct assumptions of the failure mode, so that the appropriate method can be used. Often this might entail completing calculations based on *each* failure mode and then choosing the lowest critical value to complete further analysis.

6.2 Mitigation at Sea

The mitigation of structural failure at sea starts with the ship remaining within its designated operating profile, whether that happens to be speed limitations, sea state limitations, or both. Regardless of the operating profile, it is imperative that the ship is able to perform its designed and desired missions *within* that designated profile or a failure event may occur.

6.2.1 Operating Profiles

Often a graph of sorts is built showing the specific limitations of a ship using sea state (or significant wave height) and speed as parameters. This is commonly referred to as safe operating envelope (SOE). Mitigation of failure events at sea can depend heavily on staying within the required parameters given by these SOE because of the damage that dynamic forces can cause. This type of graphical SOE is seen in Appendix 6.1 for the PC 179'. A similar SOE in tabular form can be seen in Appendix 6.2 for the WPB 123'. Although they are shown differently, both SOE's convey the same information. It is well established within this study that dynamic forces such as slamming and other effects can cause serious hull strength reduction over time and can cause the onset of catastrophic failure if yield or buckling limits are reached in particularly susceptible areas of the hull. More information on the SOE's of both ships can be seen in References (39) and (2).

6.2.2 Effect on Mission Performance

The effect of the SOE on mission performance is heavily dependent on the design criteria and in an ideal scenario, the design of the hull and its associated sea-keeping characteristics should be consistent with the types of missions required. However, when a complex scenario arises such as a retrofit of an existing, proven cutter to upgrade its capabilities, calculations of the "new" SOE based on "new" seakeeping characteristics are more difficult to accomplish. Furthermore, when a hull experiences a failure event that is, so-to-speak, within its designated

operating profile and within its normal mission capabilities, one has to question if departure from the normal operating profile in completion of its missions (based on the new hull form), previous to the failure, was partially at fault.

Once it is established that failure has in fact occurred, the next mitigation technique to limit progressive failure (discussed in Chapter 3) of the ship is to change the operating profile. For both the Navy and the Coast Guard, this has an enormous effect on mission performance. Both services and both crafts examined in this study need to be able to operate in sustained heavy sea conditions in order to complete some of their primary missions. Limiting these capabilities without a reliable plan to fix the problem essentially removes them from service and the ships will remain at the pier.

6.3 Repair Economics

At the back of every client's mind whose ship(s) endure a structural failure scenario is the overarching cost of the event (both in determining the cause and preventing it from happening again) and the difficult decisions to fix or scrap the ship. The cost of these evolutions runs into the millions of dollars and in this case, the client is the United States government. Stopping short of a full economic analysis of the relative cost fixing a ship in dry-dock, it is easy to put things into perspective by outlining the estimated cost of repair for each of the ships examined in this study. Keep in mind that both of these ships are at the low end of the spectrum in terms of overall cost because of their relatively small size. The cost to fix a ship such as a high endurance cutter, destroyer or even an aircraft carrier is tens to hundreds times more.

The following tables outline actual cost summaries for fixing the 123's and 170's. Based on available information and the different timetables of failure discussed in this study, the tables are not identical but their premise is the same.

123' Upgrade and Repair Economics	
Consideration	Cost ($M)
Original Hull Cost	343.0
Original Upgrade	67.1
Final Upgrade	80.3
Upgrade Difference (Repairs)	13.2
Overall Cost/Hull of 8 123's	17.0
Cost/Hull Repairs	1.7

Table 20: Table of USCG 123' Economics.

From the table above it is easy to see that the overall cost of the new, upgraded cutters is more than twice the original cost of a single cutter (17.0M vice 7.0M). Furthermore, the cost of repair

of each hull is nearly $2M. Of course inflation has to be considered so this number is somewhat skewed, but this shows how relative cost of ship construction has risen over the past 20 years, making the case for soundly built ships that don't have to be repaired based on faulty engineering.

170' Upgrade and Repair Economics	
Consideration	Cost ($M)
Original Hull Cost	SOCOM $
Repair of First Failure	0.2
Development & Upgrade of First	0.3
Repair & Upgrade-Rest of Class	2.8
Total Cost of Upgrade	3.4
Cost of Upgrade/Ship	0.3

Table 21: Table of 179' Economics

In this case (as seen above) even though the initial price of the ship is unknown, the total cost to repair the ships is much less per ship than the cost to repair the Coast Guard Cutter. Keep in mind that this number does not include the extension project, and should be compared with the $1.7M figure given in Table 20. This may be based on several interacting factors including severity of the damage, the location of the damage, and the time frame of repair.

Whatever the cause of damage, whatever the repair scheme and new limitation put in place due to the initial failure, incidents such as the ones discussed in this thesis constantly remind the naval ship builder, designer, and operator of one important piece of information: Through careful workmanship and safe operation within limits prescribed by its design, a ship can safely and effectively perform its mission both at minimal costs and at minimal risk to the crew for its entire prescribed service life.

Conclusions

It is relatively clear from this study that there is no simple answer as to why seemingly well designed ships have enough structural failure to cause massive overhauls and in one case, complete removal from service. Naval ship construction companies and their subsidies have been in the design and construction of naval ships for long enough that no events like this should ever occur. Obviously, without these failures and the inability to completely understand them there would have been no motivation for this work.

Over the course of this project, there were two distinct levels of work completed, though fundamentally the goal was to bridge the gap between actual events and panel theory. This was completed through investigation of global and local behavior of ship structures and structural design, considering failure modes, loading scenarios, and the uncertainties surrounding strength reduction factors at both levels.

i. Global Considerations

Globally, this analysis was less than precise. Obviously, no *hard* conclusions were drawn from the results (nor could have there been) but it seems like this might always be the case when faced with a type of situation where finger pointing becomes routine. One has to assume that competent shipbuilders used proven techniques with built in checks and balances (even if they weren't related to a governing body) to create the ship, keeping in mind of course the project was not completed by a single person or a single team. In the case of the WPB, the 110', designed 20 years prior to the retrofit, served admirably prior to the elongation and continues to serve to this day. This leads to the conclusion that sometimes, through a variety of both explainable and unexplainable circumstances and causes, a structure simply cannot withstand the environment for which it was designed. Furthermore, once that structure has been initially compromised, it is not only very difficult, time consuming and expensive to try and fix, but if kept in the same environment it may continue to weaken and subsequently be a complete structural loss.

ii. Local Considerations

Locally, the results of this study focused more on comparison of analysis techniques and how changes in geometry effect changes in overall strength, rather than analyzing strength in the context of global ship design. Experimentally, the magnitude of the strength of the panel had already been determined to be much different than what engineers had previously thought and therefore, it was best to use these results as an asset for further work. As a comparison and geometrical effects study, there was certainly resounding success. Not only were analytical

calculations shown to be closely related to finite element analysis using assumptions based the author's analysis of failure mode, geometry and loading conditions of the experiment. A review of the all three methods, coupled with considerations for the real world versus the ideal world, proved them to be extremely accurate. As an engineer, one can hardly ask for much more.

iii. Goals and Future Work

At the highest level, a major driving factor in ship structural design and its construction is cost. The ultimate goal is, therefore, to learn from past missteps and prevent future failure incidents while improving ship design practices and keeping costs down. This said, the margins that are built into the rules and optimization design approaches in order to keep ships safe also are a viable cause of cost increases and overruns. These margins exist however, due to present capabilities of modeling software and the extreme difficulty in predicting external and internal uncertainties in an ever changing field of factors. At present, the most viable way to increase the accuracy of the prediction of uncertainties (as noted in many of the discussions in this text on strength reduction factors) is to continue to examine ship structures from both global and local levels and make acceptable and viable connections between real life incidents and their associated mechanics. To truly optimize the ship structural design and construction process over time, margins must decrease through better modeling with built-in, reliable methods for calculating the strength of the hull over a variety of changing load and environmental criteria through the expected life of the ship.

This Page Intentionally Left Blank

Appendix: Chapter 1

A.1.1Representations of Primary, Secondary, and Tertiary Stresses

Primary, secondary and Tertiary stresses experienced by ship hulls are sometimes referred to as component stresses. Each respective stress is described in detail in Section 1.1.2 and visual representation of each stress can be seen below:

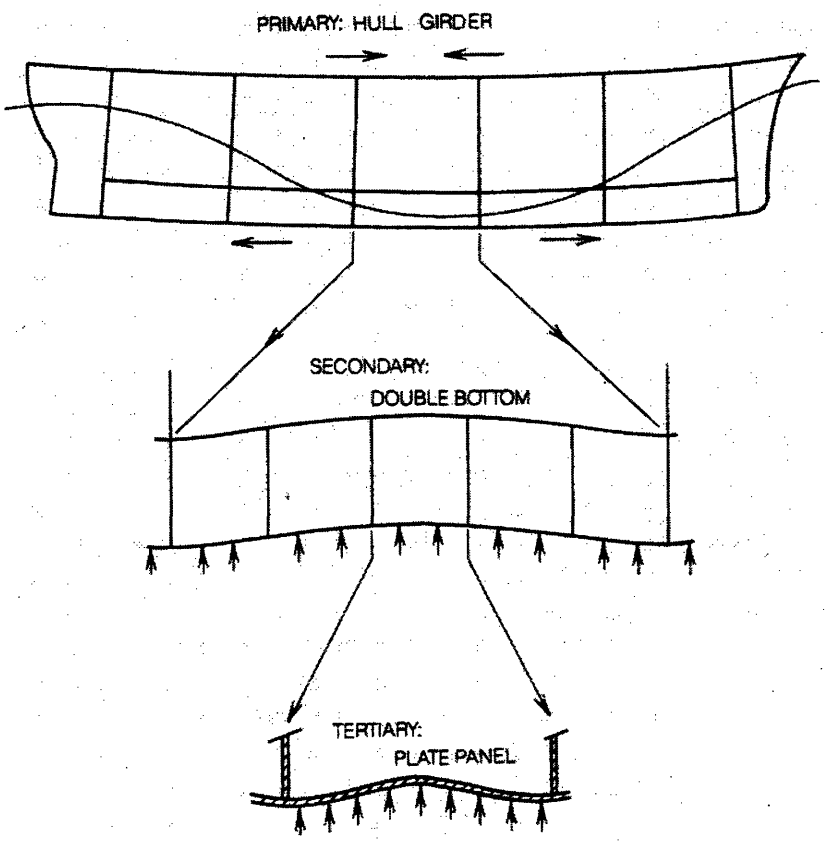

Figure 57: Primary, secondary, and tertiary stress diagram. This figure is reproduced from Reference (20).

It is quite obvious that each subsequent stress component is a more local portion of its predecessor. Therefore one can say that any single load can cause effects in each of the different component stresses in the local and global realms. Typical loads effecting more than one component are items such as pressure loads, liquid loads, or incredibly heavy machinery.

A.1.2 Overall Measure of Effectiveness

The premise of the Overall Measure of Effectiveness design philosophy method is that it provides a way to quickly assess the overall relative importance of certain design criteria and seamlessly compare different variations of the same ship with each other. These variations can then be compared with the cost

(or affordability) of the ship to determine the overall feasibility. While the actual OMOE document usually is some kind of spreadsheet calculator, the flowchart below shows an example of the results of one such calculator for a fictitious frigate-type warship. Each "relative importance" value is normalized to one.

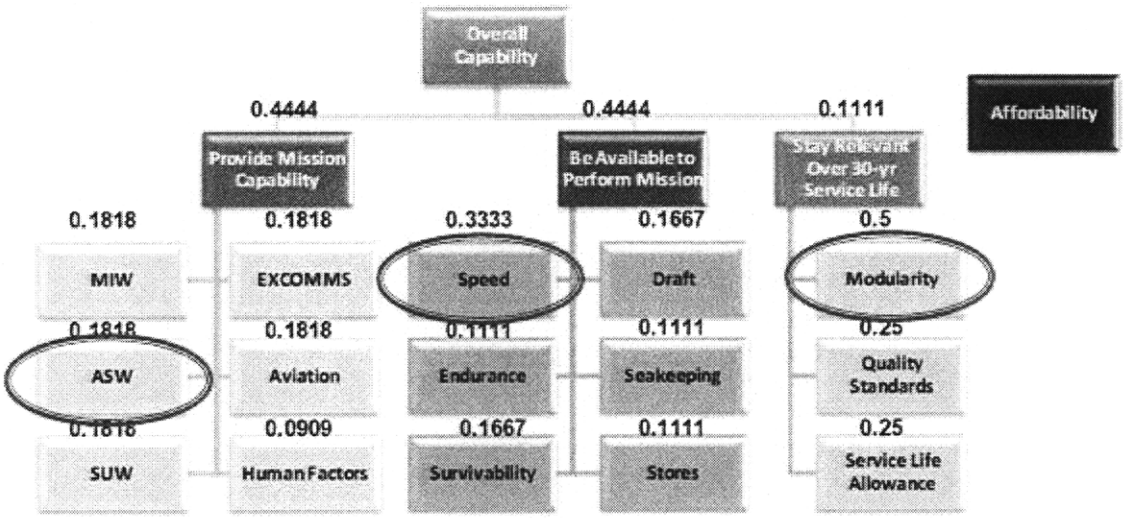

Figure 58: Overall Measure of Effectiveness Summary Flowchart. The OMOE is calculated using pair wise comparisons and simple multiplication of relevant values. The circled performance specifications signify the most significant specification for that affiliated OMOE Category.

It is clear that Mission Capability and Performance are both four times as important as relevance over service life in this particular model. Similarly, Within the Availability to Perform Missions subset, speed is determined to be twice as important and survivability and three times as important as Endurance, Sea-keeping and Stores. Of course no warship design is truly this simple, but the OMOE calculator can help to focus design teams on what is extremely relevant and important and what is less so during initial phases of design (9).

A.1.3 Table of Classification Societies

On the following page is a table of predominant Classification societies. The premise and the oversight of the classification societies are discussed in detail as part of the ship design and construction process in Chapter 1. For military ships, there is no reason to comply with any or all of the rules that are derived (usually empirically) by these governing bodies. Still, many designs are checked against a variety of rules to ensure a ship design is structurally sound. The U.S. Navy's "Naval Vessel Rules," while confidential in nature, undoubtedly cover (and may even be nearly identical in nature) many major rules also seen in these class societies.

Major Classification Societies of the World			
Name	**Abbr**	**Date**	**Head office**
Lloyd's Register of Shipping	LR	1760	London
Bureau Veritas	BV	1828	Paris
Registro Italiano Navale	RINA	1861	Genova
American Bureau of Shipping	ABS	1862	Houston
Det Norske Veritas	DNV	1864	Oslo
Germanischer Lloyd	GL	1867	Hamburg
Nippon Kaiji Kyokai	NKK	1899	Tokyo
Russian Maritime Register of Shipping	RS	1913	Sankt Petersburg
Asia Classification Society	ACS	1980	Tehran
Hellenic Register of Shipping	HR	1919	Piraeus
Polish Register of Shipping	PRS	1936	Gdańsk
Croatian Register of Shipping	CRS	1949	Split
China Classification Society	CCS	1956	Beijing
China Corporation Register of Shipping	CR	1951	Taipei
Korean Register of Shipping	KR	1960	Daejeon
Biro Klasifikasi Indonesia	BKI	1964	Jakarta
Registo Internacional Naval	RINAVE	1973	Lisbon
Indian Register of Shipping	IRS	1975	Mumbai
Brazilian Register of Shipping	RBNA	1982	Rio de Janeiro
International Register of Shipping	IROS	1993	Miami
Iranian Classification Society	ICS	2007	Tehran
Ships Classification Malaysia	SCM	1994	Shah Alam

Table 22: Table of Major World Classification Societies, along with their abbreviations and head offices (52).

Appendix: Chapter 2

A.2.1 Initial Deflection Variation

The effect of initial deflection for an Euler Column is shown below in a figure reproduced from Reference (28). Consistent with Hughes, it is clear that as the load approaches the Euler buckling load, the overall effect of the magnitude of initial deflection as it relates to the load carrying capacity is fairly insignificant. What is significant, however, is the larger the load, the more deflection will be seen, especially between 60% and 90% of the ideal Euler buckling load.

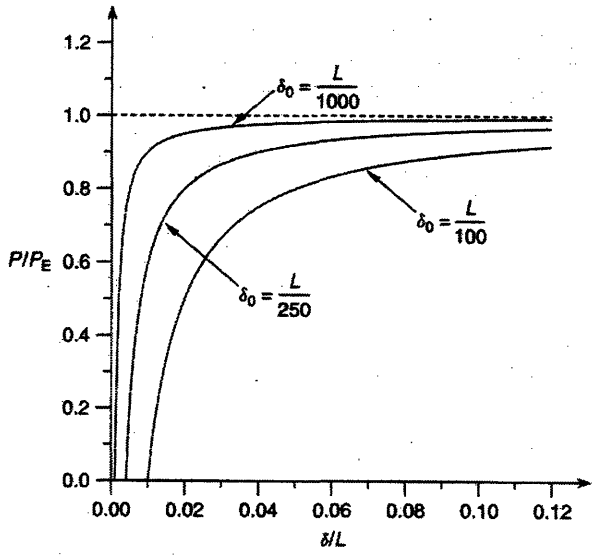

Figure 59: Euler Column behavior as subjected to initial deflection. The graph is normalized by ideal Euler Buckling Load.

As mentioned in the text, an Ideal Euler Column will collapse once its critical buckling load is reached. This is shown in the figure above by the dotted line at $P/P_E=1$.

Appendix: Chapter 3

A.3.1 Simple Plate Buckling Figure

The figure below, reproduced from Reference (5) is a visual depiction of the way a simple plate will buckle given simply, simply supported boundary conditions on all four sides. The simply, simply supported condition is a widely accepted condition when analyzing sub-plates of stiffened panels found on ships, where the condition closely mimics constraints created by transverse and longitudinal stiffeners. Using this concept, it is acceptable to analytically calculate stiffened panel buckling solutions (assuming local plate buckling is the limiting factor) by simply dividing the plate into sections between the stiffeners and then adding the result.

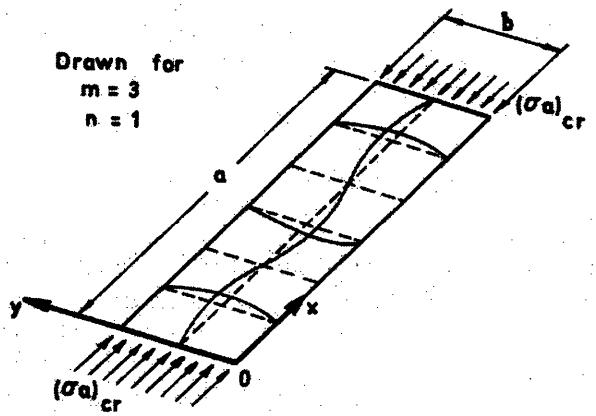

Figure 60: Simple plate buckling with four sides simply supported and a wavelength parameter of 3.

In accordance with Equations 28-31, the *n* variable for a simple plate is assumed to be unity notes above. Transversely, the plate buckles in a single half wave. The *m* variable denotes the wavelength parameter, whose calculation is detailed in the next section of this Appendix (30).

A.3.2 Buckling Wavelength Number Figure

Seen in Equation 30, the wavelength parameter, *m*, is a function of the length-to-width ratio of the simple plate. This variable is predominant in the figure seen on the following page. This figure shows the ratio of a/b where *m* shifts and the corresponding k_c values. The shift in the wavelength parameter is determined by calculating the point on the graph where each curve has equal ordinates. This is given by $k_c|_m = k_c|_{m+1}$. Further information and a derivation of this equilibrium equation can be seen in Reference (30).

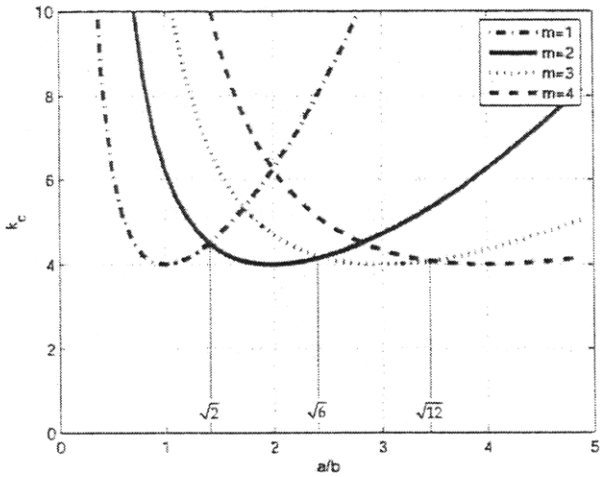

Figure 61: k_c versus length-to-width ratio detailing the effect of the wavelength parameter on the buckling load. Note the change in wavelength parameters occur at specific points where each curve is equal with respect to k_c.

The k_c versus a/b ratio diagram is useful for determining the appropriate wavelength parameter for a simply, simply supported boundary condition. Equation 30 can then be used to calculate the exact k_c value. For other boundary condition scenarios, Figure 12 or a variation is used.

A.3.3 Intermediate Boundary Condition Solution Figure

When intermediate boundary conditions are applied to a simple plate, Figure 12 in the plate buckling theory chapter is no longer valid. With the computer technology available today, different combinations of intermediate boundary conditions are easy to model in FEM or other methods. Prior to these methods, however, numerical simulations were completed to achieve graphical solutions (similar to figure 12) which can be seen below:

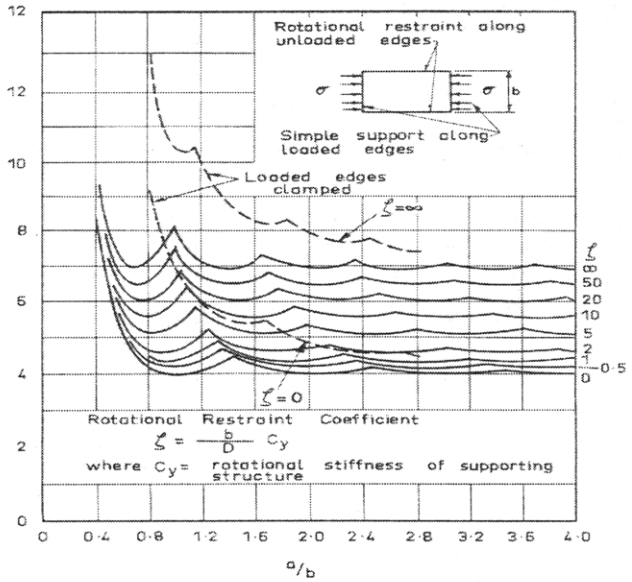

Figure 62: Graphical solution for a plate with simply supported loaded and intermediate unloaded edges. The work was completed by Ludquist & Stowell and is based upon the use of a rotational restraint coefficient (5).

Appendix: Chapter 4

A.4.1 Diagram of Failures – 123'

The following diagram shows the different failures associated with the 123'. These failures took place in a variety of different sea conditions and on a number of different ships within the 123' class. In all, 6 of the 8 cutters experienced serious debilitating structural issues and all 8 experienced stress corrosion related cracking of the aluminum hull. The figure can be seen below

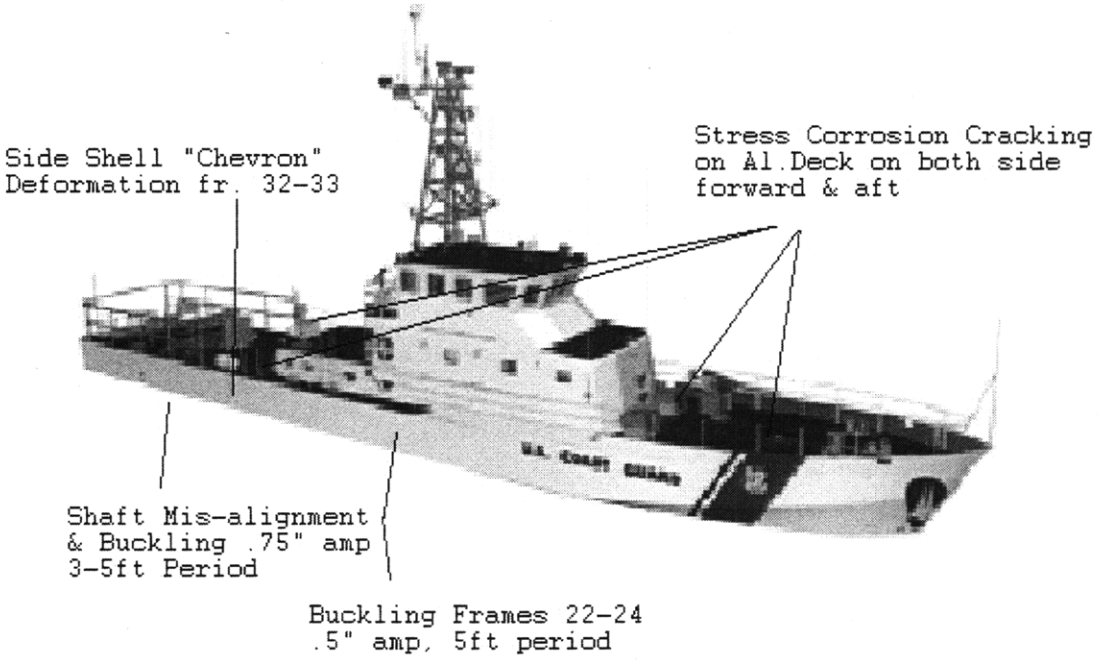

Figure 63: Visual Depiction of Failures of the 123' Class Cutter

A complete description of the failures seen on the cutter and the associated engineering explanations can be seen in the main text in section 4.1. The description of each of the failures is from interviews with participants in the 123' program (35) and Reference (2).

A.4.2 PC 179' Detailed Damage Diagram

The drawing on the next page shows the mid-ship section of the 179' pre-structural upgrade and the locations of the associated damage. Damage occurred in a progressive nature and is mainly attributed to operating outside of the designed mission envelope which caused undue severe dynamic loading both in compression and tension. The figure is reproduced from Reference (39).

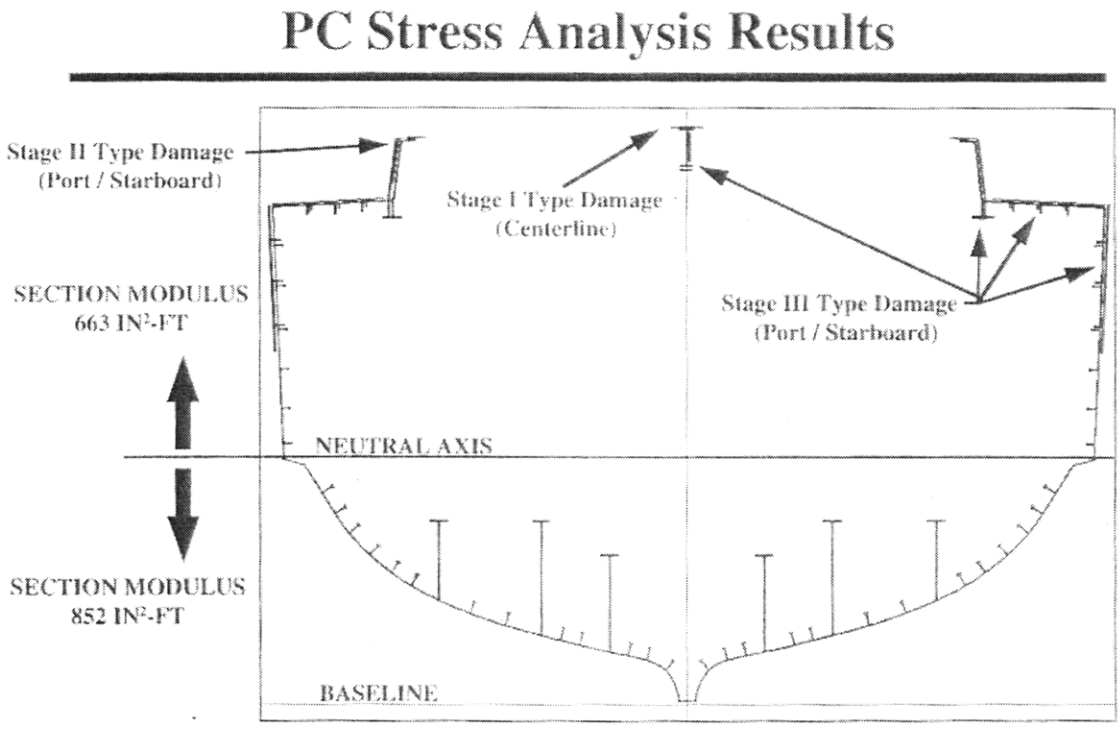

Figure 64: Locations of Damage on the 170' PC prior to its structural upgrade. The upgrade enabled several PC's to transit to take part in Operation in the Middle East and permitted the hull to be lengthened by 9'. This image is reproduced from Reference (39).

Stage I failure occurred first caused by tension loading, resulting in cracks of the centerline deck girder. Stage II failure followed as the raised engine casing was unable to hold the additional load caused by Stage I failure. Stage III compression buckling and yielding followed, caused by large compression stresses as the cracked support members were unable to hold their design load. More information on the failures can be seen in Reference (39).

A.4.3 123' Mid Ship Section

The U.S. Coast Guard 123' Midship Section is seen below as U.S. Coast Guard Drawing # WPB-123-085-031 Rev A. Note that there are some geometrical differences between the side shell plating present on the hull and that of the experimental side shell plate that is analyzed in Chapter 5. Although there is no significant discussion on why this discrepancy exists, the characteristics of the plate and stiffeners must be nearly identical (mechanical properties and rigidity, for example) for continuity purposes.

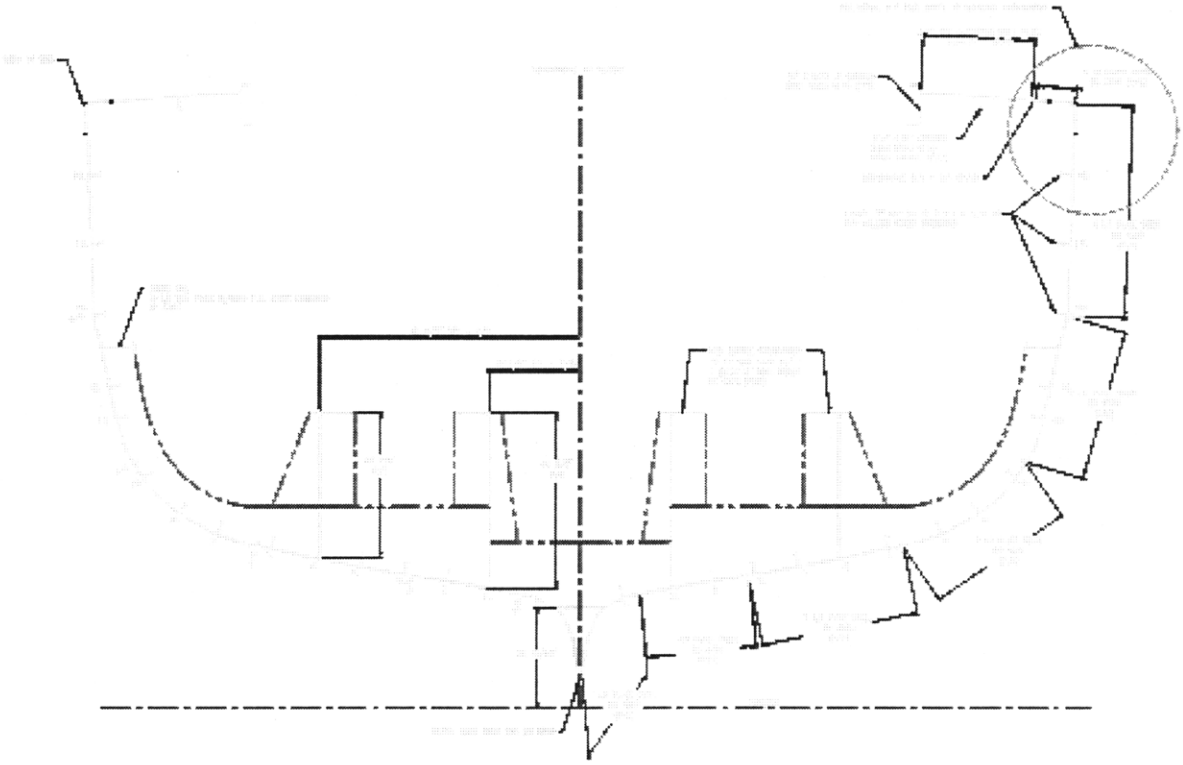

Figure 65: Midship Section for the 123'. This particular drawing, (taken directly from the ELC furnished drawings for the 123') show the doublers and sponsons that were added to all cutters after the Matagorda buckling event occurred. A magnified image of this area is available on the drawing itself, noted as Reference (37).

The mid-ship frame in this case is frame 23.5. More information on the mid ship section can be seen in the text in section 4.2.1.

A.4.4 ELC Spreadsheet Summary of 123'

In response to the structural failures of the 123', Deepwater Program officials and ELC engineers reviewed and upgraded the moment of inertia (MOI) and Section Modulus calculations for various pertinent frames. The summary of these results can be seen as Table 4-4 in Section 4.2.1. These results were drawn from Copies of Spreadsheet calculation for the mid-ship moment of inertia before and after the structural upgrade. The summary spreadsheet for the mid-ship section (fr. 23.5) is seen below:

	A	B	C	D	E	F	G	H	I	J	K
2	Mod	Item	Matl	Remarks		Side	$Y_{Centroid}$	$Area_{Current}$	AY	AY^2	I_{self}
3		Al deck	Al			S	156.54	0.68	106.72	16706.15	0.07
4		Steel deck	Stl			S	155.31	4.27	663.09	102982.26	0.69
5		Plate M	Stl			S	128.92	7.57	975.45	126846.70	575.73
6		Plate T	Stl			S	87.49	4.81	421.15	37146.66	97.10
7		Plate V	Stl			S	50.44	12.33	622.12	32488.69	95.22
8		Plate P	Stl			S	35.83	2.87	102.86	3685.70	2.16
9		Plate Q	Stl			S	29.60	7.21	213.45	6317.54	53.85
10		Plate AF	Stl			S	17.42	4.28	74.52	1298.02	79.07
11	Original	Steel Longitudinals	Stl			S	58.50	13.83	809.23	66155.87	5.88
12		Aluminum Longitudinals	Al			S	153.07	2.15	328.93	50354.13	29.47
13		Outer Engine Girder	Stl			S	0.00	0.00	0.00	0.00	0.00
14		Inner Engine Girder	Stl			S	0.00	0.00	0.00	0.00	0.00
15		**Total**					**71.95**	**60.0**	**4317.5**	**443981.7**	**939.2**
16				$D_{..}$	**SM Both Sides**			Previous		$+\Sigma AY^2 =$	443982 In4
17		**Top Fiber Height**	**156.54**	**84.59**	**3152 In3**		**5468 In3**		42%	$-(\Sigma AY)^2 / \Sigma A =$	-310651 In4
18		**Bottom Fiber Heigh**	**9.97**	**61.98**	**4302 In3**		**4801 In3**		10%	$I_{NA\ [Both\ Sides]} =$	**266662 In4**
19					1.3648024						
20											
21		Gunwale addition	Stl	**6.75" x 10#**		S	156.66	1.65	259.18	40604.46	0.01
22		Doubler Blw Dk Edge	Stl	**7.5" x 10#**		S	152.79	1.84	280.86	42913.21	8.617
23		Doubler Blw 18L	Stl	**7.5" x 10#**		S	134.79	1.84	247.78	33397.69	8.617
24	MOD 2	3x3/8" FB Longl	Stl			S	155.04	0.96	148.92	23087.92	0.720
25		**Total**					**79.25**	66.3	5254.3	144320.8	443999.7
26				$D_{..}$	**SM Both Sides**		Previous		Δ	$+\Sigma AY^2 =$	144321 In4
27		**Top Fiber Height**	**156.54**	**77.29**	**4448 In3**		3964 In3		-12%	$-(\Sigma AY)^2 / \Sigma A =$	-416414 In4
28		**Bottom Fiber Heigh**	**9.97**	**69.28**	**4963 In3**		3550 In3		-40%	$I_{NA\ [Both\ Sides]} =$	**343814 In4**
29					**1.11558**						
30		Sponson - Top	Stl	**8" x 10#**		S	155.18	1.96	304.28	47219.45	0.010
31		Sponson - Side	Stl	**11.28" x 10#**		S	149.42	2.76	413.11	61726.58	0.014
32		Sponson - Bottom	Stl	**10.7" x 10#**		S	138.43	2.62	363.04	50256.28	0.013
33		**Total**					**86.02**	73.6	6334.7	303523.1	443999.7
34	MOD 2 + Ext. Sponson			$D_{..}$	**SM Both Sides**		Previous		Δ	$+\Sigma AY^2 =$	303523 In4
35		**Top Fiber Height**	**156.54**	**70.52**	**5747 In3**		3569 In3		-61%	$-(\Sigma AY)^2 / \Sigma A =$	-544883 In4
36		**Bottom Fiber Heigh**	**9.97**	**76.04**	**5330 In3**		3550 In3		-50%	$I_{NA\ [Both\ Sides]} =$	**405280 In4**

Figure 66: Image of the Summary Spreadsheet for frame 23 on the 123'. The red numbers indicate the exclusion of the engine girders as structural members and the "previous" blocks indicate possible errors in the original calculations, acknowledged by Congress.

This spreadsheet shows the differences in the original, *post* retrofit of the stern launch structural calculations and the subsequent modifications. This summary spreadsheet has also been reviewed and modified by a Coast Guard member of the 123' Deepwater Staff. The individual part calculations and summary calculations for the other relevant frames can be seen in subsequent sheets of this Microsoft Excel file and additional files (Reference (42)), respectively.

A.4.5 ELC Structural Variation Figures for the 123'

As part of the structural calculations completed for the original 110' and the modified 123', a chart showing the relative change of significant values over the length each ship was created. Scaled versions of these images can be seen below.

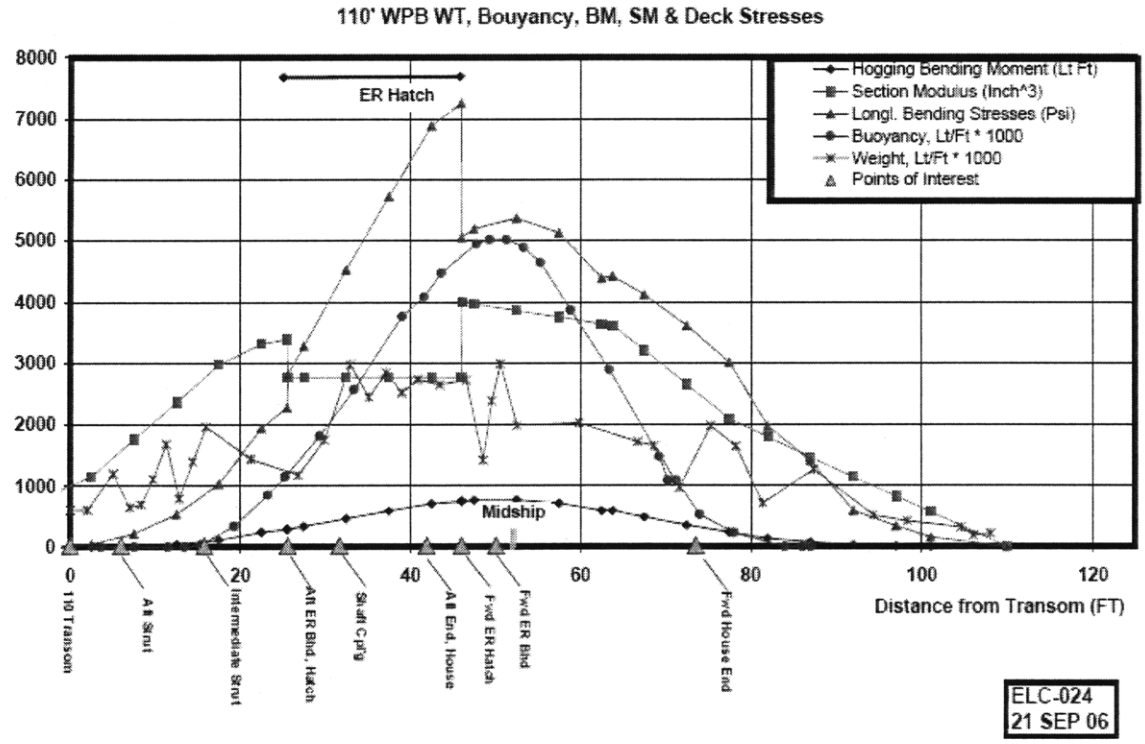

Figure 67: Notable variable trends as the x-location is varied over the length of the ship. Note the large increase in stress where the engine room soft patches are located.

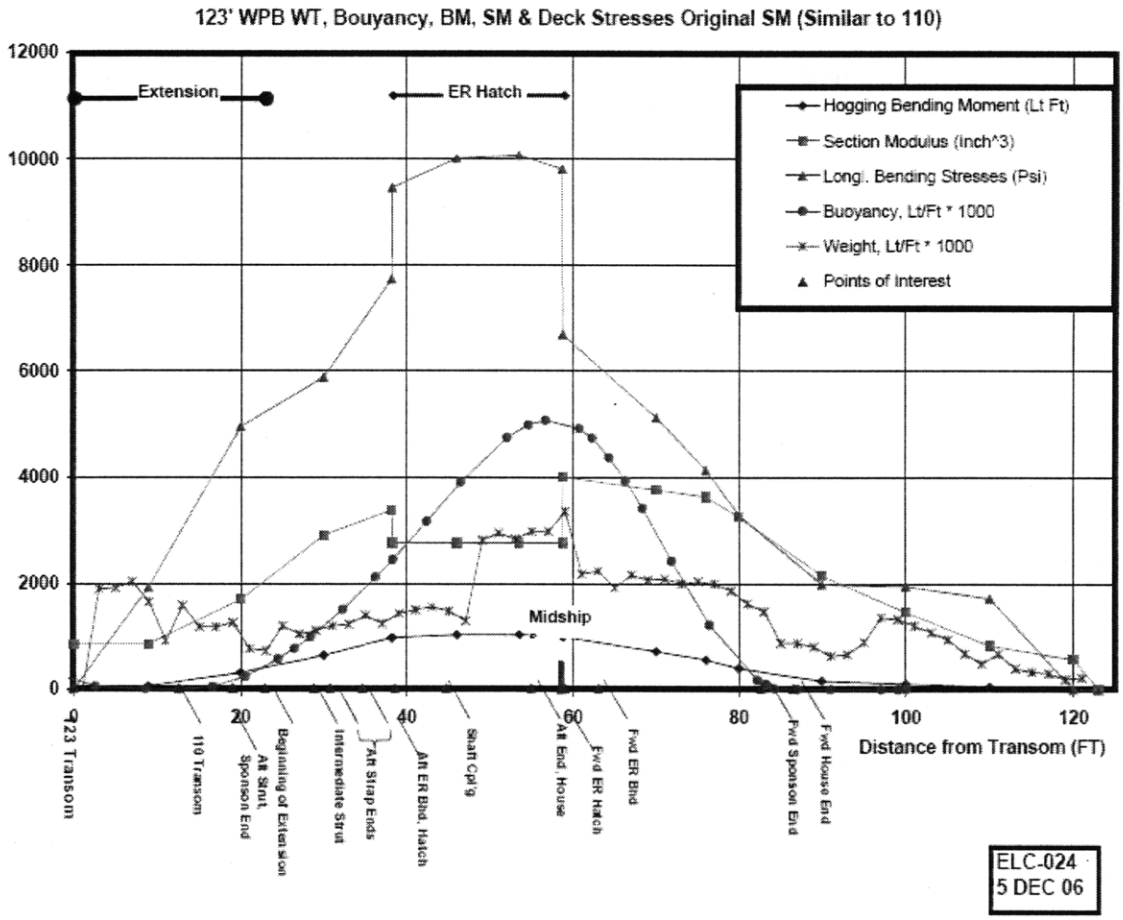

Figure 68: Notable variable trends as the x-location is varied over the length of the ship. It is obvious that there is a large increase in the primary bending stress due to the addition of the 13' extra feet. The value obtained for primary bending stress at the engine room hatch in this instance will not necessarily match up with the stress calculated in the text because of the variability in loading condition.

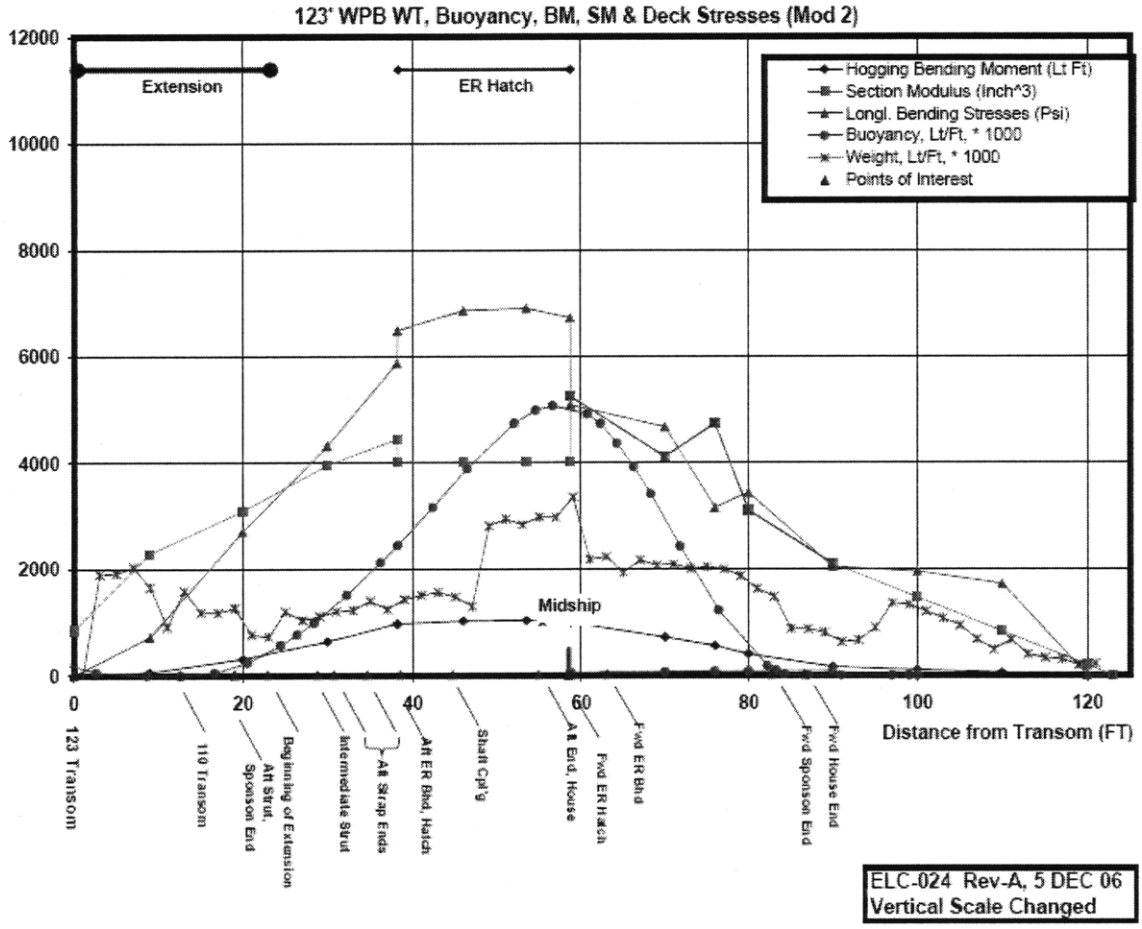

Figure 69: Graphical depiction of the changes caused by the structural upgrades in an identical loading condition as the previous figure.

The preceding figures show the changes in the "versions" of the 110' and 123' structural values. Each is reproduced from ELC-024 original files to supplement the text and to provide a visual of the variability of each structural term for this specific cutter (44). Most of these terms are discussed in length in Chapters 1 and 2 of the text.

A.4.6 Structural Variation Figure for PC

Similar to the previous section, the 170'-179' conversion case also had significant structural issues identified in the text in Section 4.2.2. Unlike the 123', no graphical analysis was completed of relevant mid-ship section structural values. However, tabular data was collected as part of the feasibility study for the 170' to 179' extension ship-alt and completed under NAVSEA. These values, along with verification that the ship meets ABS and DnV standards, are noted in Reference (46). To ensure continuity, a graphical depiction of the values seen in Tables 6 and 7 are seen below.

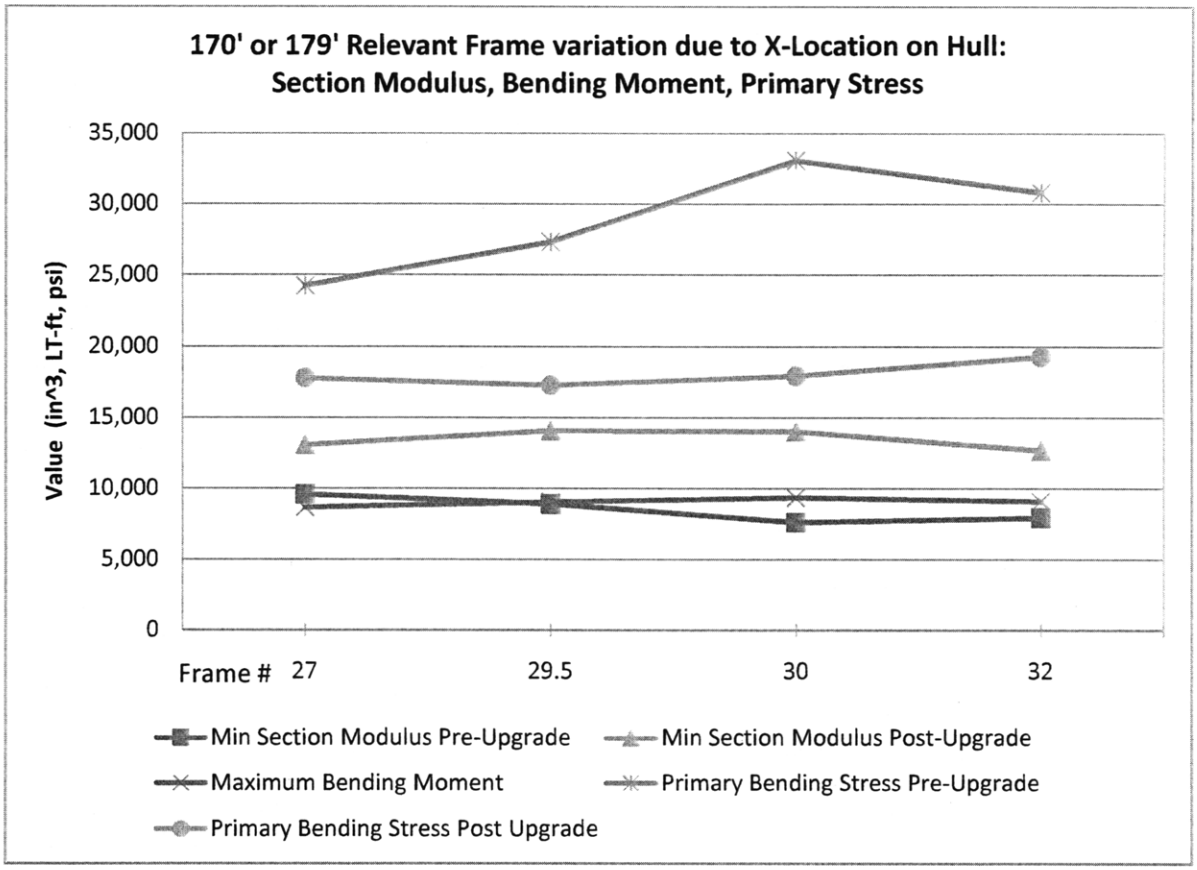

Figure 70: Notable variable trends as the x-location is varied over the relevant portion of the PC. The units for Section Modulus are inches^3 while Primary Bending Stress and Bending Moment units are psi and LT-ft, respectively. The Maximum Bending Moment trend shown is for the worst-case scenario moment identified by NAVSEA using dynamic force models.

Values in the figure above constitute a worst case sagging loading condition. It is obvious that the primary bending stresses present in the pre-structural upgrade ship are quickly closing in on the yield stress of the steel in question (BS 4360 grade British Steel). A complete discussion of the structural values associated with the 170'-179' can be seen in the text.

A.4.7 Method of Qualitative Vibration Calculations for the 123'

Scaling for the qualitative vibration characteristics was based on Mansour and d'Oliveria's work, authors of Reference (21). The scaling was completed to provide a qualitative, order of magnitude value to validate that dynamic forces (due to slamming) need to be considered.

These calculations are based upon worst case scenario correlation with the large cargo container ship that was used to quantify the bending moment due to slamming at a given wave encounter frequency, which correlates to wavelength over ship length nearing unity. Mansour and d'Oliveria show that this encounter frequency yields the largest addition in magnitude to the Bending Moment. The ship characteristics can be seen in this reference as well. Unfortunately, a time-varying computer model was used to predict the values, and although this model is valid for the 123' this is not the focus of this study and merely an order-of-magnitude correlation suffices.

The wave encounter frequency used for worst case scenario is 0.6 radians per second. This frequency correlates a bending moment of 275,000 LT-ft. This can then be scaled using both the Displacement and the Length as linear operators. The results are then compared with the 179' relative increase in bending moment to obtain the proper order of magnitude.

Mariner	Moment	2.75E+05	LT-ft
	Displacement	18674	LT
	LOA	563	ft
Island Class	Moment (displacement oper.)	**2577.1**	LT-ft
	Moment (length oper.)	**6.01E+04**	LT-ft
	Displacement	175	LT
	LOA	123	ft

Table 23: This Table notes the applicable characteristics and the results for the linear scaling of the added bending moment due to slamming.

From the results in Table 23 above, it is clear that the best correlation is the moment scaled using the displacement. The percentage correlations and results imbedded in the text can be seen in section 4.4.1.

Appendix: Chapter 5

A.5.1 Supplemental Figures from Experiment

The following figures are to be used as a supplement to the experiment conducted by the U.S. Naval Academy Structures Lab discussed in the text in section 5.2.2. They encompass actual results and are reproduced from Reference (7), the report from the Naval Academy to the U.S. Coast Guard Engineering Logistics Center.

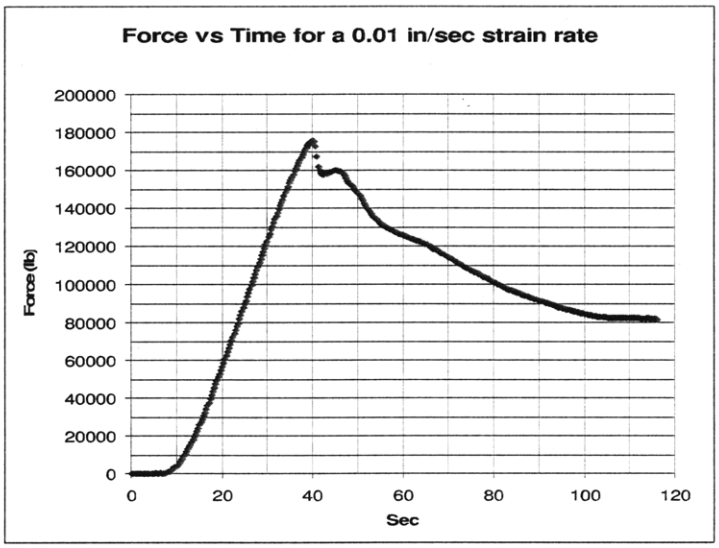

Figure 71: Load (lbs) versus rate of strain curve for the Ultimate Load Test Conducted at the U.S. Naval Academy.

In the figure above, note that this curve is based on a constant loading rate of .01 inches/second and the data has not been cropped to remove the pre-load collection data. The total displacement for the test was estimated to be approximately 1.1 inches.

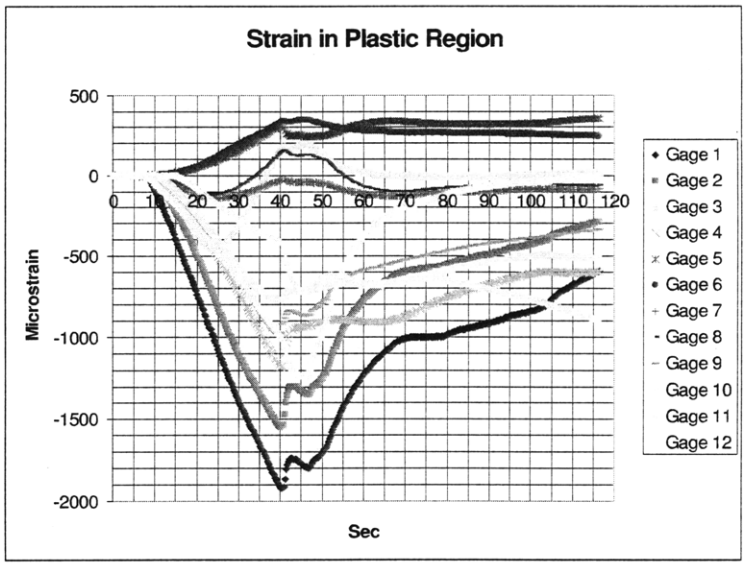

Figure 72: Strain gauge readouts for various locations on the plate surface. The placement of each gauge is noted in (7).

It is obvious right away the striking similarities in some of the strain curves to the data collection "strain" rate versus load curve. In an ideal world, the largest strain magnitude (seen on Gauge 1) can be easily translated into the maximum stress seen on the plate based on Hooke's law. Completing this calculation (assuming the micro-strain to be 1920 in/in and Young's Modulus to be 2.96E+7 psi), the maximum stress equals 56,832 psi, just under the ultimate stress of 58 ksi.

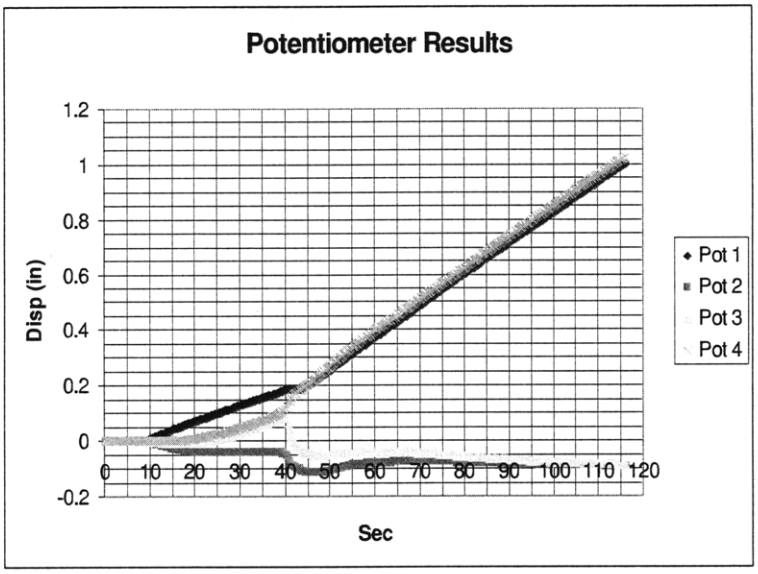

Figure 73: Data Collection lines for 4 mounted potentiometers during the ultimate load test.

In this case, it is obvious that potentiometers 1 and 2 lie very close to the edge of the plate while the other two are farther away from the compression mechanism. This explains the sudden return to a near normal location as the plate moves farther into the plastic realm. The exact Potentiometer locations can be seen in the reference.

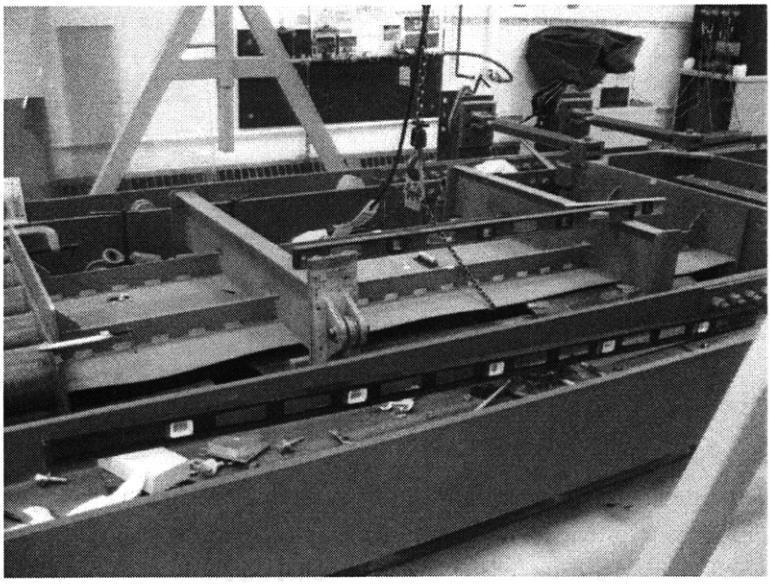

Figure 74: An image of the compression apparatus at the U.S. Naval Academy Structures Laboratory.

The figure above provides a good image of the scale of both the test panel and the apparatus.

A.5.2 Summary of Finite Element Methods

The FEA data collected is the compilation of numerical inputs and outputs relating to a mesh-like calculation completed by the ABAQUS/CAE software platform.

The ABAQUS/CAE solver uses both implicit and explicit methods to solve Finite Element Models (FEM) with complex geometries that would otherwise be difficult to accurately model. The differences in the Static, General and the Static, Riks modules within ABAQUS essentially solve the experimental plate load displacement problem in the implicit and explicit realms, respectively. Usually, complex models that have fast developing loads such as blast or impact (high frequency) loads are better modeled with an explicit scheme but in the long run they may be slightly less accurate. Low frequency, relatively long duration loads (such as the displacement load experienced by the test) are modeled accurately and decisively in the implicit scheme. A complete explanation of FEM methods can be found in References (29) and (53).

A.5.3 Explanation of Geometrical Parameter Calculations

Calculations pertaining to how different parameters were chosen for the study are actually quite straight-forward. They are derived from the drawings of the original Plate drawing (seen as Figure 36) and create variations that are fundamentally very similar to the plate itself.

The doubler smear variation in both the cropped plate and the actual test panel was accomplished by simple algebra. The doubler plate was said to be #10.2 lb steel which correlates to 0.239 inches as per the tabular data seen in Reference (18). The total volume of the doubler plate was then determined using the appropriate measurements from Figure 5-1 and that volume was added to the total volume of the base plate with the original thickness of .112 inches, or #5 lb steel. Then the area of the base plate was divided out per the desired dimensions, and the new thickness was determined. The calculation is below:

$$h_{New} = \frac{V_{Doubler} + V_{Plate}}{A_{PlateSurface}}$$

$$\therefore V_{Doubler} = l \times w \times h = 82" \times 7.5" \times 0.239" = 147.0"$$

$$V_{Plate} = l \times w \times h = 94 \times 32 \times 0.112" = 336.9"$$

$$\therefore h_{new} = \frac{147.0" + 336.9"}{94" \times 32"}$$

$$h_{New} = 0.161"$$

Depending on the overall geometry of the plate-stiffener combination, the procedure above was slightly modified in several instances to provide a more accurate assessment of the elastic-plastic characteristics of some of the specimens. This was true for the stiffened panel that only considers the center bay. Experts have stated (also repeated in Reference (18)) that appropriate analysis of this nature can be completed using only a single frame or several frames because the results should ideally be the same.

It should be noted that on the actual hull, the doubler plates and sponsons (seen in pictures of the hull and in Coast Guard Official Drawings) extend nearly 40% of the way down the hull. This is to ensure they are legitimately counted in the mid-ship section moment of inertia and subsequent section modulus calculations. The Official Coast Guard reasoning is for "robustness" (2).

A.5.4 Finite Element Analysis Buckling Data

The data seen below is from the FEA Buckle module as completed through a series of "runs" at a variety of different geometries and boundary conditions. It is well established that boundary conditions that are more restrictive than the "Alpha" condition are not necessarily plausible for the side shell of a ship but they are included for comparison purposes. The data values that are missing were removed due to being extreme outliers. In this data set, ABAQUS was only solving for a buckling instability and some of the geometrically sound structures noted towards the bottom of the table will certainly fail in yield prior to buckling.

All data point units are in pounds	4 Sides SS	Load SS Unload FR (Frmod)	Load SS Unload CC	Alpha	Load CC Unload SS	4 Sides CC
18X46 Simple Plate	11993.4	295.38	20792	11998.98	30004.2	34088
32X46 Simple Plate	9731.2	535.68	10143	10137.6	13435.2	14627
32X46 Stiffened Panel	36597.8	30764.8	35503	35514.04	49153	46444
32X46 Doubler Smear Stiff. Panel	117803.8	95418	113240	113285.6	154876.6	145510
32X46 Stiff Panel w/ s Xtra stiff	152040.3	110076.8	148613	161806.5	190994.4	190994
Exp. Plate FEA w/o doubler	35999.68	31252.34	36071	36092.78	52489.4	52592
Exp. Plate w/ Smear Doubler	101543.6	83603.8	102144	102265.6	147234.8	148132
Exp. Plate w/ Extra Stiffener	128530.9		147965	148128.9	200526.9	200974
Exp. Plate w/ Smear & xtra Stiff.		119126.2				

Table 24: Finite Element Data Table for tests run in the ABAQUS/CAE FEM modeler. The graphical representation of this chart can be seen in the text as Figure 42.

In each case, only the length x width geometry is given. In this case, it shall be assumed that the original #5 Plate thickness (0.112in) was used except in the case where a smear doubler was noted. For the Experimental plate, the new smear thickness is 0.161 inches and for the 32"x46" plate the equivalent smear thickness is 0.168 inches.

A.5.5 Selected Finite Element Analysis Buckling Images

The following are a selected group of FEA buckling images. They were generated in ABAQUS/CAE. The numerical results of each image are seen in the table in the preceding section. Each figure seen below is labeled as appropriate for each test. The rest can be seen at the request of the author.

The images are generally grouped in pairs unless otherwise noted, showing the loaded edge simply supported, unloaded edge free (or free modified) condition, followed by the simply, simply supported condition. In some cases the alpha condition is added (if any obvious change is seen) for each geometry.

More on what encompasses each boundary condition can be found in the text in Chapters 3 and 5 or any mechanics textbook.

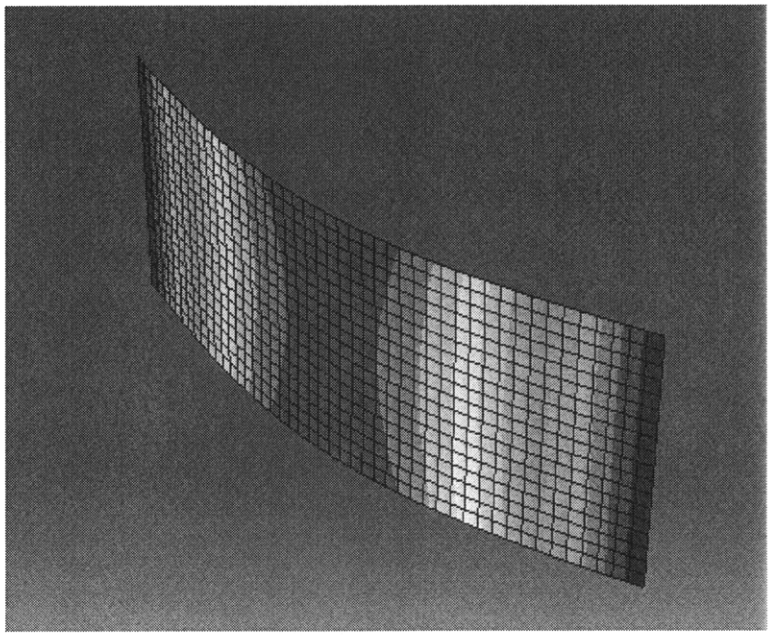

Figure 75: 18"x46" Simple plate in first mode buckling (Euler)

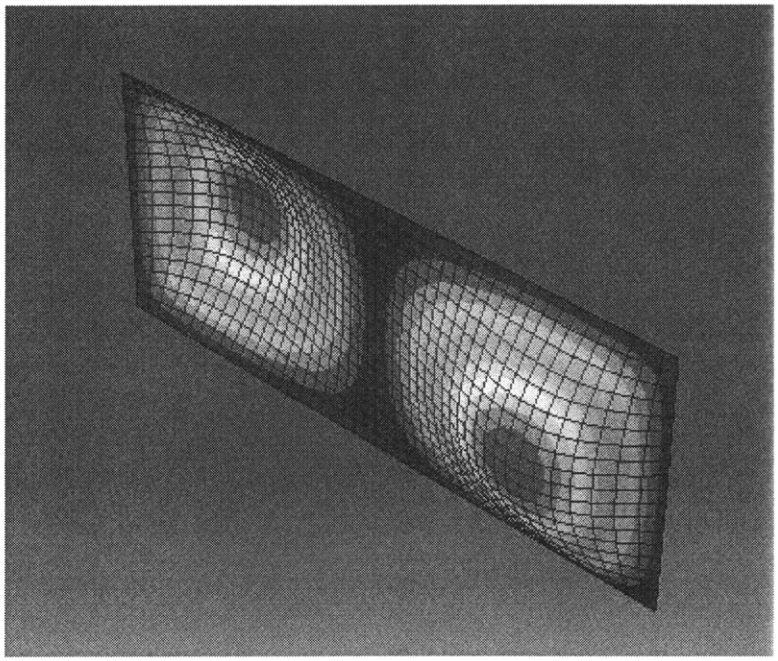

Figure 76: 18"x46" Simple plate in 2 mode buckling (simply, simply supported)

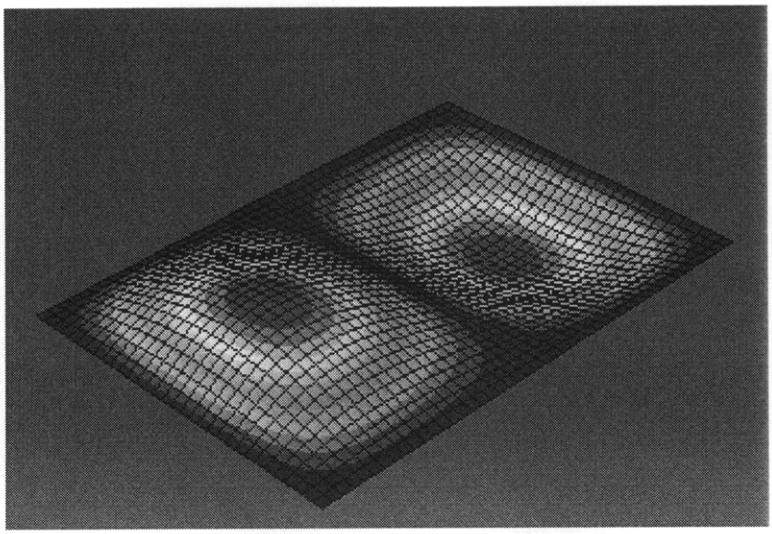

Figure 77: 32"x46" Simple plate in 2 mode buckling (simply, simply supported)

The following images show the modified longitudinally stiffened 46"x32" panel with original thickness.

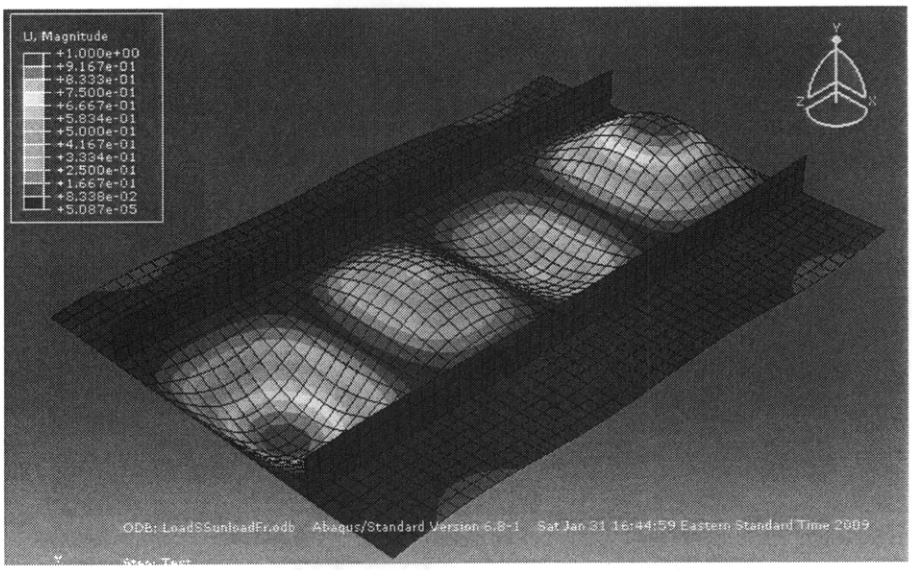

Figure 78: 32"x46" Longitudinally stiffened panel in 4th mode buckling (Euler).

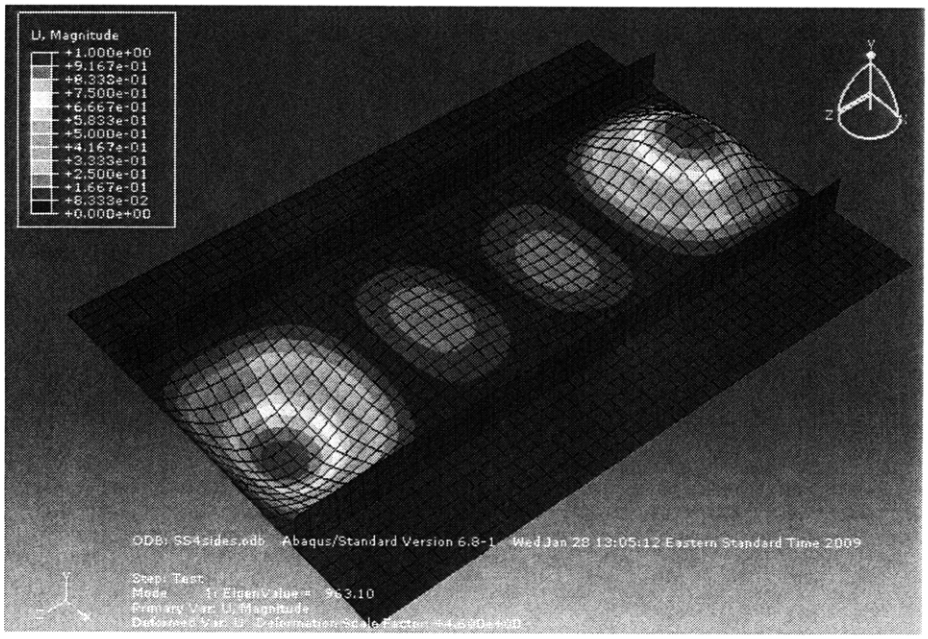

Figure 79: 32"x46" Longitudinally stiffened panel in 4th mode buckling (simply, simply supported).

While the preceding two figures show the original stiffened panel, the figure below shows the change in buckling mode due to a change in thickness by considering the doubler in the simply, simply supported mode. The Euler mode figure is seen in the text as Figure 41.

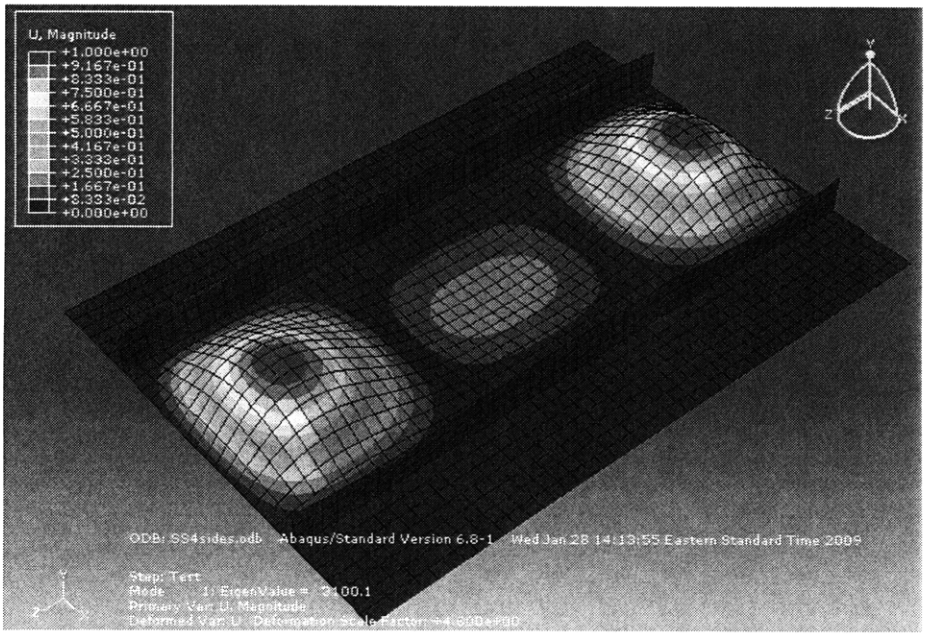

Figure 80: 32"x46" Longitudinally Stiffened Panel in 3rd Mode buckling with the doubler smear considered (0.168 inch thickness-simply, simply supported).

The rest of the images on the following pages show actual Eigen-value buckling solutions for the Finite Element Geometry detailing the 3 bay panel used in the experimental testing. Considerations for the doubler are noted if applicable in the figure captions.

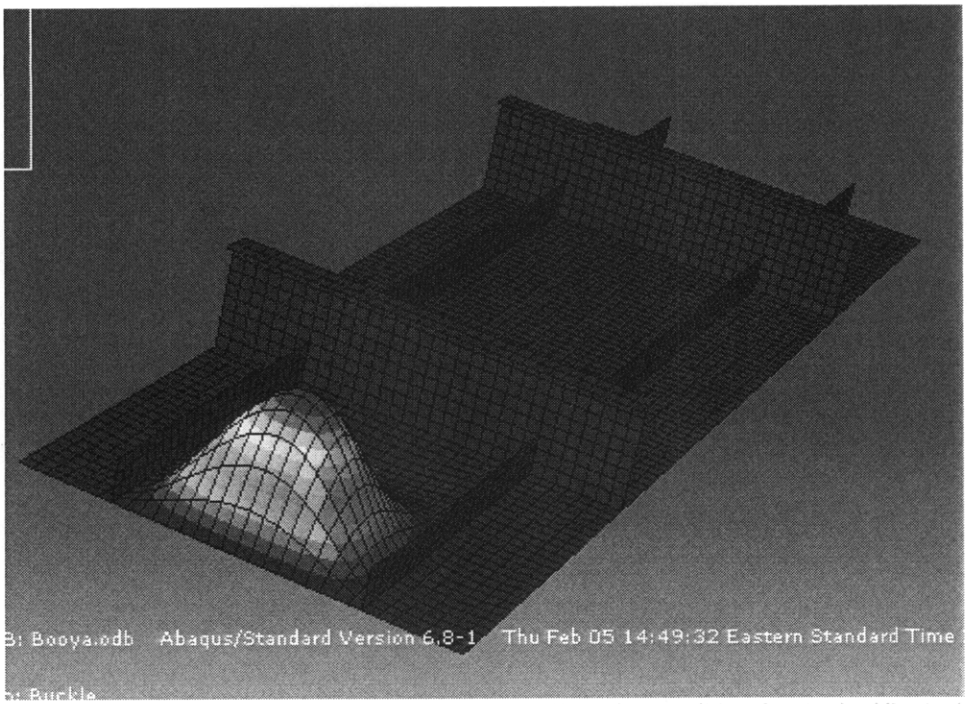

Figure 81: Actual Experimental plate with a simply, simply supported boundary condition showing buckling in the end bay.

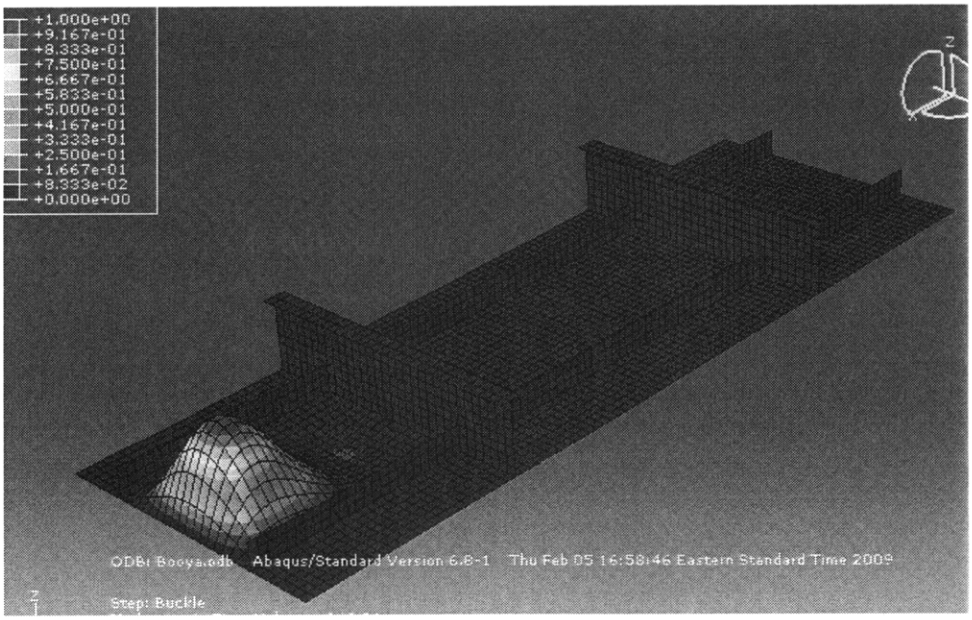

Figure 82: Experimental plate buckled in the end bay in the "Alpha" boundary condition. Note the slight depression in the negative z-direction indicating the end bay buckling in a slightly different configuration than that of a simply, simply supported plate.

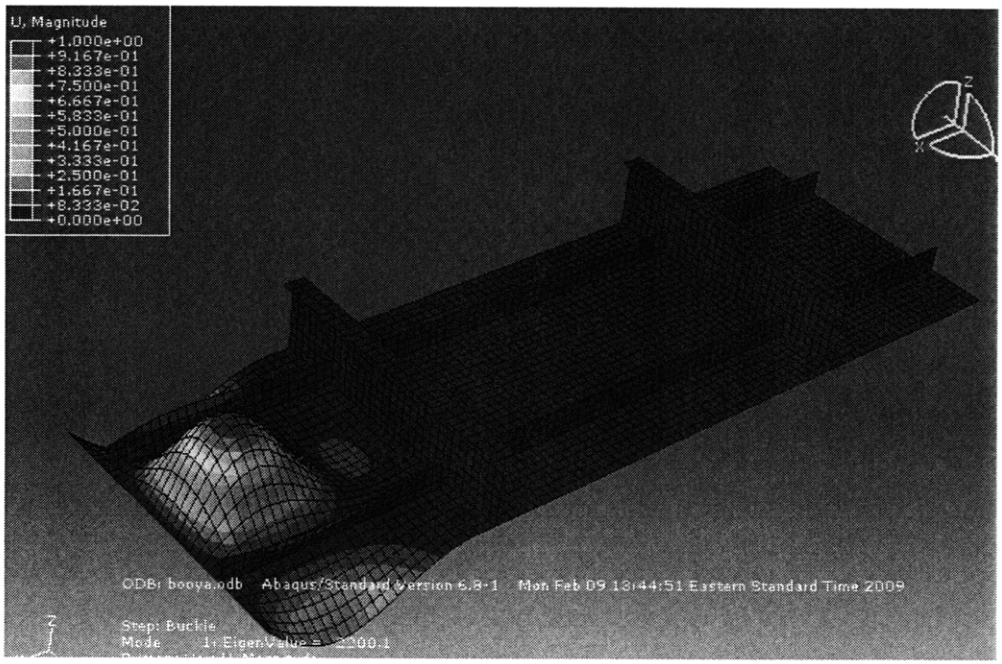

Figure 83: Experimental plate with Euler boundary conditions and accounting for the doubler smear. Note that the buckling characteristics do somewhat resemble what was seen on the actual panel testing.

A.5.6 Analytical Plate Theory Buckling Calculations

In most cases, the mathematical calculations shown in this portion of the Appendix were completed in Microsoft Excel. Whenever possible, all variables are shown and different intermediate steps are also generally given. Since many of the spreadsheet calculations dealt with more than one data set, the numbers actually filling the tables show only one set of data collected. For more clarity on the calculation process or intermediate steps, information can be found in Section 5.2.2 or the appropriate references. These calculations are based on basic plate theory outlined in Section 3.1.2 of the text. The material properties for BS 4360 Steel are detailed in Section 5.2 and can also be found in Reference (49).

Plate Theory Calculations					
Variables	**Values**	**Units**	**Variables**	**Values**	**Units**
v	0.3	n/a	v	0.3	n/a
E	2.96E+07	psi	E	2.96E+07	psi
a	46	inches	a	46	inches
b	18	inches	b	32	inches
m	3	wavelength	m	2	wavelength
a/b	2.5555556	n/a	a/b	1.4375	n/a
D	11312.19	lbs-inch	D	12852.775	lbs-inch
h	0.161	inches	h	0.168	inches
Kc	4.1037234	n/a	Kc	0.45	n/a
PxCr	25453.765	lbs	PxCr	1783.8536	lbs

Table 25: This Table shows the Spreadsheet calculations for simple plate theory. For the simply, simply supported calculations or Euler Calculations, k_c is determined using Equation 30 in the text or wide column theory, respectively. For other boundary conditions, a graphical approach is used based on Figure 12.

The two tables seen below are meant to be a supplement to the buckling theory calculations and to Table 11, seen in the text. Each show applicable k_c factors based on geometry and the differences in buckling mode determined in analytical and finite element methods. Each covers basic plate theory.

18"x46" k_c and Wave Response Data					
	SS-Free	SSSS	SS-CC	CC-SS	CCCC
kc factor	0.14	4.1	6.95	4.45	7.7
wave # in FEA	1	2	3	2	3
wave # in analytic	1	3	4	2	3

32"x46" k_c and Wave Response Data					
	SS-Free	SSSS	SS-CC	CC-SS	CCCC
kc factor	0.45	4.45	7	5.4	8.75
wave # in FEA	1	2	2	2	2
wave # in analytic	1	2	2	1	2

Table 26: (a&b) The tables above show buckling mode (wave response numbers) for each applicable boundary condition across two methods of analysis and two separate geometries.

A.5.7 Analytical Stiffened Panel Theory Calculations

The following Spreadsheet calculations stem from the different acceptable methods used to calculate the overall axial loading capabilities of longitudinally stiffened panels. These calculations are completed on the premise that the transverse and longitudinal stiffeners act as simply supported boundary conditions where applicable. Every effort is made to account for the free or free-modified unloaded edge condition seen in the experimental testing.

As discussed in the text in section 5.2.2, two independent sources allow basic Euler column theory to be used when determining the axial strength of a plate-stiffener combination. Just like Euler theory, however, this approximation only holds true when buckling occurs in the overall mode. Since the Euler method (Section 3.1.1) is based upon material properties, an effective length and the moment of inertia with constant multipliers, the spreadsheet below accounts for the plate-stiffener M.O.I. using a $b_{effective}$ for the width of the plating consistent with Von Karman. Just as in previous portions of this appendix, the spreadsheet only shows one iteration of the M.O.I. although more than one was conducted based upon geometrical changes.

Calculation of Moment of Inertia (Used in Euler Buckling Theory)								
Piece	t	w	A (in ^2)	dn (in)	A-dn (in^3)	A-dn^2 (in^4)	h (in)	io (in^4)
Plate	0.168	8.8	1.4784	0.084	0.1241856	0.01043159	0.168	0.0034772
Stiffener	0.375	3	1.125	1.668	1.8765	3.130002	3	0.84375
						PI	3.141593	
A	2.6034	in^2				E	2.96E+07	
Dg	0.7684895	in				I	2.450155	
In	3.9876608	in^4				Leff	46	
Io	2.4501549	in^4	Moment of Inertia			Load Calc:	338274.6	
	R. of Gyn 2, plate thick 0.112			1.001				
	R. of Gyn 2, plate thick 0.168			0.97		Radius Of gy.	0.970122	

Table 27: Moment of Inertia calculation spreadsheet for ideal Euler column buckling. This method is only valid for plate-stiffener combinations that fail in mode I. The method of calculation for the MOI is replicated from (4).

The effective width calculation is used in Euler column theory and is therefore inserted at this point in the Appendix. While effective width was originally developed for simple plates, it is applicable to stiffened panels. The table seen on the following page incorporates two geometries; the reasoning behind this is discussed in the text. The $b_{effective}$ coefficient is determined using the relationship between the k_c value and the constants seen in Equation 31. Using this coefficient, $b_{effective}$ is then calculated using Equation 39, incorporating the relationship between several material properties, and the thickness of the plating. The $b_{effective}$ value can then be used to approximate ultimate load of a plate.

$b_{effective}$ Calculation (Von Karman)		
$k_c = 4.45$	b_{eff} Coefficient	2.005
Geometry 32"x46"	b_{eff}	9.17
$k_c = 4.103$	b_{eff} Coefficient	1.926
Geometry 18"x46"	b_{eff}	8.80

Table 28: The spreadsheet used for the effective width calculation based on Von Karman's approach. The theory behind this can be seen in the text in Chapter 3 and more extensive information can be found in Reference (30).

In addition to the effective width calculation used to approximate ultimate load which is essentially based on buckling theory, Von Karman also used a similar approach to approximate longitudinally stiffened panel strength under axial load by treating each piece of plating between stiffeners as an individual slender plate. Although his work was completed assuming all sides of the panel to be simply supported, the method was modified to consider each of the outer plates to have one unloaded edge simply supported and the other edge free. This theory is noted in Section 3.1.3. The table below shows the calculation of each piece and the subsequent summation.

Von Karman Analytical Calculation of Stiffened Panel Buckling Load						
	Sides	Middle				
k_c	0.43	4.10		Summation	2Stiff	3 Stiff
Pi Squared	9.87	9.87		BC 4SS	28,915.17	57,830.33
D	12,852.78	12,852.78		BC 4SS	7,792.33	15,584.65
S (width)	7.00	18.00		BC 4SS	7,792.33	
P_{cr}	7,792.33	28,915.17		Totals	44,499.82	73,414.98

Table 29: This table shows the spreadsheet calculation for stiffened panel axial buckling load using a Von Karman approach. This method essentially adds the different plate segments between each longitudinal stiffener based on applicable B.C's.

As before, this Table was used as a calculation spreadsheet so not all runs are shown above. The different summation columns to the right are indicative of different geometrical considerations and are summarized by Equation 35, to aid in the calculation of the variation of strength due to the addition of extra support.

A.5.8 Analytical Ultimate Load Calculations

Ultimate load calculations are based upon Von Karman's effective width theory discussed in Chapter 3 and in previous sections of this Appendix. Von Karman's method is modified slightly to account for stiffeners, as presented in Equation 43. The calculation of ultimate load is based on the relationship of the yield stress and the overall effective area designated by b_{eff} and a thickness (in this case, the cross sectional area of the stiffeners was included to allow for a better approximation). The spreadsheet where the ultimate load calculations were completed can be seen below. A complete table of the results is seen in the text as Table 15.

Calculation	No Doubler Smear: h = 0.112 in	Doubler Smear: h = 0.168 in
$B_{effective}$	5.87 inches	8.80 inches
P_{ult} Load	142,595 lbs	208,272 lbs

Table 30: Excel Spreadsheet used to calculate Ultimate Load based on Equations in Chapter 3 of the text.

The calculation above is based upon the 18"x46" sub-plate geometry. Using this geometrical representation (basically formulating all of the calculations off of the center region of the panel) provides the best approximation because of the lowest critical buckling mode. If overall mode one failure occurred first, the plate-stiffener combination would be most likely be better modeled by the 32"x46 geometry.

A.5.9 Finite Element Load Displacement Curves

The following load displacement curves represent all of the data collected from ABAQUS/CAE based the experimental plate seen in its drawing as Figure 36 with transverse and longitudinal stiffeners. Variations in plate thickness are shown, as well as the addition of an extra longitudinal stiffener, bisecting the original two. In each figure, the effect of different boundary conditions is noted while geometry remains the same. The geometry is noted in each figure title. The Static, General FEA method was used in this instance.

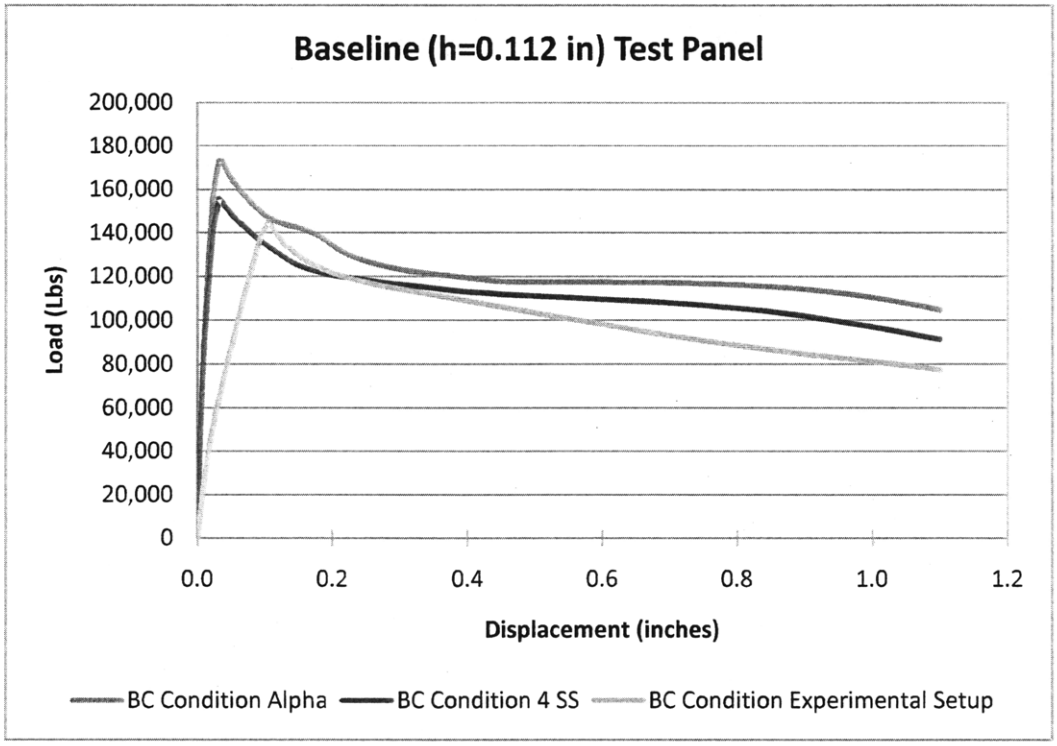

Figure 84: This figure shows the baseline stiffened panel with no doubler added. These curves represent an ideal plate.

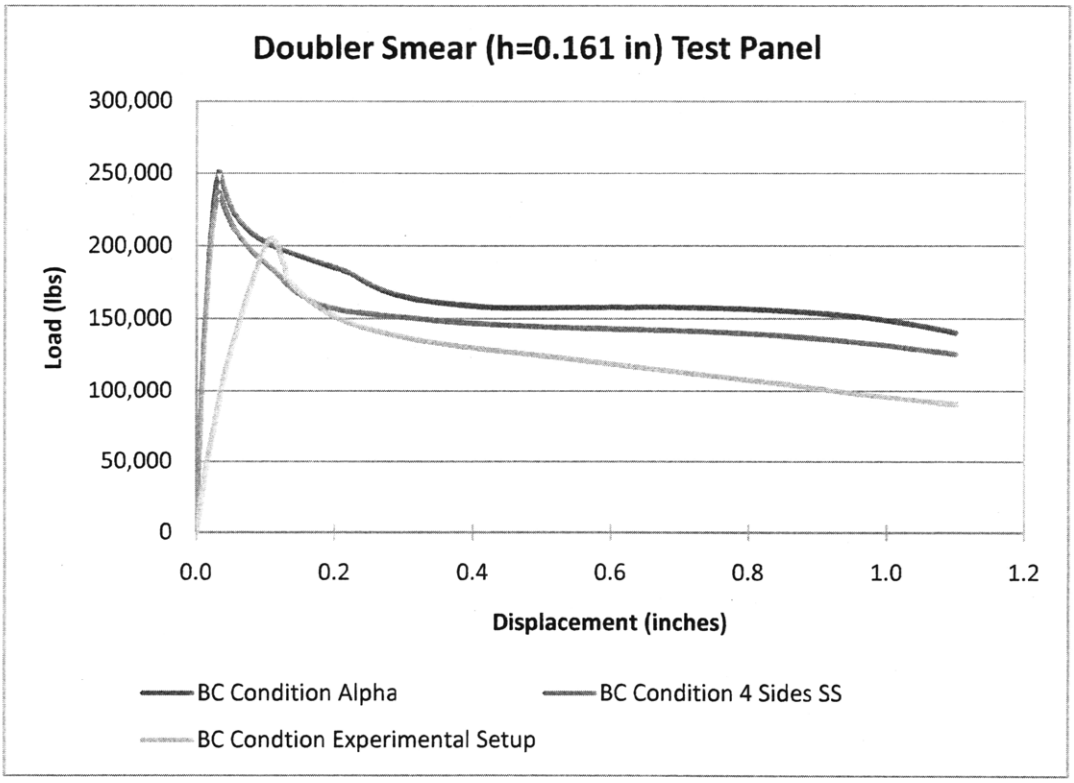

Figure 85: This figure shows the stiffened panel with the doubler smear added. These curves represent an ideal plate.

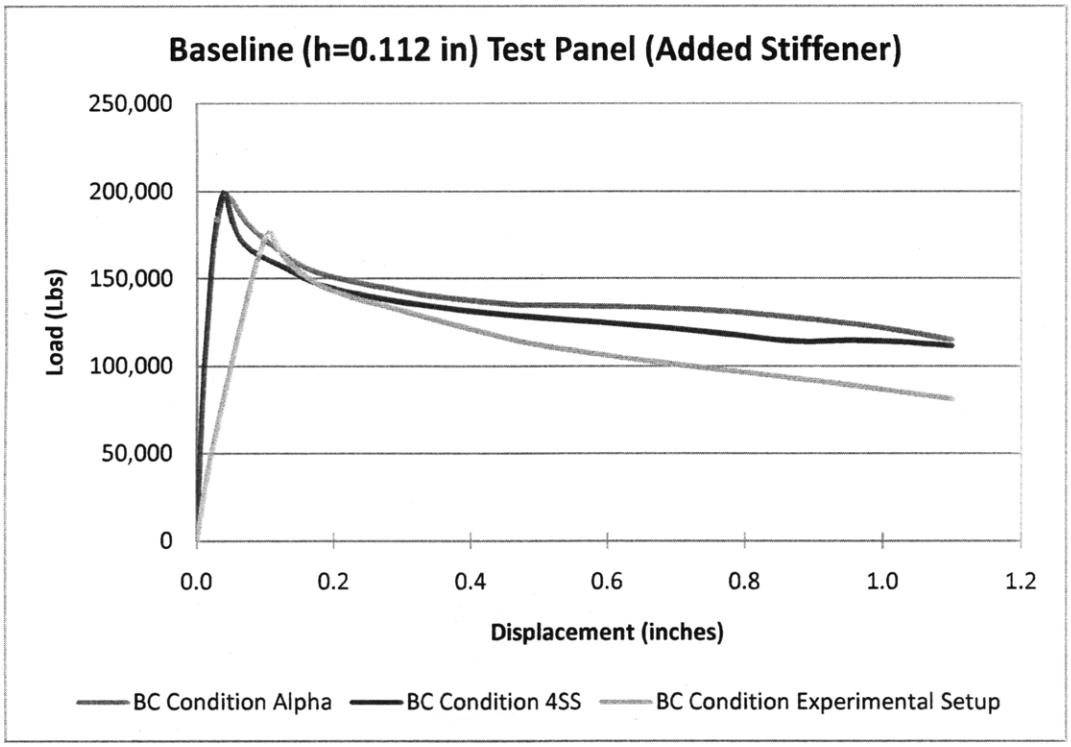

Figure 86: This figure shows the baseline stiffened panel with an extra stiffener added but no consideration for the doubler. These curves represent an ideal plate.

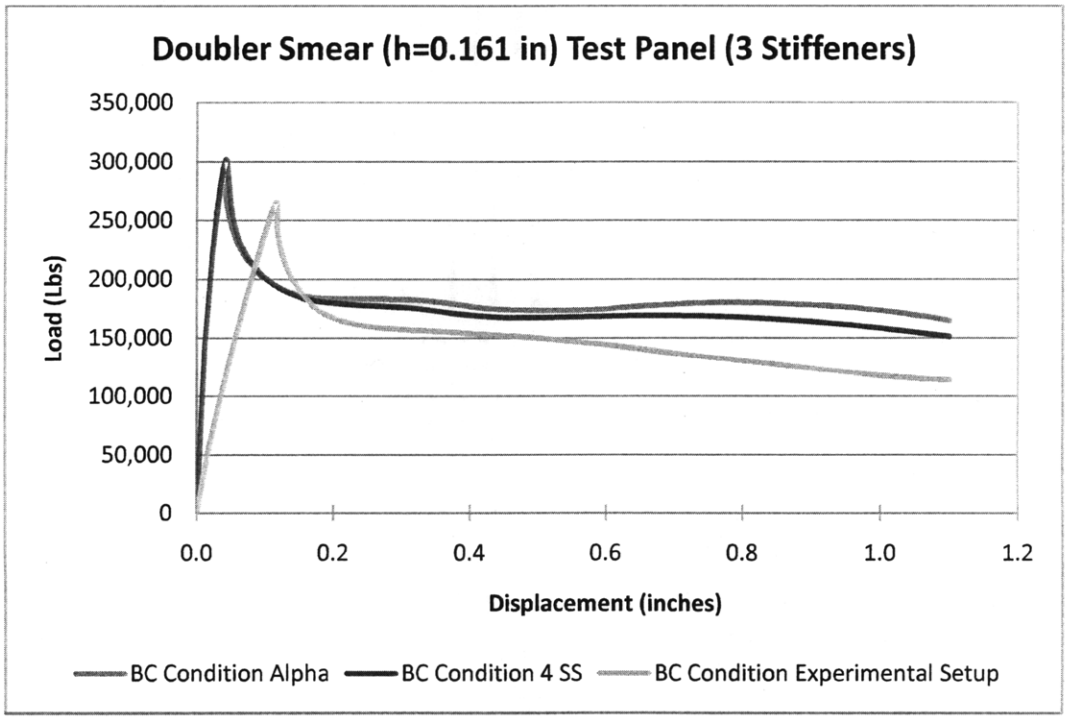

Figure 87: This Figure shows the stiffened panel with the doubler smear added, as well as an extra stiffener. These curves represent an ideal plate.

A.5.10 Selected Finite Element Analysis Ultimate Load Images

The following images correspond to the load displacement curves seen in the preceding section. The images seen below are grouped according to geometric specifications and show boundary conditions used in the experimental test, (for comparison) and either the simply, simply supported boundary condition or the Alpha condition. The rest of the pertinent images can be seen at the request of the author.

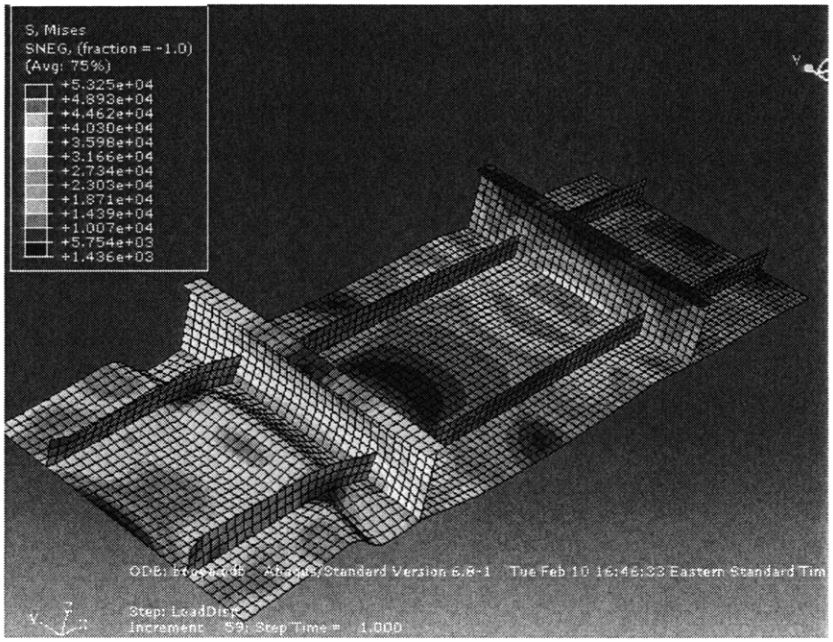

Figure 88: This image corresponds to the baseline panel with experimental (Euler) boundary conditions. These results are for an ideal plate.

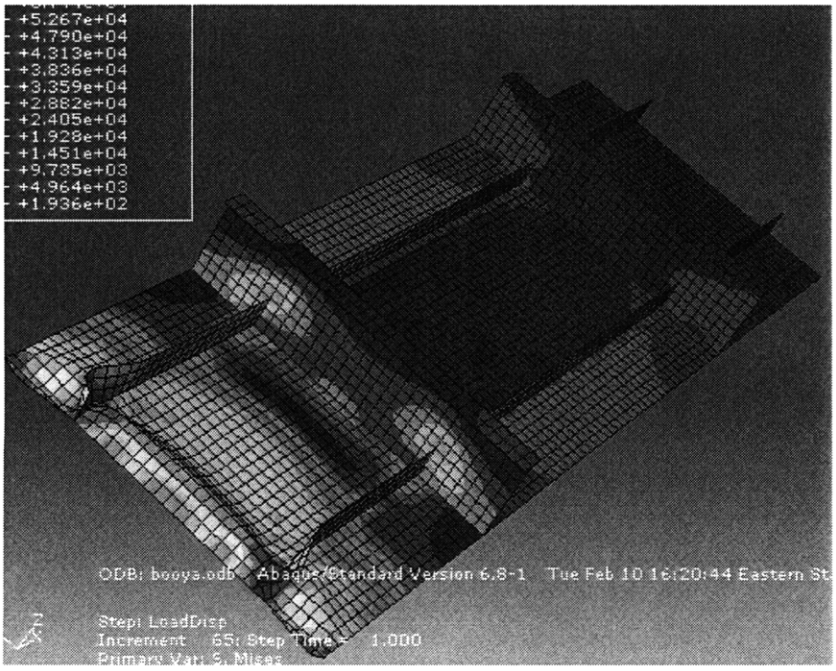

Figure 89: This image corresponds to the baseline panel with 4SS boundary conditions. These results are for an ideal plate.

The next several images show the baseline panel with additional thickness to account for the smeared doubler plate. Note the changes in the stress distributions caused by the base plate thickness change.

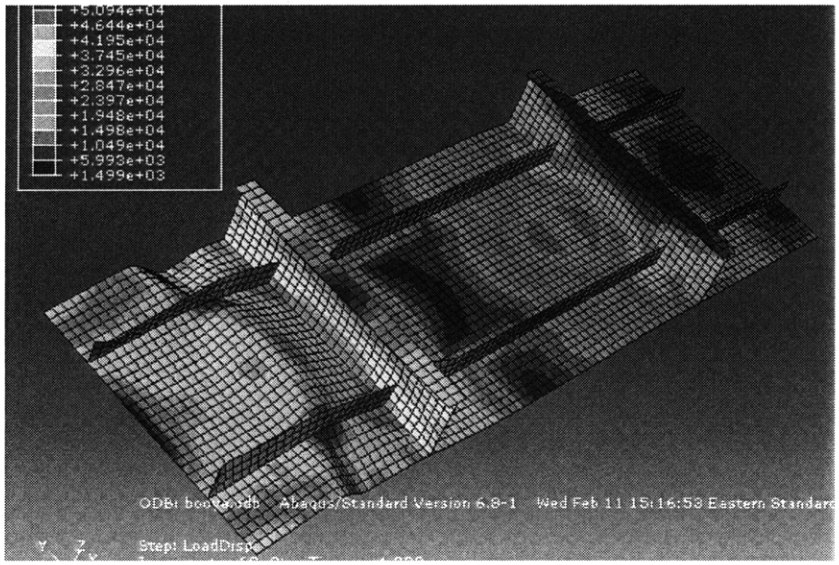

Figure 90: This image corresponds to the baseline panel with experimental (Euler) boundary conditions and an increase in thickness to account for the doubler. These results are for an ideal plate. These results were used to provide an "ideal plate" ultimate load to compare with the experimental results.

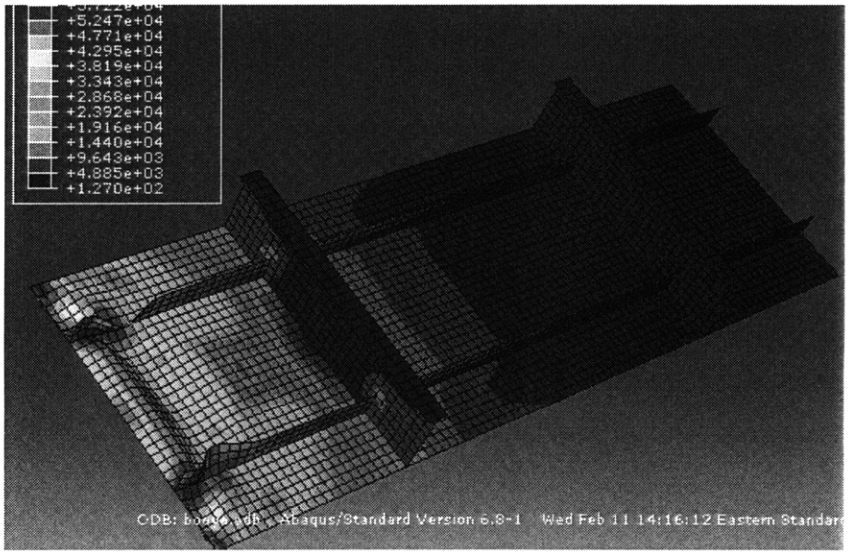

Figure 91: This image corresponds to the baseline panel with condition Alpha boundary conditions and an increase in thickness to account for the doubler. Note the relative change in the stress distribution due to the change in boundary conditions. These results are for an ideal plate.

The next set of images seen on the next several pages show the new stress distribution based on the addition of an extra stiffener. The resulting ultimate loads calculated by ABAQUS/CAE are seen graphically in the previous section of this Appendix.

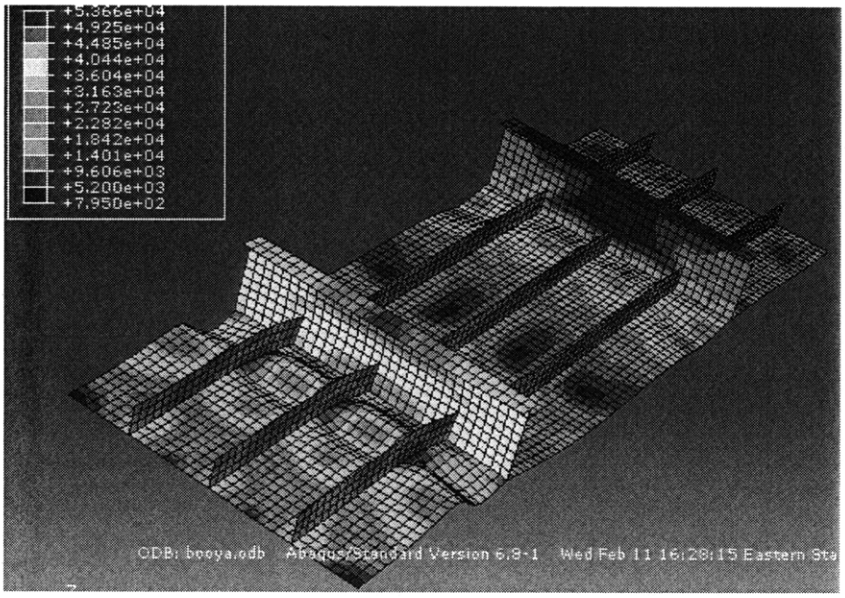

Figure 92: This image corresponds to the baseline panel with experimental (Euler) boundary conditions and an extra stiffener added. This test run is a result of a recommendation from an outside body that an extra, intermediate stiffener could be added to strengthen the 123's hull. These results are for an ideal plate.

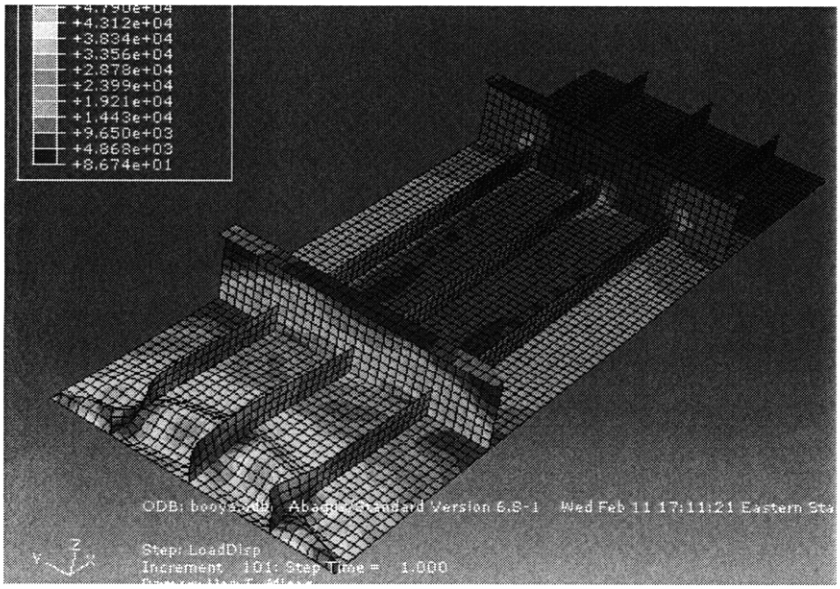

Figure 93: This image corresponds to the baseline panel with simply, simply supported boundary conditions and an extra stiffener added. These results are for an ideal plate.

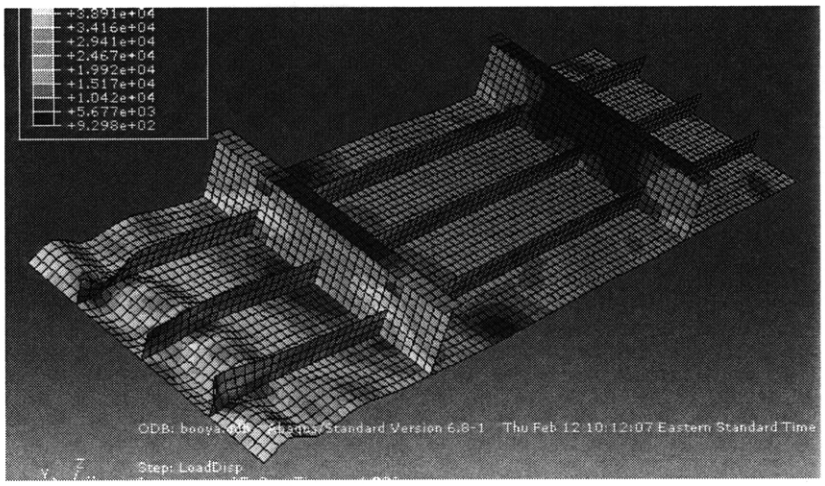

Figure 94: This image corresponds to the baseline panel with experimental (Euler) boundary conditions, an increase in thickness to account for the doubler, and the addition of an extra stiffener. These results are for an ideal plate

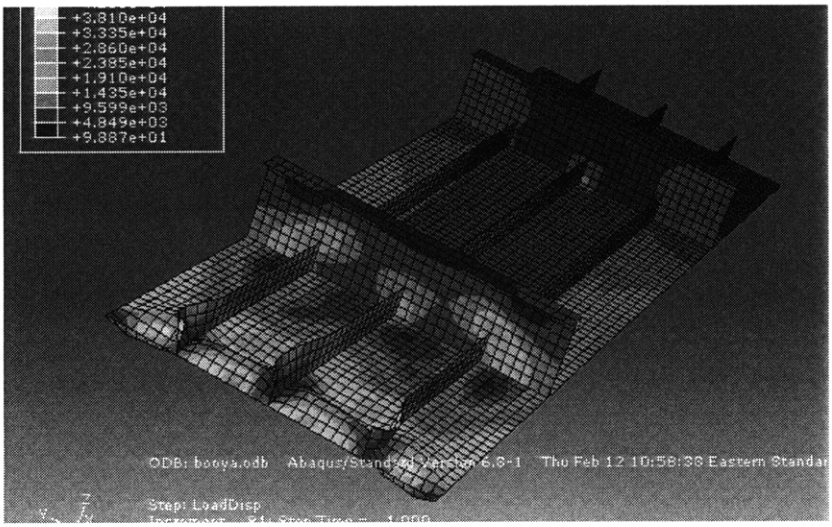

Figure 95: This image to the baseline panel with Alpha boundary conditions, an increase in thickness to account for the doubler, and the addition of an extra stiffener. These results are for an ideal plate.

A.5.11 Selected F.E.A Images with Consideration for Initial Deflection

The images below represent the changes in the failure of the test plate (as per Coast Guard Drawing) that occur when an initial deflection is added. The initial deflection was added using an additional distributed load under plate bending theory, discussed in Section 5.3.3. These images represent an initial deflection of 1% and 10% of the thickness considering the doubler to be smeared into the plate. All other images can be seen at the request of the author.

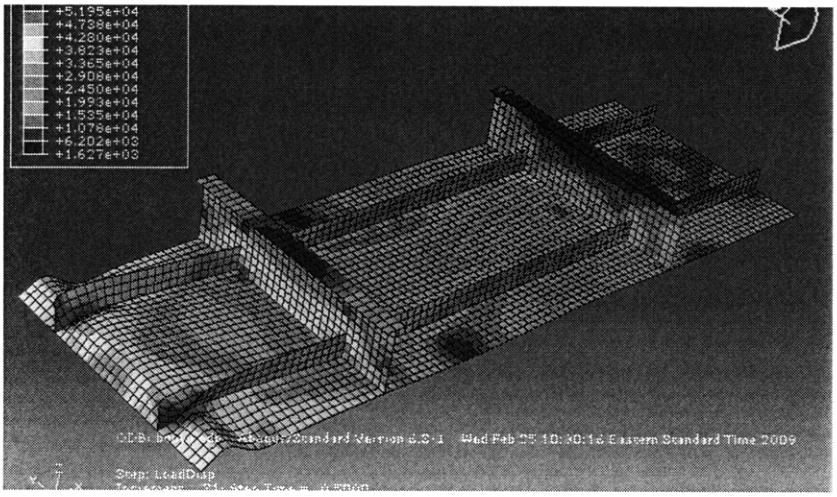

Figure 96: Baseline Test Panel with smear consideration and experimental boundary conditions. This image shows a maximum initial deflection equal to 1 % of the thickness of the plate.

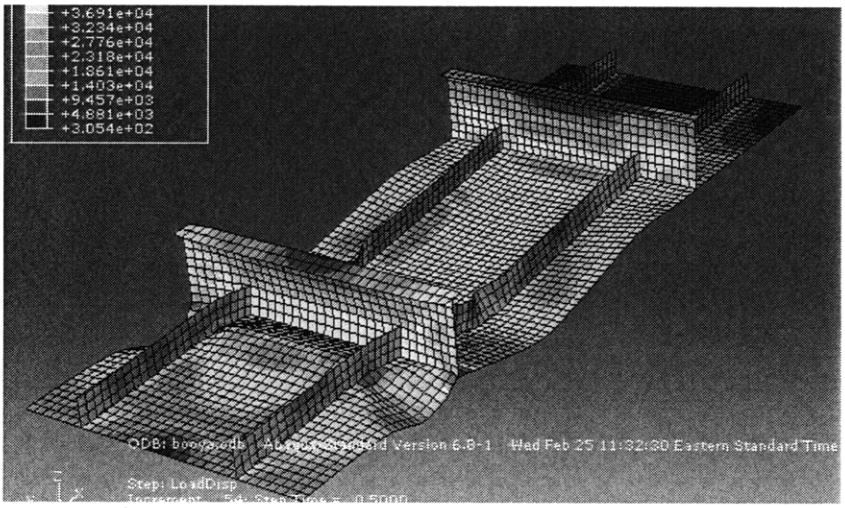

Figure 97: Baseline test panel with smear consideration and experimental test boundary conditions at 10% initial deflection. While the panel displays slightly different failure characteristics than are actually seen in the experiment, it is interesting to see how Von Karman's effective width theory is validated by the stress distribution on the loaded edge. The dark blue semi-circle seen on the edge shows the relatively less stress in that area as compared to the area by the stiffeners.

The only boundary condition that was considered for the initial deflection study was the one used in the experiment (free, modified). The results of this study and the corresponding loss in strength can be seen in the text as Table 17.

A.5.12 Local Plate Strength Reduction Consideration Calculations

The following spreadsheet calculations correspond to section 5.4 of the text which discusses calculations that are based on various local plate strength reduction concerns. This is what bridges the gap when working with actual plates versus ideal plates. Finite element results for initial deflection consideration are discussed in Section 5.3.3 of the text and the load-displacement results were seen in Appendix Section 5.11. Analytically, the allowances for initial deflection are based on the slenderness

ratio (ß) and empirically derived formulas discussed in Reference (5). Verification calculations of F.E.M. are seen below.

Slenderness Ratio	Allowable Initial Deflection
1.56	0.05

Table 31: Allowable Initial Deflection Calculation

The slenderness ratio was calculated considering smear for the doubler and the stiffeners. The allowable initial displacement is approximately 30% of the thickness of the base plate and therefore will within limits. Methodology for the calculation of the slenderness ration is seen in Appendix 5.13.

Unlike initial deflection considerations which are a very real issue with the test panel, the shear stress considerations used on the test panel were actually considered using the maximum shear stress seen on the *entire* ship to prove, that in this scenario, they are of little consequence. The shear stress factor is calculated using Equation 54 assuming shear stress is calculated from Equations 8 and 9 in the text. The resultant loss in load capability is extrapolated based on the stress-equals-load-over-area relationship. The spreadsheet is below.

Shear Calculation:	Value	Units
Q	124,444.4	lbs
Q/I	0.4667	lbs/in^4
m	870.43	in^3
τ	1,372.3	lbs/in^2
r_τ	0.9982	psi/psi
P_{ult} Difference	164.4	lbs

Table 32: Shear stress spreadsheet calculation

The maximum shear force on the 123' assumes normal beam theory applies. Shear appears insignificant.

Imperfection calculations were completed based on the ANSI modification to Von Karman's effective width method. A doubler smear is considered, but worst case imperfections are considered by not smearing the stiffeners. The calculation is below:

Imperfection Calculations:	Value	Units
Buckling Cr	9,604	(from V.K)
Stress Yield	40,000	psi
b	18	inches
b_{effnew}	7.87	(h=0.168)
P_{ult} New	195,878.3	Lbs
P_{ult} Difference	12,393.7	Lbs

Table 33: Imperfection spreadsheet calculation

The critical buckling load was determined using Von Karman's relationship between σ_y and σ_{cr} based on a given slenderness ratio.

The considerations for residual stress were completed using theory normally reserved for simple plates. Due to the lack of information regarding the welding characteristics of the stiffened panel, this approximation is certainly the most accurate. The spreadsheet calculation below is based on Equation 10 and its applicable sub-equations, including the eccentricity factor, discussed in Reference (5).

Residual Stresses Calculation:	Value	Units
Eccentricity Factor	0.14	eta
Residual Stress present	57.34	psi
P_{ult} Difference (using b_{eff})	296.79	lbs

Table 34: Residual Stress spreadsheet calculation

In this case, the b_{eff} that is used is based upon a smeared doubler to increase similarity with the experiment.

Although important in the case of the 179', considerations for cracking does not affect the validation of theoretical methods with regards to the experiment using the Coast Guard furnished stiffened panel. A calculation was completed, however, based on fictitious crack geometry, to qualitatively determine the extent of degradation due to cracking. Equation 56 in the text is used. The calculation is below:

Crack Calculation:	Value	Units
b	8.8	in
C_p	2.2	in
t	0.161	in
σ_y	40,000	psi
h_w	3	in
c_s	1.5	in
t_w	0.375	in
Numerator (Eqn 5-6)	65,004	lbs
Denominator (Eqn. 5-6)	2.5418	in^2
σ_{ult}	25,574	psi
P_{ult}	130,008	lbs
% Difference	37.57	lbs/lbs

Table 35: Crack Consideration Spreadsheet Calculations.

In this case, the reduction in P_{ult} was calculated to be 37%. The crack size is arbitrary and with changes in the geometry of the plate and the crack size the strength reduction will change.

A.5.13 Calculation of Slenderness Ratio and Normalized Stresses

The premise of (algebraically) the calculation for the slenderness ratio (ß) that best accounts for the complex geometry of the plate-stiffener calculation is seen in section 5.3 of this Appendix. The slenderness ratio is given by Equation 38 in the text.

In order to determine a valid thickness to account for the stiffeners, first the entire cross sectional area of the entire 32"x46" plate (with stiffeners) was determined and then to calculate the equivalent thickness over an 18" piece the area was divided by that length. This was completed for a baseline and doubler smear scenario. These results are plotted in Figure 55 in the text.

Appendix: Chapter 6

A.6.1 170' (179') Safe Operating Envelope

The figure below depicts the SOE for the 170' (179'). In this particular instance, it is in graphical form. The figure is based upon two parameter, namely Ship Speed (Knots) and Significant Wave Height (Feet).

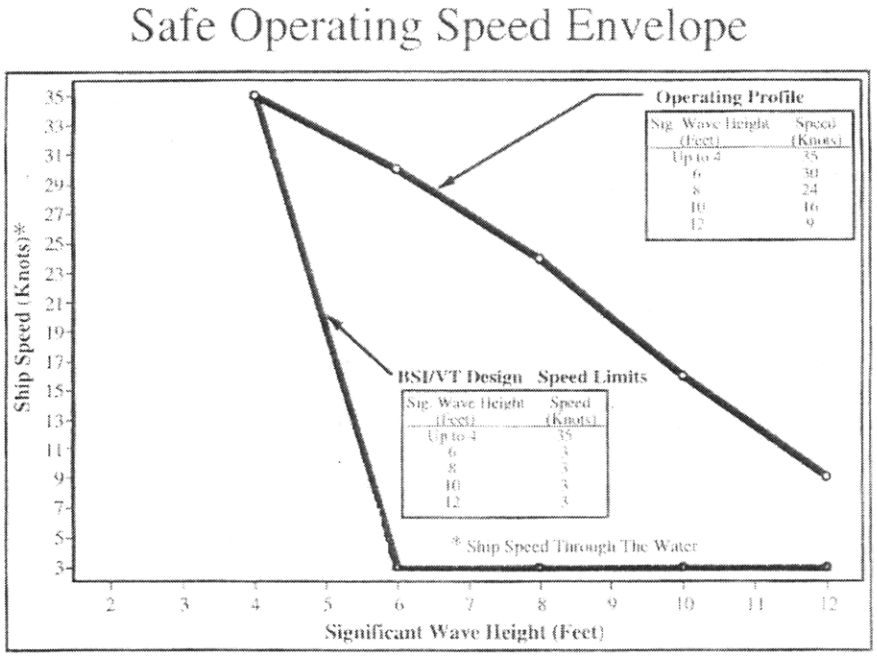

Figure 98: Operating Speed Envelope for the 179'. The curves are limitations that the ship must remain below to stay within limits. These curves are derived from the design seakeeping characteristics of the ship.

The different curves on the graph represent different operating envelopes. The curve all the way to the right signifies the original operating envelope (and current operating envelope) of the 179' while the BSI/VT curve shows the original Thorneycroft design envelope. The figure above is modified and reproduced from reference (39).

A.6.2 110' (123') Safe Operating Envelope

The SOE of the 110' (123') is seen on the following page in tabular form. Like the operating profile seen in the previous appendix, it is based on the seakeeping characteristics of the ship, the ship speed and both significant wave height and sea state. In this particular case, it is broken down into a P-spec (performance specification detailing mission defining capabilities) and a pure operating envelope where survivability is the leading variable input. The charts on the following page are reproduced from Reference (2).

110 WPB Operating Envelope[1, 5] (Speeds and Sea States)

Sea State[2]	Significant Wave Height[2] (ft)	Speed	Heading
3	1.6 - 4.1	Unrestricted, Involuntary Reduction[3]	Any
4	4.1 – 8.2	Unrestricted, Involuntary Reduction[3]	Any
5	8.2 – 13.1	Begin Voluntary Reduction[4]	Any
6	13.1 – 19.7	Voluntary Reduction[4]	Any

Notes:

1. Based on 1982 Circular Of Requirements, 1987 R&DC Report and 1991 Structural Improvements.
2. Lee and Bales 1984, "Environmental Data for Design of Marine Vehicles" SSC/SNAME Arlington, VA.
3. Involuntary Speed Reduction – Due to Added Drag and Reduced Available Power (Reduced Propulsive Efficiency) in a Seaway (Full Engine Power Can Be Applied).
4. Voluntary Speed Reduction – By the Operator to Reduce Slamming and Deck Wetness. Alternatively, Operator Can Change Ship's Heading to Reduce Slamming, Crew Discomfort and Deck Wetness.
5. The 110 WPB is Considered a "Coastal Naval Craft" as per "Guide..." (ABS HSNC Rules, 2003).

This means 110 WPB is restricted to 300 NM from safe refuge during summer and 150 NM during winter.

6. Restricted to 70 Knot Beam Wind; Must Avoid Eyes of Hurricanes.

RIB Launch and Recovery up to Sea State – 5 at Slow Speed at Best Heading.

Table 36: 110' (123') Operating Envelope with survivability based on seakeeping parameters of the hull as the primary input. References to which seakeeping analysis criteria were used for the envelope analysis are noted below the table.

Performance Requirements	Environmental Conditions
Refueling and Strike-down Underway	Sea State 3 (1.6 – 4.1 ft) Ship takes best heading
Continuous Efficient Operation	Sea State 3 (1.6 – 4.1 ft) All ship headings
Limited Operation and Capability of Continuing Mission without Returning to Port for Repairs after Sea Subsides	Sea State 4 (4.1 – 8.2 ft) Ship takes best heading
Survive without Serious Damage to Mission-Essential Systems	Sea State 5 (8.2 – 13.1 ft) Ship takes best heading

Table 37: Performance Specification based on mission requirements for the WPB.

Using the tables above and Figure 98 in the previous section of the Appendix, it is easy to compare seakeeping characteristics even though the operational speed of each craft is slightly different.

Bibliography

1. **Wikipedia.** Liberty Ships. [Online] 2008. http://en.wikipedia.org/wiki/Liberty_Ship.

2. **Integrated Deepwater Systems.** *123' WPB Program Summary: Senate Brief.* s.l. : United States Coast Guard, Department of Homeland Security, 2006.

3. **d'Entremont, Richard.** *179' Damage Summary.* October 2008.

4. **Zubaly, Robert B.** *Applied Naval Architecture.* Jersey City, NJ : The Society of Naval Architecture and Marine Engineering, 1996.

5. **Hughes, Owen F.** *Ship Structural Design.* Jersey City, NJ : The Society of Naval Architects and Marine Engineers, 1988.

6. **Hibbler, R.C.** *Mechanics of Materials, Fourth Edition.* Upper Saddle River, NJ : Prentice Hall, Inc., 2000.

7. **Miller, Paul H and Stettler, Jeffrey W.** *USCG 123 FT WPB Side Shell Panel Buckling Test.* Annapolis, MD : United States Naval Academy Department of Engineering and Weapons, 2006.

8. **Purcell, Edward S, Allen, Stephen J and Walker, Richard T.** Structural Analysis of the U.S. Coast Guard Island Class Patrol Boat. *SNAME Transactions.* 1988, Vol. 96.

9. **Gooding, Trent.** *2.703 Principles of Naval Ship Design Notes.* Cambridge, MA : Massachusetts Institute of Technology, 2008.

10. **American Bureau of Shipping.** ABS News Room - Fact Sheet. *ABS, American Bureau of Shipping Ship Classification Society.* [Online] 2009. http://www.eagle.org/news/newsroom-factsheet.html.

11. **American Bureau of Shipping.** *Guide for Building and Classing High Speed Naval Craft.* Houson, TX : American Bureau of Shipping, 2007.

12. **Collella, Kurt.** *Ship Structures Notes.* New London, CT : United States Coast Guard Academy, 2004.

13. **O'Rourke, Ronald.** *CRS Report for Congress: Coast Guard Deepwater Acquisition Programs.* Washington, DC : Congressional Research Service, 2008.

14. **Navy Ship Structural Design Standards.** *DDS 100-6.* Washington, DC : NAVSEA, Department of the Navy.

15. **Koenig, Philip C.** *Technology and Management in the Global Shipbuilding Industry.* Cambridge, MA : Massachusetts Institute of Technology, 2008.

16. **Lamb, Thomas ed.** *Ship Design and Construction Vol. I.* Jersey City, NJ : The Society of Naval Architects and Marine Engineers, 2003.

17. **Rawson, KJ and Tupper, EC.** *Basic Ship Theory Fifth Edition.* Boston, MA : Butterworth-Heinneman, 2001.

18. **Sensharma, Pradeep and Willis, Malcolm.** *Structural Analysis of 123-FT A-Class WPB.* Arlington, VA : BMT Designers & Planners, Inc, 2005.

19. **PEO Ships.** *PC History.* Washington, DC : Department of the Navy, 2006.

20. **Lewis, Edward V, ed.** *Principles of Naval Architecture Second Revision Volume I.* Jersey City, NJ : The Society of Naval Architecture and Marine Engineering, 1988.

21. **Mansour, A and d'Oliveira, J.M.** *Hull Bending Moment due to Ship Bottom Slamming.* Cambridge, MA : Massachusetts Institute of Technology, 1973.

22. **Becker, H, Goldman, R and Pazerycki-Mithras, J.** *Compressive Strength of Ship HUll Girders.* Washington, DC : Ship Structure Committee, 1970.

23. **Masubuchi, Koichi.** *Analysis of Welded Structures.* New York, NY : Pergamon Press, 1980.

24. **Todd, F. H.** *Ship Hull Vibration.* London, UK : Edward Arnorld, Ltd., 1961.

25. **Mothander, Matthew K.A.** *A Study of Forced and Natural Vibration Characteristics of the United States Coast Guard Academy Training Boats.* New London, CT : United States Coast Guard Academy, 2005.

26. **Bleile, Henry R and Rodgers, Stephen D.** *Shipboard Corrosion Engineering.* Washington, DC : NAVSEA, Department of the Navy, 1984.

27. **MO-307, NAVFAC.** Corrosion Type Stress Corrosion Cracking. [Online] Corrosionist, 2009. http://www.corrosionist.com/Corrosion_Type_Stress_Corrosion_Cracking.htm.

28. **Paik, Jeom Kee and Thayamballi, Anil Kumar.** *Ultimate Limit State Design of Steel-Plated Structures.* West Sussex, UK : John Wiley & Sons, Ltd., 2003.

29. **Wierzbicki, Tomasz.** *2.080 Structural Mechanics Notes.* Cambridge, MA : Massachusetts Institute of Technology, 2007.

30. **Wierzbicki, Tomasz.** *2.081 Plates and Shells Notes.* Cambridge, MA : Massachusetts Institute of Technology, 2008.

31. **Paik, Jom Kee and Kim, Bong Ju.** Ultimate Strength Formulations for Stiffened Panels Under Combined Axial Load, in Plane Bending, and Lateral Pressure: A Benchmark Study. *Thin Walled Structures.* 2002, Vol. 40.

32. **Chen, Yong.** Ultimate Strength Analysis of Stiffened Panels using a Beam-Column Method. Blacksburg, VA : Virginia Polytechnic Institute, 2006.

33. **Global Security.** WPB-123' Patrol Boat. [Online] 2008. http://www.globalsecuriy.org/military/systems/ship/wpb-123.htm.

34. **Deepwater.** Deepwater Collage. [Online] http://huntingandgathering.org/images/NAVY_USCG_Deepwater_Collage_lg_1_.gif.

35. **Pierce, LCDR Frank A, USCG.** *123' Damage Summary.* August 2008.

36. **United States Coast Guard.** USCG: About Us - Aircraft, Boats, and Cutters. *USCG.* [Online] United States Coast Guard. http://www.uscg.mil/datasheet/110wpb.asp.

37. **USCG Office of Naval Engineering.** USCG Drawing 123-WPB-085-031. Washington, DC : United States Coast Guard, Department of Homeland Security, 2004.

38. **Matyas, Chris.** Cyclone Class PC's - World War 2 - PCSA. [Online] Patrol Craft Sailor Association, 2008. http://www.ww2pcsa.org/cyclone-patrol-coastals.html.

39. **PMS 325J Project Managment Office.** *Patrol-Coastal (PC) Cyclone Class Structural Damage Investigation and Analysis Status.* Washington, DC : NAVSEA, Department of the Navy, 1998.

40. **Naval Sea Sytems Command.** NAVSEA Drawing 7291814. Washington, DC : NAVSEA, Department of the Navy, 2000.

41. **Jensen, J.J.** *Load and Global Response of Ships.* New York, NY : Elsevier, 2001.

42. **USCG Engineering Logistics Center.** *123' Section Modulus Calculations with Revisions.* Washington, DC : United States Coast Guard, Department of Homeland Security, 2006.

43. **Hull Girder Primary Strength.** *SDS 100-1.* Washington, DC : NAVSEA, Department of the Navy.

44. **USCG Engineering Logistics Center.** *123' Load-Shear-Moment-Stress Curves.* Washington, DC : United States Coast Guard, Department of Homeland Security, 2006.

45. **Wendell, Peter.** *179' Naval Architecture.* February 2009.

46. **Naval Sea Systems Command.** NAVSEA Drawing 5106697. Washington, DC : NAVSEA, Department of the Navy, 1998.

47. **Rizzo, LT(jg) Joseph USCG.** *110' Underway Specifications.* March 2009.

48. **Guillot, Michael.** *Corrosion Testing of Alumimum Samples from Patrol Boats.* Baton Rouge, LA : Stress Engineering Services Inc, 2007.

49. **Maryland Metrics.** BS 4360 HR Steel for General Engineering Purposes. Owings Mills, MD : Maryland Metrics, 2008.

50. **Timoshenko, S and Gere, J.** *Theory of Elastic Stability.* New York, NY : McGraw-Hill , 1961.

51. **Timoshenko, S and Woinowsky-Krieger, S.** *Theory of Plates and Shells.* New York, NY : McGraw-Hill Book Company, Inc, 1959.

52. **Wikipedia.** Classification Society. [Online] Wikimedia Foundation, Inc., 2008. http://www.wikipedia.org/wiki/Classification_society.

53. **Simulia.** *Abaqus/cae Documentation 6.8.* Providence, RI : Dassault Systemes, 2008.